Compactons in strongly nonlinear lattices

Dissertation

zur Erlangung des akademischen Grades
Doktor der Naturwissenschaften (Dr. rer. nat.)
in der Wissenschaftsdisziplin Statistische Physik / Chaostheorie

eingereicht an der
Mathematisch-Naturwissenschaftlichen Fakultät
Universität Potsdam

von
Karsten Ahnert

Potsdam, 2. November 2010

Published online at the
Institutional Repository of the University of Potsdam:
URL http://opus.kobv.de/ubp/volltexte/2010/4853/
URN urn:nbn:de:kobv:517-opus-48539
http://nbn-resolving.org/urn:nbn:de:kobv:517-opus-48539

Abstract

In the present work, we study wave phenomena in strongly nonlinear lattices. Such lattices are characterized by the absence of classical linear waves. We demonstrate that compactons – strongly localized solitary waves with tails decaying faster than exponential – exist and that they play a major role in the dynamics of the system under consideration. We investigate compactons in different physical setups. One part deals with lattices of dispersively coupled limit cycle oscillators which find various applications in natural sciences such as Josephson junction arrays or coupled Ginzburg-Landau equations. Another part deals with Hamiltonian lattices. Here, a prominent example in which compactons can be found is the granular chain. In the third part, we study systems which are related to the discrete nonlinear Schrödinger equation describing, for example, coupled optical wave-guides or the dynamics of Bose-Einstein condensates in optical lattices.

Our investigations are based on a numerical method to solve the traveling wave equation. This results in a quasi-exact solution (up to numerical errors) which is the compacton. Another ansatz which is employed throughout this work is the quasi-continuous approximation where the lattice is described by a continuous medium. Here, compactons are found analytically, but they are defined on a truly compact support. Remarkably, both ways give similar qualitative and quantitative results.

Additionally, we study the dynamical properties of compactons by means of numerical simulation of the lattice equations. Especially, we concentrate on their emergence from physically realizable initial conditions as well as on their stability due to collisions. We show that the collisions are not exactly elastic but that a small part of the energy remains at the location of the collision. In finite lattices, this remaining part will then trigger a multiple scattering process resulting in a chaotic state.

Zusammenfassung

In der hier vorliegenden Arbeit werden Wellenphänomene in stark nichtlinearen Gittern untersucht. Diese Gitter zeichnen sich vor allem durch die Abwesenheit von klassischen linearen Wellen aus. Es wird gezeigt, dass Kompaktonen – stark lokalisierte solitäre Wellen, mit Ausläufern welche schneller als exponentiell abfallen – existieren, und dass sie eine entscheidende Rolle in der Dynamik dieser Gitter spielen. Kompaktonen treten in verschiedenen diskreten physikalischen Systemen auf. Ein Teil der Arbeit behandelt dabei Gitter von dispersiv gekoppelten Oszillatoren, welche beispielsweise Anwendung in gekoppelten Josephsonkontakten oder gekoppelten Ginzburg-Landau-Gleichungen finden. Ein weiterer Teil beschäftigt sich mit Hamiltongittern, wobei die granulare Kette das bekannteste Beispiel ist, in dem Kompaktonen beobachtet werden können. Im dritten Teil werden Systeme, welche im Zusammenhang mit der Diskreten Nichtlinearen Schrödingergleichung stehen, studiert. Diese Gleichung beschreibt beispielsweise Arrays von optischen Wellenleitern oder die Dynamik von Bose-Einstein-Kondensaten in optischen Gittern.

Das Studium der Kompaktonen basiert hier hauptsächlich auf dem numerischen Lösen der dazugehörigen Wellengleichung. Dies mündet in einer quasi-exakten Lösung, dem Kompakton, welches bis auf numerische Fehler genau bestimmt werden kann. Ein anderer Ansatz, der in dieser Arbeit mehrfach verwendet wird, ist die Approximation des Gitters durch ein kontinuierliches Medium. Die daraus resultierenden Kompaktonen besitzen einen im mathematischen Sinne kompakten Definitionsbereich. Beide Methoden liefern qualitativ und quantitativ gut übereinstimmende Ergebnisse.

Zusätzlich werden die dynamischen Eigenschaften von Kompaktonen mit Hilfe von direkten numerischen Simulationen der Gittergleichungen untersucht. Dabei wird ein Hauptaugenmerk auf die Entstehung von Kompaktonen unter physikalisch realisierbaren Anfangsbedingungen und ihre Kollisionen gelegt. Es wird gezeigt, dass die Wechselwirkung nicht exakt elastisch ist, sondern dass ein Teil ihrer Energie an der Position der Kollision verharrt. In endlichen Gittern führt dies zu einem multiplen Streuprozess, welcher in einem chaotischen Zustand endet.

Acknowledgements

During this work many people have supported me. Escpecially, I want to thank

- Prof. Dr. Arkady Pikovsky,
  for giving me the opportunity to write this thesis, for his superb supervision, and for many interesting scientific discussions.
- Prof. Dr. Dima Shepelyansky,
  for inviting me to Toulouse and for many discussions about lattices and related problems.
- Prof. Dr. Philip Rosenau,
  for helpful discussions concerning compactons in general and problems in this work in particular.
- Mario Mulansky and Priv.-Doz. Dr. habil. Markus Abel,
  for many physical and non-physical discussions and for proof-reading the manuscript.
- Arthur Straube,
  for giving me the possibility to join him at the Humboldt-University Berlin.
- Marlies Path,
  for all the sweets and her help with all organisatorical questions.
- The group of statistical physics and chaos theory,
  as well as the institute of physics for a very warm and inspiring atmosphere.
- My parents and my friends,
  which supported me throughout my way of eduction, especially my brother Kristof for preparing some graphics and Janina Wowros for her patience and love.

Contents

Chapter 1

Introduction

Everybody knows what happens if two billiard balls hit each other – they exchange momentum. A similar phenomenom appears in the toy "Newton's cradle" depicted in Fig. 1.1. If one ball on the side is pulled away and then released, it hits the next ball and the ball on the other side is knocked away. Momentum conservation is responsible for this observation. One could repeat the experiment with two (or in general n) balls pulled away resulting in two (or n) balls knocked away. But what happens exactly in the time between the initial stroke and the release of the last ball? How is the momentum transferred through the chain and how long does the whole process take?

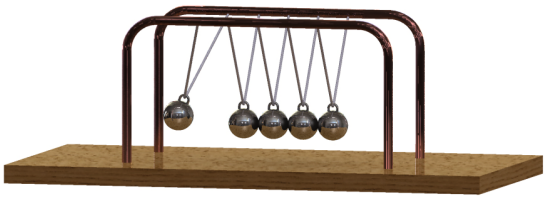

Figure 1.1: Newton's cradle

To answer such questions experiments with hard spheres arranged in one line have been performed. This setup is also called a granular chain. One could observe that momentum is transferred in very narrow pulses, typically involving five balls [1]. The velocity of these pulses depends on the amplitude and follows a power law.

Nowadays, the results of the experiments with the granular chain are viewed in the context of solitons and solitary waves [2, 3]. Roughly speaking, a soliton is a wave which travels with a constant velocity and does not change its shape during the evolution. From a mathematical point of view, solitons appear only in integrable systems, i.e. systems with an infinite number of conservation laws and without dissipation. The interaction between two or more solitons is elastic, such that their properties are not destroyed during collisions. In non- or nearly-integrable systems solitary waves also exist [4, 5]. But here, their interactions are not elastic and these waves are not exact solitons. In the last decade, a special class of non-integrable systems has been introduced which allows

for the formation of *compactons* – solitary waves with compact support [6]. The basic mechanism behind this remarkable property is nonlinear dispersion [7].

The aim of the present work is to investigate compactons in discrete systems. One possible application is the above mentioned granular chain. But we will look on this topic from a broader perspective. In particular, we will not exclusively study granular systems, but also phase oscillator lattices and systems related to the discrete nonlinear Schrödinger equation (DNLS). As we will see, nonlinear interaction is responsible for the emergence of compactons and compact structures.

This thesis is organized as follows. In the remaining part of the introduction the differences between discrete and continuous systems are discussed. Furthermore, nonlinear structures, like solitons, breathers or kinks and the classical compacton are introduced and applications are presented. In chapter 2 we will analyze compactons and related phenomena in dispersively coupled **phase oscillator lattices**. We will observe that besides compactons a large variety of stable traveling wave structures exist. **Hamiltonian lattices** are studied in chapter 3. The granular chain belongs to this class of systems and we will see that the above mentioned pulses are in fact compactons. The topic of chapter 4 is a generalization of the **discrete nonlinear Schrödinger equation**. Finally, the thesis is completed with concluding remarks and open questions in chapter 5.

1.1 Dynamics of lattices

In this thesis, we will study discrete dynamical systems

$$\dot{u}_k = f_k(u_k) + f_k^{\mathrm{coup}}(u_1, \ldots, u_N) \ . \tag{1.1}$$

Here, and in the following the overdot $\dot{u} = \mathrm{d}u/\mathrm{d}t$ always means differentiation with respect to time. u_k is the quantity under observation, which can be vector-like, and its internal dynamics is given by $f_k(u_k)$. $k = 1, \ldots, N$ is the index of the k-th "particle" and N is the total number of "particles".

The function f_k^{coup} denotes the coupling and contains all informations about the interactions of the individual units. Especially, it describes the interaction type (e.g. two-, three-, ... particle interaction) and the topology of the lattice. In this work we will mainly concentrate on two-particle interaction and regular lattices in one or two dimensions. In Fig. 1.2 some explanatory lattice topologies are shown. The first one (Fig. 1.2a)

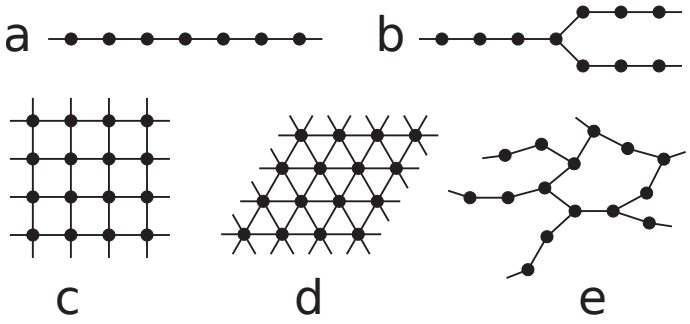

Figure 1.2: Different lattice topologies

is a one-dimensional regular chain. The nodes (black dots) represent u_k and the lines interaction between two nodes. The second one (Fig. 1.2b) shows three 1D chains which are connected at one particular site. The third and the fourth diagrams (Fig. 1.2c and 1.2d) show two-dimensional regular lattices in a square and a hexagonal configuration and the fifth lattice topology (Fig. 1.2e) is a random network. As stated above, this work will only deal with regular lattices, although interesting effects can also be expected on irregular topologies, like random networks or coupled chains.

There is a natural way to compare the dynamics of a regular lattice with the dynamics of a continuous medium – the discrete lattice is approximated by a continuous variable. If the wave length (or spatial scale) is much larger then the lattice spacing this method is known as long wave approximation and the spacing enters as a small parameter. In this way, the Korteweg-de Vries equation could be derived from the Fermi-Pasta-Ulam problem [8]. Contrary, if the wave length and the lattice spacing are of same order a small parameter does not exist and the continuous approximation is more or less arbitrary [9–11]. Therefore, it is called the quasi-continuous approximation (QCA) and its validity has to be checked, either by numerics or by comparison with experiments. Throughout this work, we will heavily utilize the QCA to compare and validate our findings in the lattice.

1.2 Nonlinear and compact structures

Genuine nonlinear structures have attracted much attention in the scientific community. It started with the discovery of solitons in the Korteweg-de Vries equation [8] and further investigations lead rapidly to a full theory of solitons in integrable systems [3]. Besides continuous systems, integrable lattices have been studied, mainly by means of the famous Toda Lattice [12–14].

Other typical nonlinear structures are breathers – time-periodic and localized solutions of either a continuous media equation or a lattice. Prominent examples are the sine-Gordon and the nonlinear Schrödinger equation [15, 16], where breather solutions can be written down analytically. Furthermore, breathers occur in Hamiltonian lattices [17, 18]. Sometimes, the terms breathers and solitons are used synonymously [19].

In 1993 Philip Rosenau introduced a model which allows for the formation of compactly localized solitary waves [6]. In contrast to the usual solitons which possess exponentially

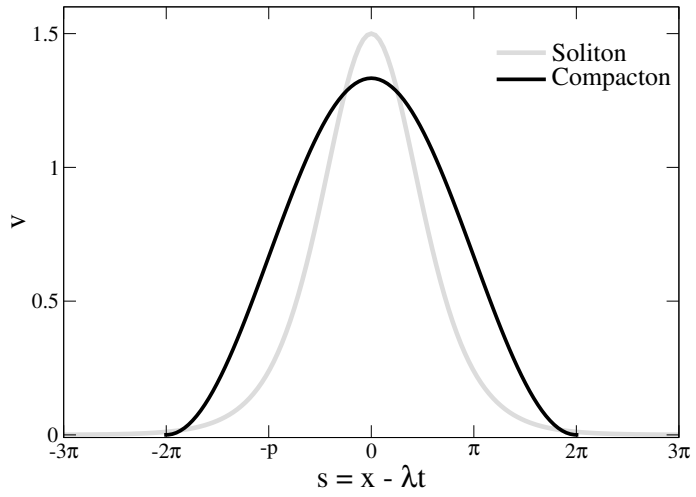

Figure 1.3: The soliton and the compacton solution of the KdV and the $K(2,2)$ equation.

decaying tails his solution is truly compact, being defined only on a small part of the domain. In detail, he studied the $K(m,n)$-equation

$$\dot{v} + [v^m]_x + [v^n]_{xxx} = 0 \ . \tag{1.2}$$

For $m = 2$ and $n = 1$ this equation reduces to the well know Korteweg-de Vries equation, which has soliton solutions in the form

$$v_{KdV}(x,t) = \frac{3}{2}\lambda \,\mathrm{sech}\left(\frac{\sqrt{\lambda}}{2}s\right) \ , \tag{1.3}$$

where $s = x - \lambda t$ is the coordinate in a frame moving with velocity λ. The tails of this soliton decay exponentially with $v_{KdV} \to \mathrm{e}^{-\sqrt{\lambda}s}$ for $s \to \infty$. In contrast, the $K(2,2)$ equation possesses the solution

$$v_{K22}(x,t) = \begin{cases} \frac{4\lambda}{3}\lambda \, \cos^2\left(\frac{1}{4}s\right) & \text{for } |s| < 2\pi \\ 0 & \text{else,} \end{cases} \tag{1.4}$$

which has been named compacton due to its compact nature. It is a combination of the constant solution $v = 0$ and a periodic solution. At the edge $s = 2\pi$ every term in the $K(2,2)$-equation is exactly zero and no balancing between various terms takes place, hence one can "glue" together the two solutions. Furthermore, all terms in the $K(2,2)$-equation are continuous and smooth, including the edge. Fig. 1.3 shows the soliton of the KdV equation and the compacton of the $K(2,2)$ equation for $\lambda = 1$.

The formation of the compacton happens due to nonlinear dispersion [6, 7]. Around $v = 0$ linear terms are completely absent and the state $v = 0$ is degenerate. In the

lattice the situation is different; one does not expect a truly compact traveling wave due to the discrete nature of the medium. But we will show that purely nonlinear interaction between neighboring lattices sites will lead to the formation of super-exponential tails, decaying faster than exponential ones. In this case, linear terms are not present in the interaction and the linear approximation of the basic state does not yield any results. In particular, exponential or periodic solutions from linearized equations can not be obtained.

1.3 Applications and models

In this work we will study three kinds of lattice equations where strongly nonlinear interaction between the constituents is crucial.

1.3.1 Dispersively coupled limit cycle oscillators

The first class of systems which is investigated are dispersively coupled limit cycle oscillators [20], which are studied in chapter 2. Limit cycle oscillators can be found nearly everywhere in nature. They have been used to model social, biological, physical or chemical systems, see for example [21–25] or the textbooks [26, 27] and references therein.

In general, a limit cycle oscillator is described by the phase φ, which is 2π-periodic and obeys $\dot{\varphi} = \omega$, where ω is its frequency. In chapter 2 we will consider lattices of such oscillators which are coupled to their nearest neighbors. In the one-dimensional case and under the assumption that the coupling is weak the dynamics are governed by

$$\dot{\varphi}_k = q(\varphi_{k+1} - \varphi_k) + q(\varphi_{k-1} - \varphi_k) \ , \tag{1.5}$$

where $q(\varphi)$ represents the interaction between the oscillators. In many examples the coupling between the oscillators is dissipative, meaning that $q(v)$ is an odd function $q(-\varphi) = -q(\varphi)$. In this case, the phases try to equalize each other, which results in the well known phenomenon of synchronization or entrainment [27]. But, the motivation of our studies is dispersive coupling, which leads to conservative dynamics. Such systems have been studied in the course of magnetic systems and spin waves [28, 29] or Josephson junctions [30]. Dynamics similar to Eq. (1.5) also appears in discrete Ginzburg-Landau lattices with dispersive coupling [30].

1.3.2 Hamiltonian lattices

The study of Hamiltonian lattices has a long history. One remarkable mile stone on their exploration is surely the Fermi-Pasta-Ulam-paradox [31, 32], which was one of the first

numerical experiments and which triggered a huge amount of scientific research. One outcome of these studies was the discovery of solitons [8]. Another important point is the existence of genuine discrete breathers [17, 18] in such lattices.

Hamiltonian lattices are usually written as

$$H = \sum_k \frac{p_k^2}{2} + V_k(q_k) + W_k(q_1, q_2, \ldots, q_N) \ , \tag{1.6}$$

where q_k and p_k are the canonical variables and the equations of motion are obtained from $\dot{q}_k = \partial H/\partial p_k$, $\dot{p}_k = -\partial H/\partial q_k$. The potential energy is split into two parts, a local onsite potential $V_k(q_k)$ and an interaction potential $W_k(q_1, \ldots, q_N)$ coupling the indiviual units. In many situations the interaction is assumed to involve only the nearest neighbors. Then $W_k(q_1, \ldots, q_N)$ simplifies to $W(q_k, q_{k+1})$.

Due to their simplicity and practical relevance, Hamiltonian lattices have been widely used in theoretical physics. For example, the original work of Fermi, Pasta and Ulam dealt with a problem of thermalization. Other examples are the study of heat conduction [33], the interplay between nonlinearity and disorder [34, 35] or dislocations of crystal lattices [36].

Granular systems: Granular materials consist of a very large number of small, but macroscopic solid particles interacting with each other. The size of each particle has to be large enough, such that thermal fluctuations are not significant. Although granular materials consist of solids, they can show a fluid-like behavior [37, 38]. Examples are sand, powders, food (rice, coffee, corn, etc.), coal and coke or planetary rings and asteroid belts. Due to their wide-spread occurrence they are subject of intense theoretical and applied research.

One particular example is the above mentioned granular chain where the contact force follows the Hertzian law $F \sim \delta^{3/2}$. This system has been studied experimentally and theoretically [39, 40] and it could be observed that traveling pulses are very narrow and of quasi-compact nature.

1.3.3 Discrete nonlinear Schrödinger lattices

The third part deals with lattices related to the discrete nonlinear Schrödinger (DNLS) equation:

$$\mathrm{i}\dot{\Psi}_k = \Psi_{k+1} + \Psi_{k-1} + \beta|\Psi_k|^2\Psi_k \ . \tag{1.7}$$

Here, Ψ_k is the complex field at lattice site k and β is the nonlinearity parameter. The study of this equation dates back to the 70s where the DNLS has been used in some biophysical models [41]. Today, it is widely used in physical and mathematical studies. It is a generic equation describing many interesting phenomena. A overview

over recent experimental and theoretical results related to the DNLS is given in [42]. Strictly speaking, the DNLS is also Hamiltonian with complex canonical variables.

Slowly varying amplitude: The discrete nonlinear Schrödinger equation can be derived from a lattice of nonlinear oscillators

$$\ddot{q}_k + \omega^2 q_k = \kappa\big(q_{k+1} - 2q_k + q_{k-1}\big) + \beta q_k^3 \ . \tag{1.8}$$

Here, ω is the base frequency of each oscillator and β and κ are some parameters. Writing q_k now as $q_k = 1/2(\Psi_k \mathrm{e}^{-\mathrm{i}\omega t} + \Psi^* \mathrm{e}^{\mathrm{i}\omega t})$ and considering only terms rotating with $\mathrm{e}^{\mathrm{i}\omega t}$ yields the DNLS (1.7). Thus, it describes the slowly varying amplitude of Eq. (1.8).

Optical waveguides arrays: An optical waveguide is a device in which light beams (electromagnetic waves with wavelengths of the order 100 nm-1000 nm) are guided. Here, the nonlinear Kerr-effect can lead to a self trapping of the beam. In the late 90s it has been shown experimentally that coupled arrays of optical waveguides allow the formation of discrete solitons [43, 44]. These experiments can be described by the discrete nonlinear Schrödinger equation [45] where Ψ_k is interpreted as the complex amplitude of the electrical field in waveguide k and the time is replaced by the spatial coordinate in the direction of the waveguides. The nonlinearity arises from the nonlinear Kerr effect.

Dynamics of Bose-Einstein condensates: The discrete nonlinear Schrödinger equation also describes with great success recent experiments in the field of ultra-cold atomic gases. At sufficiently low temperatures all particles of a dilute bosonic gas occupy the same quantum state. This effect is the famous Bose-Einstein condensation [46] and the gas in this state is called a Bose-Einstein condensate (BEC). BECs have been observed first in 1995 [47, 48] with rubidium and sodium atoms. To create BECs the atoms are trapped magnetically and then evaporatively cooled to temperatures below the critical temperature. Then, the trap is switched off. The BEC can now expand and its properties are recorded. These experiments triggered a huge amount of experimental and theoretical work, for reviews see [49] or the book of Pethick and Smith [46]. To a certain extent Bose-Einstein condensates can be modeled by the Gross-Petaevskii equation (GP) (a variant of the nonlinear Schrödinger equation), especially if the temperature is well below the critical temperature T_c and if two body interaction is considered.

Quasi one-dimensional BECs can be loaded into optical lattices, which are created by the superposition of two interfering laser beams. The potential experienced by the BEC is then periodic, with the period of the interferences. Such experiments have been realized in 1998 [50]. They are modeled by the DNLS and nonlinear structures have been observed [51]. Effects of disorder could be studied too, resulting in an experimental realization of Anderson localization of BECs in optical lattices [52, 53].

Chapter 2

Compactons in phase oscillator lattices

In this part, we study lattices of coupled autonomous oscillators. They have a broad range of application and can be found in many scientific disciplines. If the coupling between the oscillators is weak one can describe them by their phase and neglect the amplitude [26, 27]. We call them phase oscillators and without coupling their dynamics is trivial: the phase is growing with a constant rate. Hence, nontrivial effects can only arise from the interaction. In general, two types of coupling exist: dissipative and dispersive coupling. Dissipative coupling tends to equalize the phases, such that a stable uniform state might establish. It is the basic mechanism for synchronization and has been discussed widely in the scientific community [54–59].

Here, we will concentrate on lattices of dispersively coupled phase oscillators. Such systems have some conservative properties and are similar to Hamiltonian lattices; in some cases it is even possible to write down a Hamiltonian. It is a well known fact that localized nonlinear structures, like breathers, kinks or solitons exist in Hamiltonian lattices [17, 19, 36, 44]. As we will see in this work, such structures also exist in phase lattices. In detail, we will investigate solitary waves and kinks, as well as periodic nonlinear waves. These waves usually appear in families, parameterized by their energies or their amplitudes.

Dispersive coupling of phase oscillators can be strongly nonlinear. The coupling function in our basic model is generic and in the ground state linear terms are absent. We will show that this leads to the formation of compact solitary waves – the *phase compactons*. Furthermore, classical solitary waves with exponential tails exists as well as periodic waves.

This chapter is organized as follows. First, we present a numerical example of coupled autonomous oscillators with dispersive coupling where one can observe the emergence of phase compactons. Then, we will introduce the basic lattice model in section 2.1, where

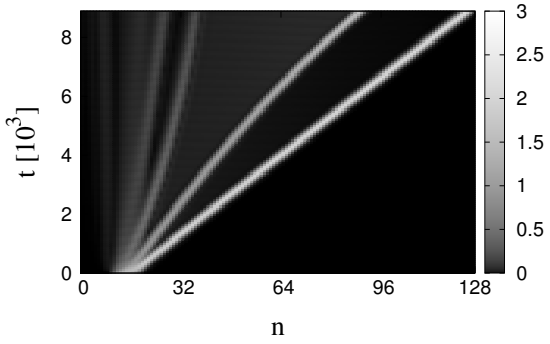

Figure 2.1: Phase compactons in the van der Pol system (2.2) with $\mu = 0.2$ and $\varepsilon = 0.1$. The phase difference between neighboring sites is shown and one observes a series of phase compactons emerging from the initial perturbation. With increasing amplitude, the velocity of these waves also increases.

we also discuss its properties and the quasi-continuous approximation. Section 2.2 is devoted to the study of traveling waves. Here, we will show that compactons exist in the lattice and in the continuum, along with conventional traveling waves like solitons and periodic waves. In section 2.3 we investigate the lattice numerically, that is, we show the stability of phase compactons against collisions and solve the initial value problem. Two-dimensional lattices of phase oscillators are studied in section 2.4.

Example: Coupled van der Pol oscillators

A famous example of an autonomous oscillator is the van der Pol (VdP) oscillator, which has been derived to describe an electrical circuit with a vacuum tube:

$$\ddot{x} = -x + \mu(1 - x^2)\dot{x} \ . \tag{2.1}$$

This oscillator exhibits a remarkable balance between energy supply and dissipation. For small amplitudes of x the second term on the RHS of Eq. (2.1) is positive and acts as negative damping, hence the amplitude of x will grow. On the other hand, for large values of x, this term is negative and energy is dissipated. These two effects are responsible for the limit cycle, which balances enery dissipation and supply.

Consider now a chain of coupled van der Pol oscillators

$$\ddot{x}_k = -x_k + \mu\big(1 - x_k^2\big)\dot{x}_k + \varepsilon\mu\big(x_{k+1} - 2x_k + x_{k-1}\big) \ . \tag{2.2}$$

Here, ε controls the coupling strength between each oscillator. The coupling is dispersive, hence it allows for the emergence of phase compactons. In Fig. 2.1 we show the evolution of a localized perturbation of the phase in the VdP chain with $\mu = 0.2$ and $\varepsilon = 0.1$. The

phase of each oscillator can approximately be described by $\varphi_k = \arctan(\dot{x}_k/x_k)$ and the phase difference $v_k = \varphi_{k+1} - \varphi_k$ is shown. One observes traveling objects leaving the initial perturbation. These objects are the phase compactons.

2.1 The basic model

We study lattices of weakly coupled autonomous oscillators. Each unit possesses a limit cycle with a characteristic frequency ω_k and the dynamics is described by the phase $\varphi_k(t)$ obeying $\dot{\varphi}_k = \omega_k$. The amplitude $A_k(t)$ of the oscillator can vary during one cycle, but must be periodic $A_k(t) = A_k(t + T_k)$, where $T_k = 2\pi\omega_k^{-1}$ is the period. Of course, the limit cycle needs to be stable, such that any initial condition in its surrounding asymptotically reaches the cycle. From a physical point of view each limit cycle oscillator balances energy supply and dissipation. In some regions of the phase space it gains energy while in other regions energy is dissipated.

If such an oscillator is now weakly coupled to its neighbors the equation for the phase reads

$$\dot{\varphi}_k = \omega_k + \sum_{l \in M_k} \tilde{q}_{kl}\left(\varphi_l, \varphi_k\right) \ , \tag{2.3}$$

where M_k is the index set of the neighbors of the k-th oscillator and $\tilde{q}_{kl}$ is the coupling function, being 2π-periodic in every argument. The smallness of the coupling assures that amplitude effects does not enter the game and the phase description is still valid for the coupled system. Now, fast oscillations are averaged out and if the frequencies $\omega_k = \omega$ are all equal the coupling function in Eq. (2.4) can be written as a function of the phase differences:

$$\dot{\varphi}_k = \omega + \sum_{l \in M} q\left(\varphi_l - \varphi_k\right) \ . \tag{2.4}$$

From here, we assume that the coupling is equal for all oscillators. The complete derivation of Eq. (2.4) is given in appendix A.1. The case of different frequencies $\omega_k \neq \omega_l$ is also shown there.

Up to now, Eq. (2.4) describes a set of coupled phase oscillators but nothing is said about their specific topology. A simple configuration is a one-dimensional chain of N oscillators. In such a chain, the indices k can be sorted according to the position in the chain and Eq.(2.4) reads

$$\dot{\varphi}_k = q(\varphi_{k+1} - \varphi_k) + q(\varphi_{k-1} - \varphi_k) \ . \tag{2.5}$$

The chain might be open, where the first and the last oscillator obey $\dot{\varphi}_1 = q(\varphi_2 - \varphi_1)$ and $\dot{\varphi}_N = q(\varphi_{N-1} - \varphi_N)$, or arranged on a ring with $\dot{\varphi}_1 = q(\varphi_2 - \varphi_1) + q(\varphi_N - \varphi_1)$ and $\dot{\varphi}_N = q(\varphi_1 - \varphi_N) + q(\varphi_{N-1} - \varphi_N)$. For some theoretical purposes it might also be convenient to consider infinite chains. Other interesting and easy-to-analyze topologies

are regular two- or higher-dimensional lattices, which are studied in section 2.4. They are natural generalizations of the one-dimensional chain.

For the one-dimensional chain it is possible to express the evolution in terms of the difference coordinates

$$v_k = \varphi_{k+1} - \varphi_k \ . \tag{2.6}$$

Building the derivative of this equation with respect to time and inserting the equation for the chain (2.5) yields

$$\dot{v}_k = q(v_{k+1}) + q(-v_k) - q(v_k) - q(-v_{k-1}) \ , \tag{2.7}$$

which is equivalent to Eq. (2.5) except one constant. In section 2.4 we also show, how one can express the two-dimensional square lattice in terms of differences. In general, the differences are a description of the connections between the lattice nodes. In this sense, Eq. (2.5) describes the evolution of the system in terms of the nodes, and Eq. (2.7) in terms of the edges.

Every function $q(v)$ can be written as a sum of an even and an odd function $q(v) = q_e(v) + q_o(v)$, where $q_e(v) = q_e(-v)$ and $q_o(v) = -q_o(-v)$. With this definitions Eq. (2.7) reads

$$\begin{aligned} \dot{v}_k &= q_e(v_{k+1}) - q_e(v_{k-1}) + q_o(v_{k+1}) - 2q_o(v_k) + q_o(v_{k-1}) \\ &= \nabla_d \, q_e(v_k) + \Delta_d \, q_o(v_k) \ . \end{aligned} \tag{2.8}$$

∇_d and Δ_d are the discrete nabla- and Laplace operators. The part with $\Delta_d \, q_o(v_k)$ introduces dissipation and for $q_o(v) = \sin v$ a stable state $v_k = 0$ exists. In this study, we will concentrate on purely even coupling functions. Such couplings induce dispersion and dissipation is absent. For the one-dimensional chain and identical oscillators our model reads now

$$v_k = q(v_{k+1}) - q(v_{k-1}) \ . \tag{2.9}$$

For simplicity we have dropped the index e here. For open boundaries the equations for the first and the last oscillator in the chain are $\dot{v}_1 = q(v_2)$ and $\dot{v}_N = q(v_{N-1})$ and for periodic boundaries $\dot{v}_1 = q(v_2) - q(v_N)$ and $\dot{v}_N = q(v_1) - q(v_{N-1})$.

The most simple 2π-periodic and even function is surely $q(v) = \cos v$. Many results in this chapter are obtained for this coupling, although we formulate all problems for general even functions.

A particularity of the even coupling function is the existence of a singular point with $q'(v) = 0$ at $v = 0$. Taylor expansion of order 2 around this point leads to $\dot{v}_k = v_{k+1}^2 - v_{k-1}^2$. Interestingly, this equations possesses an explosive solution [30] $v_k = A(t) \sin \frac{2\pi k}{3}$ with $A(t) = A_0/(1 - A_0\sqrt{3/4}(t - t_0))$. In the phase model (2.9) this explosive solution will grow until the full nonlinearity will slow it down. We will see later that this instability is crucial for the evolution of the lattice, especially in the two- or higher-dimensional case.

2.1.1 Properties

First of all, we note that the phase volume of the infinite chain is conserved, hence Eq. (2.9) fulfills the Liouville property $\sum_k \partial \dot{v}_k/\partial v_k = 0$. Secondly, the infinite chain (2.9) possesses the following conserved quantities

$$C_1 = \sum_k v_k \tag{2.10a}$$

$$C_2 = \sum_k (-1)^k v_k \tag{2.10b}$$

$$C_3 = \sum_k Q(v_k, v_0) \ , \qquad \text{where } Q(v,u) = \int_u^v q(x)\mathrm{d}x \ . \tag{2.10c}$$

In finite chains we have to introduce boundary conditions at both ends of the chain. For periodic boundary conditions the conservation laws for C_1 and C_3 are valid. The validity of C_2 depends on the number of oscillators; if N is even C_2 is conserved, otherwise not. In the open chain only C_3 is conserved and for odd N another conservation law exist

$$C_4 = \sum_k v_{2k-1} \ . \tag{2.11}$$

Remarkably, for open boundary conditions the Eq. (2.9) can be derived from a Hamiltonian

$$H = \sum_{k=1}^{m} Q(p_k) + Q(s_1) + \sum_{k=1}^{m-1} Q(s_{k+1} - s_k) + Q(C_4 - s_m) \qquad \text{for } N = 2m+1$$

$$H = \sum_{k=1}^{m} Q(p_k) + Q(s_1) + \sum_{k=1}^{m-1} Q(s_{k+1} - s_k) \qquad \text{for } N = 2m \ .$$

The canonical variables are defined via $s_k = \sum_l v_{2l-1}$ and $p_k = v_{2k}$ and the evolution equations are given by $\dot{s}_k = \partial H/\partial p_k$, $\dot{p}_k = -\partial H/\partial s_k$. Note, that the energy is equivalent to $H = C_3$ and the kinetic energy is C_4.

2.1.2 The quasi-continuous approximation

Now, we establish a continuous description of the lattice equation (2.9). That is, we assume $v_k = v\big(x = kh\big)$ and Taylor expand $q(v_{k\pm1})$ up to third order

$$q(v_{k\pm1}) = \left[1 \pm h\partial_x + \frac{h^2}{2}\partial_{xx} \pm \frac{h^3}{6}\partial_{xxx}\right] q(v) \ . \tag{2.13}$$

h denotes the spatial distance between the lattice nodes. Inserting this equation into (2.9) results in the partial differential equation

$$\frac{\partial v}{\partial t} = 2\left[h\partial_x + \frac{h^3}{6}\partial_{xxx}\right] q(v) \ , \tag{2.14}$$

which is the quasi-continuous approximation (QCA) of the lattice. Note, that this approximation is not based on a small parameter. The spatial scale is not defined on the lattice and its introduction in the QCA is more or less arbitrary. In the following we will set $h = 1$. The cut-off of the Taylor-series at order three is also arbitrary. If the QCA successfully describes the lattice has to be shown by direct comparison of the lattice and the continuum.

Eq. (2.14) describes the phase differences and one might wonder if an approximation of the original phase equation (2.5) would yield the same QCA. Of course, it is possible to expand $\varphi_{k\pm1}$ in Eq. (2.5). Then, the analogon to (2.14) reads

$$\dot{v} = 2\left[h\partial_x + \frac{h^3}{6}\partial_{xxx}\right] q(v) - \frac{h^3}{12}\partial_x\Big(q''(v)v_x^2\Big) \ . \tag{2.15}$$

The full derivation of this equation is given in appendix A.2. This approximation introduces one additional term. But since a term proportional to $q''(v)v_x^2$ is also included in the first part of the RHS of Eq. (2.15) the overall structure does not change and we expect that both approximations yield similar results.

For small v the coupling function in Eq. (2.14) can be approximated by $q(v) \approx q(0) + \alpha v^m$, where m is a positive integer. For example, the small amplitude version of (2.14) for $q(v) = \cos v$ reads (after an appropriate rescaling)

$$\dot{v} = 2\big[v^2\big]_x + \frac{1}{3}\big[v^2\big]_{xxx} \ . \tag{2.16}$$

This is the $K(2,2)$ equation in [6] and it possesses compacton solutions.

2.2 Traveling waves

In this section we investigate traveling waves in the phase oscillator lattice (2.9) and compare them with their continuous counterparts in Eq. (2.14).

2.2.1 Traveling waves in the quasi-continuum

First, we start with the QCA (2.14). Any constant $v = v^*$ is a solution and we will look for traveling waves on the base v^* in the form $v(x,t) = v(x - \lambda t) = v(s)$, where λ is

the wave velocity. Inserting this ansatz into Eq. (2.14) and integrating once yields

$$\lambda(v - v^*) + 2(q(v) - q(v^*)) + \frac{1}{3}\frac{\mathrm{d}^2}{\mathrm{d}s^2}q(v) = 0 \ . \tag{2.17}$$

The left boundary of the integration starts at s_0 where the wave profile is constant $v(s_0) = v^* = \text{const}$. This assumption can not be valid for periodic waves where the curvature of $q(v(s_0))$ has to enter (2.17). However, this curvature is a constant which can be absorbed in the constants in (2.17).

Eq. (2.17) can be written as a first-order ordinary differential equation (ODE)

$$\frac{\mathrm{d}v}{\mathrm{d}s} = u \quad , \quad \frac{\mathrm{d}u}{\mathrm{d}s} = -\frac{3\lambda(v - v^*) + 6\big(q(v) - q(v^*)\big) + q''(v)u^2}{q'(v)} \ , \tag{2.18}$$

which will be used to calculate and characterize the traveling wave solutions. In some cases, we also need the linearization of (2.18) around $v = v^*, u = 0$ provided $q'(v^*) \neq 0$. The stability of this state is determined by the eigenvalues of the according Jacobian

$$l_{1,2} = \pm\sqrt{-(3\lambda + 6q'(v^*))/q'(v^*)} \ . \tag{2.19}$$

Interestingly, Eq. (2.17) can be written in a potential-like form. To see this, we have to multiply Eq. (2.17) by $\mathrm{d}q(v)/\mathrm{d}s$ and integrate it once, such that we obtain

$$\lambda\Big[q(v)\big(v - v^*\big) - Q(v, v^*)\Big] + \big(q(v) - q(v^*)\big)^2 + \frac{1}{6}\left[\frac{\mathrm{d}q}{\mathrm{d}s}\right]^2 = 0 \ , \tag{2.20}$$

where the function $Q(v, v^*)$ is defined in (2.10c). This equation can be transformed to

$$\left(\frac{\mathrm{d}q}{\mathrm{d}v}\right)^2 \left[\frac{1}{2}\left(\frac{\mathrm{d}v}{\mathrm{d}s}\right)^2 + U(v)\right] = 0 \ , \tag{2.21a}$$

with the potential

$$U(v) = 3\frac{\lambda[q(v)(v - v^*) - Q(v, v^*)] + \big(q(v) - q(v^*)\big)^2}{(q'(v))^2} \ . \tag{2.21b}$$

With the equations (2.17)-(2.21) we are now able to investigate all kinds of traveling wave phenomena in the QCA. First, we will introduce different types of traveling waves. Secondly, we will analyze a few coupling functions in detail and show the transitions and bifurcations of the waves.

Solitary waves

Solitary waves are homo-clinic orbits in Eq. (2.18) and Eq. (2.21) of the fixed point v^*. They start from v^*, grow to a peak at v_m, and return back to their origin v^*. At the peak, they have to fulfill $U(v_m) = 0$ which gives a condition for the wave velocity λ_S on the knowledge of v^* and v_m

$$\lambda_S = \frac{\big(q(v_m) - q(v^*)\big)^2}{Q(v_m, v^*) - q(v_m)(v_m - v^*)} \ . \tag{2.22}$$

Solitary waves with compact tails – compactons. As mentioned above, the coupling function possesses some points where linear terms are absent. At least at $v^* = 0$ this is the case, but depending on $q(v)$ other points are possible. At such points, compact structures may occur. $q'(v^*) = 0$ and linear waves can not exists in the vicinity of v^*.

One example is the coupling function $q(v) = \cos v$ with solitary waves on the background $v^* = 0$. Approximation of $q(v)$ up to second order yields $q(v) \approx q(0) + av^2$, with $q(0) = 1$ and $a = -1/2$. Inserting this approximation into (2.17) yields the traveling wave ansatz for the $K(2,2)$ equation in [6]. One solution of the $K(2,2)$-equation is given by $v(s) = -A\cos^2(Bs)$, with appropriate constants $A = 2\lambda(3a)^{-1}$ and $B = \sqrt{3/8}$. Interestingly, this solution degenerates at $s = \pm\sqrt{2/3}\pi$, such that every term in Eq. (2.17) is identical to zero. There is no balancing between different terms and one can match the periodic solution with the trivial solution $v(s) = v^* = 0$ without violating any continuity conditions. So, one solution reads

$$v(s) - v^* = \begin{cases} -\frac{2\lambda}{3a}\cos^2\left(\sqrt{\frac{3}{8}}s\right) & |x| < \pi\sqrt{\frac{2}{3}} \\ 0 & \text{else,} \end{cases} \tag{2.23}$$

which is the classical compacton. It is a single humped solitary wave, where the amplitude depends on the wave velocity while the width is independent of amplitude or velocity. The hump is defined on a compact domain. For the full coupling function we can now expect that traveling wave solutions will behave according to Eq. (2.23) in the surrounding of v^* and only the shape of the hump will be affected by the full coupling.

In Fig. 2.4 below we show a compacton in the QCA for the coupling function $q(v) = \cos v$ and $v^* = 0$. This solution has been obtained by numerical solution of (2.18). The wave velocity was chosen to $\lambda = 2/\pi$.

Solitary waves with exponential tails. If the fixed point fulfills $q'(v^*) \neq 0$ one expects the usual exponential tails which can be observed in many soliton bearing equations like the KdV or the sine-Gordon equation. In this case we can use the linearization

around v^* to classify the tails and the traveling wave. Especially, for the existence of a homo-clinic trajectory one needs the fixed point of Eq. (2.18) to have one stable and one unstable direction, hence v^* has to fulfill

$$-\frac{3\lambda + 6q'(v^*)}{q'(v^*)} > 0 \ . \tag{2.24}$$

This condition yields a critical velocity $\lambda_C = -2q'(v^*)$, which separates a saddle-type stationary solution from a center.

A solitary wave with exponential tails is shown in Fig. 2.4 below. The coupling function is $q(v) = \cos(v)$ and the background is $v^* = \pi/4$. The wave velocity is a free parameter, but bounded by the above condition. For the case $v^* = \pi/4$ and $v_m > v^*$ this results in $\lambda > 2\sin\pi/4 = \sqrt{2}$. In Fig. 2.4 the wave velocity was chosen to $\lambda = \pi/2$. The tails of the solitary wave decay exponentially, corresponding to the eigenvalues of the stationary state v^*.

Kinks

Another class of traveling wave solutions that can be studied and observed in the QCA as well as in the lattice are kinks. In contrast to solitary waves, kinks are hetero-clinic orbits connecting two fixed points v^* and $\bar{v}^*$. The kink between v^* and $\bar{v}^*$ has to fulfill two basic conditions, first the peak condition (2.22), and secondly it has to be a fixed point of (2.21), such that $U'(\bar{v}^*) = 0$ or

$$\lambda_K = 2\frac{q(\bar{v}^*) - q(v^*)}{v^* - \bar{v}^*} \ . \tag{2.25}$$

This condition can also be derived from (2.17) where one assumes, that $\bar{v}^*$ is a constant solution. Combining the two conditions (2.22) and (2.25) results in the final condition for the kink

$$Q(\bar{v}^*, v^*) = \frac{(q(\bar{v}^*) + q(v^*))(\bar{v}^* - v^*)}{2} \ . \tag{2.26}$$

Note, that a solution of this equation might yield a kink $(v^*, \bar{v}^*)$ which encloses a singularity in Eq. (2.18) with $q'(v) = 0$. In this case, these two points can not be connected by a hetero-clinic orbit. In general, points with $q'(v) = 0$ separate the phase space of (2.18) into independent regions, but it might be possible that for some specific values of the wave velocity the singularity can be removed and a trajectory crosses that point.

For $q(v) = \cos v$ the kink is given by $\bar{v}^* = \pi - v^*$. The velocity belonging to this kink is $\lambda_{max} = \lambda_K = 4\cos v^*/(\pi - 2v^*)$. For other coupling functions the structure of the kink levels is more complicated.

Kinks with exponential tails. Kinks with exponential tails have to fulfill Eq. (2.24) and an example is shown in Fig. 2.5. The coupling function is $q(v) = \cos(v)$ and $v^* = \pi/4$, $\bar{v}^* = 3\pi/4$. The velocity is $\lambda = \sqrt{32}/\pi$.

Compact kinks. If v^* and $\bar{v}^*$ fulfill $q'(v^*) = q'(\bar{v}^*) = 0$ both tails will become compact and may form a compact kink–anti-kink pair, named *kovaton* [60]. An example of this wave form is shown in Fig. 2.5, with $q(v) = \cos v$ and $v^* = 0$, $\bar{v}^* = \pi$ and $\lambda_K = 4/\pi$.

Exponential-compact kinks. In addition to kinks with exponential *or* compact tails one can also observe *semi-compact* kinks possessing one exponential and one compact tail. Consider the coupling $q(v) = \cos v + a \cos 2v$ with $a = 0.2$. In this special case $v^* = 0$ fulfills $q'(v^*) = 0$ and $\bar{v}^* = 2.39955$ is the kink satisfying (2.26) with the velocity (2.25) $\lambda_K = 1.60011$. This kink is shown in Fig. 2.5. It is compact at $v = v^*$ and exponential at $v = \bar{v}^*$.

Periodic waves

Periodic waves around v^* exist if the eigenvalues $l_{1,2}$ in (2.19) are purely imaginary. A periodic wave in the QCA is shown in Fig. 2.6(a). The velocity of a periodic wave must satisfy the condition resulting from (2.18):

$$-\frac{3\lambda + 6q'(v^*)}{q'(v^*)} < 0 \ . \tag{2.27}$$

For $q(v) = \cos v$ and $0 < v^* < \pi$ this condition yields $\lambda < 2 \sin v^*$. At $\lambda = \lambda_C = -2q'(v^*)$ a bifurcation from periodic to solitary waves occurs.

Exemplary coupling function $q(v) = \cos v$

Now, we will study the particular coupling function $q(v) = \cos v$. The regions of existence of the traveling wave solutions in the parameter space (v^*, λ) are shown in Fig. 2.2(a). Due to the symmetry of the coupling function, only the part $0 \leq v^* \leq \pi/2$ is shown. For $\pi/2 \leq 0 \leq \pi$ the plot has to be mirrored around $v^* = \pi/2$ and for $v^* < 0$ it has to be inverted.

The velocity of the kinks for this coupling function is $\lambda_K = 4 \cos v^*/(\pi - 2v^*)$. If the velocity is larger than this value the trajectories in the $v, \dot{v}$ plane become unstable and no traveling wave solutions exists. Hence, this velocity defines an upper bound for the existence of traveling waves. Below λ_K the solutions are solitary waves until λ reaches the critical velocity λ_C, which separates solitary and traveling waves. For $q(v) = \cos v$ the critical velocity is given by $\lambda_C = 2 \sin v^*$. Below λ_C all solutions are periodic waves.

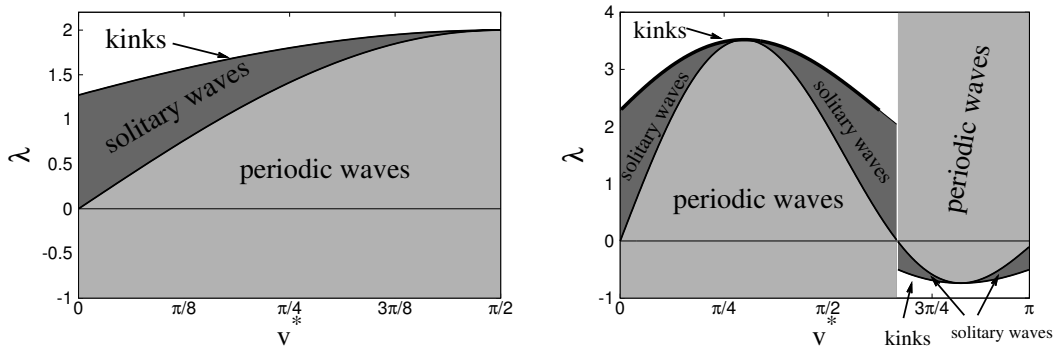

(a) $q(v) = \cos v$ (b) $q(v) = \cos v + 1/2 \cos 2v$

Figure 2.2: Regions of existence of traveling waves in the parameter space (v^*, λ). In (a) the coupling is $q(v) = \cos v$. The function $\lambda_C = 2 \sin v^*$ separates periodic from solitary wave solutions. The upper bound $\lambda_K = 4 \cos v^*/(\pi - 2v^*)$ defines the kink solutions. Compactons arise from $v^* = 0$ and the according kink becomes compact on both sides. In (b) the coupling function is $q(v) = \cos v + 1/2 \cos 2v$. At $v = \arccos(-1/2) \approx 2.0944$ a singularity ($q'(v) = 0$) exists, which divides the phase space into two independent parts. Between $1.95841 \lesssim v \lesssim 2.0944$ the soliton solutions are not bounded by a kink solution for increasing λ, but become directly unstable.

As stated above, compact structures occur if $q'(v^*) = 0$, which results in $v^* = 0$. Around this point only compactons and compact kinks exist and periodic waves are absent. The according kink is located at $\bar{v}^* = \pi$ and fulfills $q'(\bar{v}^*) = 0$, hence it is compact on both sides.

Exemplary coupling function $q(v) = \cos v + a \cos 2v$

Another interesting coupling function is $q(v) = \cos v + a \cos 2v$, which introduces the second harmonic parameterized by a. For small values of a we do not expect a qualitative difference to the harmonic coupling with $a = 0$, but the shape of the wave regions will slightly change, as well as the position of the kinks.

Remarkably, a second singularity ($q'(v) = 0$) appears for $|a| > 1/4$ at $v_c = \pm \arccos\big(-1/(4a)\big)$ and the phase space of (2.18) is effectively divided at this point. In Fig. 2.2(b) we show the regions of existence of the traveling wave solutions in the parameter space (v^*, λ) for $a = 0.5$. At $v_c = \arccos(1/2) \approx 2.0944$ the phase space is divided. Below v_c we observe a similar behavior as for the harmonic coupling, whereas above v_c the situation is inverted. Interestingly, between $1.95841 \lesssim v < v_c$ kink solutions are not possible. In this case, the kink lies below the critical point $v = 0$ and the solitary wave becomes immediately unstable if the velocity crosses that critical point.

2.2.2 Traveling waves in the lattice

Now, we turn our attention to traveling waves in the lattice (2.9). In particular, we are looking for solutions of the form

$$v_k(t) = v(k - \lambda t) = v(s) \tag{2.28}$$

with the wave velocity λ. Inserting (2.28) into (2.9) yields

$$\dot{v} = \frac{1}{\lambda}\Big(q\big(v(s-1)\big) - q\big(v(s+1)\big)\Big) \ . \tag{2.29}$$

This equation is an advance-delay equation, containing terms going forward and backward in time. Advance-delay equation typically describe traveling waves solutions in discrete systems [61–63]. They are difficult to solve and to analyze, even numerically [64]. But, it is possible to write Eq. (2.29) as an integral

$$v(s) - v^* = \frac{1}{\lambda}\int_{s-1}^{s+1} \big[q(v^*) - q(v(\tau))\big]\mathrm{d}\tau \ , \tag{2.30}$$

where it is supposed, that $v(s < s_0) = v^*$. It will turn out below, that this integral representation is relatively easy to solve numerically. We will propose a simple method based on this integral equation, which reveals the traveling wave solutions.

If one requires that $v(s) = \bar{v}^*$ is a constant solution, hence a kink exists, the corresponding velocity λ_K has to satisfy

$$\lambda_K = 2\frac{q(v^*) - q(\bar{v}^*)}{\bar{v}^* - v^*} \ . \tag{2.31}$$

This condition is exactly the condition (2.25) for the QCA.

Fixed point analysis

Similar to the fixed point analysis in the QCA, one can analyze the behavior of traveling waves close to the background v^* by linearization [62, 63]. To this end we approximate $q(v) \approx q(v^*) + a(v - v^*)$ in (2.29) and apply the exponential ansatz $v(t) = A\exp lt$. This yields the characteristic equation

$$l = \frac{a}{\lambda}(e^{-l} - e^{l}) \ . \tag{2.32}$$

Note again, that $a = q'(v^*) \neq 0$, meaning that this approximation does not hold for compacton backgrounds.

We split l into its real and imaginary part $l = p + \mathrm{i}q$ to obtain

$$p = -2\frac{a}{\lambda}\cos q \sinh p \qquad \text{and} \quad q = 2\frac{a}{\lambda}\sin q \cosh p \ . \tag{2.33}$$

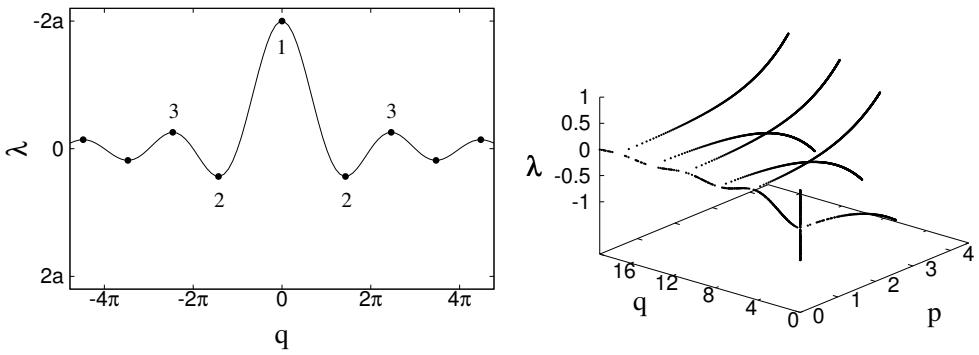

Figure 2.3: (a): Wave speed λ in dependence of the complete imaginary eigenvalue q in Eq.(2.33). The dots mark possible bifurcation points to real eigenvalues. (b): Wave speed λ vs. the real and the imaginary part of the eigenvalues, with $a = \sin(0.2)$. Only the positive parts of the real and imaginary axes are shown.

For purely imaginary eigenvalues $p = 0$ these equations result in the condition $q = -2\frac{a}{\lambda}\sin q$ or $\lambda = -2a\frac{\sin q}{q}$. This function is plotted in Fig. 2.3(a). In this plot, the dots mark possible points for transitions to eigenvalues with real parts. In Fig. 2.3(b) all eigenvalues $l = p + \mathrm{i}q$ are shown. Purely real eigenvalues are given by $p = -2\frac{a}{\lambda}\sinh p$ or $\lambda = -2a\frac{\sinh p}{p}$. So, when λ crosses $-2a$ (point 1 in Fig. 2.3(a)), a bifurcation from two purely imaginary eigenvalues to two purely real eigenvalues occurs. This scenario corresponds to the transition from periodic to solitary waves and the critical velocity is $\lambda_C = -2a$. This transition is analogous to the bifurcation in the QCA. The critical velocities are identical.

Another bifurcation occurs, when λ crosses point 2, see Fig. 2.3. There, the center changes to a stable and an unstable spiral point. This refers to a transition from periodic to solitary waves with oscillating tails and exponentially decaying amplitude. Since the bifurcation occurs on the imaginary axis, one can calculate the critical velocity from (2.33) by setting $\lambda'(q) = 0$. For the special case $q(v) = \cos v$ one obtains $\lambda \approx -2a \cdot 0.217$. Note, that this transition has no counterpart in the quasi-continuum.

Numerical determination of traveling waves

As mentioned above, it is possible to construct a numerical scheme from (2.30) to find solitary wave solutions of the lattice [30, 65, 66]. Therefore, one initially guesses a wave profile $v_0(s)$ and then iterates

$$\tilde{v}(s) = v^* + \frac{1}{\lambda}\int_{s-1}^{s+1}\big(q(v^*) - q(v_k(\tau))\big)\mathrm{d}\tau \qquad v_{k+1} = \left(\frac{||v_k||}{||\tilde{v}||}\right)^{3/2}\tilde{v}\ , \tag{2.34}$$

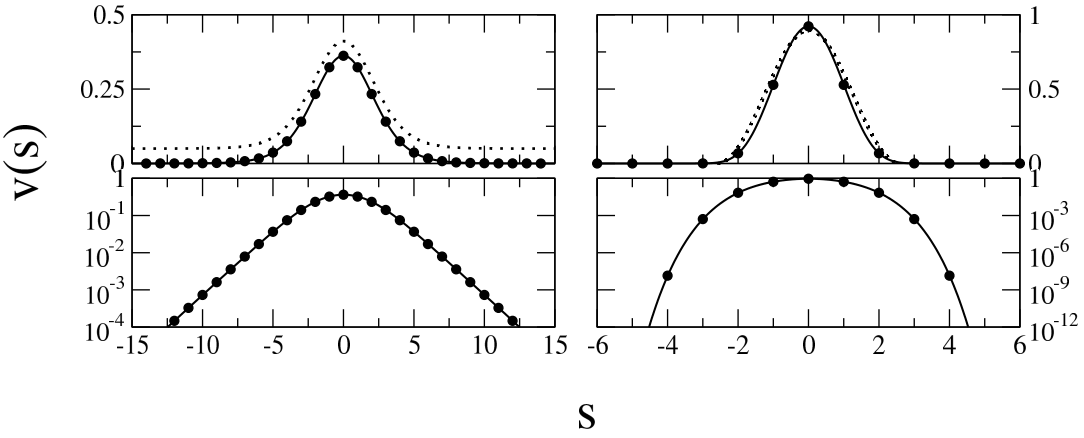

Figure 2.4: Soliton solutions for the coupling function $q(v) = \cos v$. In the left row the soliton travels on the background $v^* = \pi/4$ with velocity $\lambda = \pi/2$, and possess exponential tails. In the right row the background is $v^* = 0$ and the velocity is $\lambda = 2/\pi$. The tails are super-exponential here, hence this solitary wave is a compacton. The upper plots show the waves in original scale, whereas the lower ones in logarithmic scale. Here and in the following figures bold dots show the traveling wave solutions on the lattice and the dashed line the solution of QCA (2.17) which has an additional offset for better visibility.

where $||\cdot||$ denotes the L_1-norm. The normalization is needed in order to prevent the algorithm from converging to the trivial solution $v^* = 0$ and we have used the normalization exponent $\alpha = 3/2$. The integral is calculated by a high order Lagrangian integration rule [67]. To construct kink solutions, one has to omit the normalization in (2.34) by setting $v_{k+1} = \tilde{v}$ and apply appropriate boundary conditions. Periodic waves can be obtained by a slight modification of (2.34). Here, the wave length w is introduced and periodic boundary conditions $\tilde{v}(0) = \tilde{v}(w)$ are assumed in (2.34). For backgrounds different from 0 one has to shift the coordinates $v \mapsto v^* + v$.

Solitary waves

Solitary waves with exponential tails. In Fig. 2.4 we show a solitary wave with exponential tails, computed with the scheme (2.34). The coupling is $q(v) = \cos v$ and the background is $v^* = \pi/4$. The velocity was chosen to $\lambda = \pi/2$, fulfilling the condition $(\lambda + 2q'(v^*))/q'(v^*) > 0$. In the same figure we also show the solution of the quasi-continuum with the same parameters and one can see that both solution coincide very well.

Compact solitary waves. The condition $q'(v^*) = 0$ allows for the formation of quasi-compact tails and we call these waves compactons. In Fig. 2.4 we show a compacton on the background $v^* = 0$ for the coupling $q(v) = \cos v$. The wave velocity was set here to

$\lambda = 2/\pi$. The compacton is not purely compact, but has super-exponentially decaying tails [30]. Thus, although there is a qualitative difference between the lattice and the QCA, quantitatively these solutions are very close to each other.

It is possible to estimate the super-exponential decay rate of the tails. In the vicinity of v^* one can write Eq. (2.30) as

$$v(s) = \frac{a}{\lambda} \int_{s-1}^{s+1} v^2(\tau) \mathrm{d}\tau \ , \tag{2.35}$$

where a is a constant (for the harmonic coupling function $q(v) = \cos v$ this constant is $a = 1/2$). Assuming now $v(s) = \exp(-f(s))$ with an appropriate monotone function $f(s)$ and that the tails decay fast yields in first approximation

$$\exp(-f(s)) = C \exp(-2f(s-1)) \ . \tag{2.36}$$

Here, we have written the integral as $\int_{s-1}^{s+1} \exp(-2f(\tau))\mathrm{d}\tau \approx C \exp(-2f(s-1))$, with a constant C. Such an approximation can be obtained if the exponent is expanded around $s-1$, for further details see section 3.2.2. Note further, that we have absorbed the wave velocity in Eq. (2.36) into the constant C. Taking the logarithm of Eq. (2.36) and neglecting $\ln C$ yields $f(s) = 2f(s-1)$. One solution of this delay equation is $f(s) = C \exp(\ln 2s)$. Finally, we can write the decay of the tails as

$$v(s) \sim \exp(-C \exp(\ln 2s)) \ . \tag{2.37}$$

Clearly, this function shows super-exponential behavior. In [30] some corrections in the approximation of the integral have been performed, with similar results.

Kinks

Kinks can also be observed in the phase lattice (2.9). But here, the position of the kinks can not be calculated as easy as in the QCA. Nevertheless, we assume, that the kinks in the lattice are the same as in the QCA (2.26). The velocity can then be obtained from Eq. (2.31).

Kinks with exponential tails. In Fig. 2.5 we show the shape of a kink. The coupling is $q(v) = \cos v$ and the background is $v^* = \pi/4$. The velocity of the kink is given by Eq. (2.31) $\lambda_K = \sqrt{32}/\pi$. A qualitative comparison with the continuum yields very good coincidence.

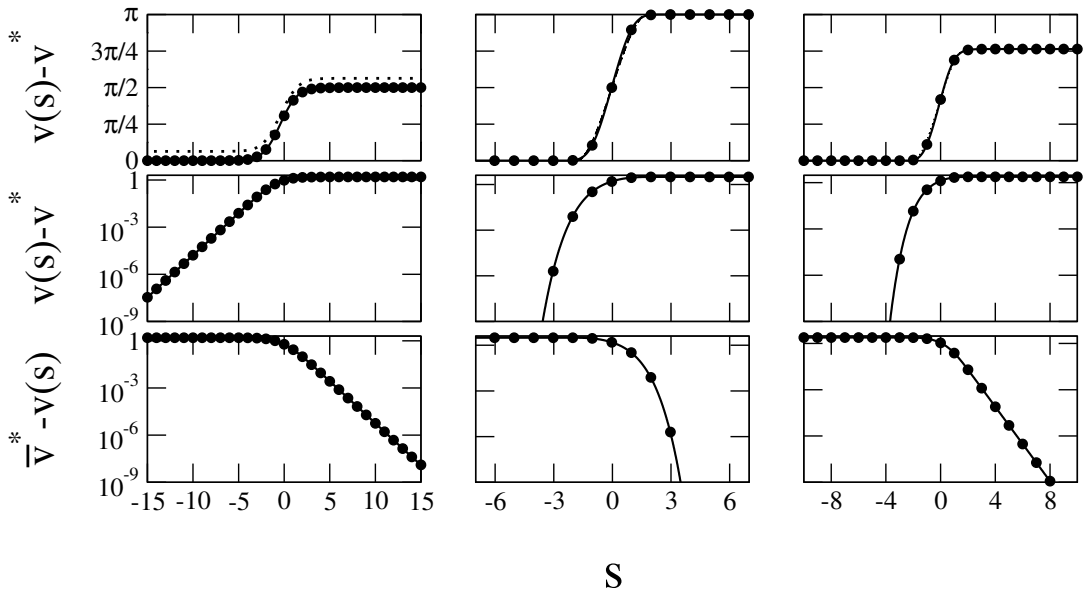

Figure 2.5: Kinks in the phase lattice. Left column: A kink with exponential tails for $q(v) = \cos v$; the kink is located between $v^* = \pi/4$ and $\bar{v}^* = \pi - v^*$ and the speed is $\lambda = \sqrt{32}/\pi$. The middle column shows a compact kink between $v^* = 0$ and $\bar{v}^* = \pi$ for $q(v) = \cos v$. In the right column, a semi compact kink is show in the model $q(v) = \cos v + a\cos 2v$ with $a = 0.2$, see the text. In the upper row the kinks are shown in normal scale, in the middle row in logarithmic scale around v^* and in the lower row in logarithmic scale around $\bar{v}^*$.

Kinks with compact tails. One can observe compact kinks, if $q'(v^*) = 0$ and $q'(\bar{v}^*) = 0$. For the coupling $q(v) = \cos v$ such a case exists with $v^* = 0$ and $\bar{v}^* = \pi$. The shape of this compact kink is shown in Fig. 2.5. Here, the velocity is $\lambda = 4/\pi$. Again, a good coincidence between the kink with compact tails in the quasi-continuum is observed. Note further, that the tails for the compact kink can be estimated in the same way as for the compacton. They decay with the same super-exponential law $v(s) \sim \exp(-C\exp(\ln 2s))$.

Semi-compact kinks. It also possible to observe kinks with one exponential and one compact tail. This is the case for $q(v) = \cos v + a\cos 2v$ with $a = 0.2$. For $v^* = 0$, $\lambda = 1.60011$ and $\bar{v}^* = 2.39955$ the kink condition (2.26) is satisfied and a semi-compact kink is found by the numerical method described above. In Fig. 2.5 we show a semi-compact kink, which conincides well with the one from the QCA.

Periodic waves

Periodic waves can be calculated with (2.34) and periodic boundary conditions. A simple example is shown in Fig. 2.6(a). As mentioned above, the wave length w has to

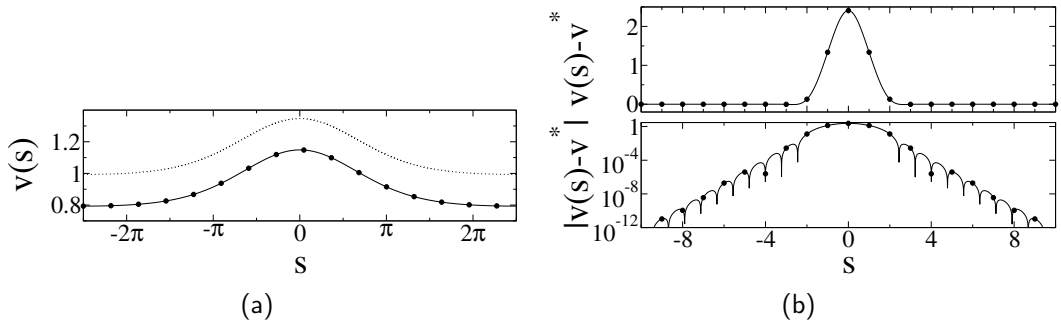

Figure 2.6: Left panel: The shape of a periodic wave for $q(v) = \cos v$. The offset is $v^* = \pi/4$, the wave length is $w = 5\pi$ and the velocity $\lambda = \pi/2$. Right panel: Solitary wave with periodic and exponentially decaying tails, $v^* = -0.2$ and $\lambda = 1.0$.

be introduced. In the example $w = 5\pi$, $v^* = \pi/4$ and the velocity is $\lambda = \pi/2$. Note again, how the periodic wave in the lattice matches the wave in the QCA.

Solitary waves with periodically decaying tails

From the fixed point analysis of the advance-delay equation (2.29) a bifurcation occurs at point 2 in Fig. 2.3(a). So, if the velocity λ reaches the critical point λ_C, the fixed point changes its type from a center to a stable spiral point. This corresponds to a solitary wave with oscillatory decaying tails. In Fig. 2.6(b) we show an example of such a wave. The offset is $v^* = -0.2$ and the wave velocity is $\lambda = 1.0$. This behavior does not occur in the quasi-continuum.

2.3 Numerical studies of the one-dimensional chain

In this last section we have shown that traveling wave structures like solitary waves, kinks and periodic waves exist in the lattice (2.9), but so far, nothing has been said about their stability and their physical relevance. In this section, we will demonstrate numerically how these waves emerge from generic initial conditions and how they propagate in the lattice. Furthermore, we show how a chaotic state may appear from the collisions of compactons.

Collision between two compacton and between a compacton and a kink have been analyzed in detail in [30]. There, it could be shown numerically, that the collisions are nearly elastic. Nevertheless, is has also observed that a collision between a compacton and its anti-compacton (possessing negative velocity and negative amplitude) may lead to the formation of a large-amplitude compacton–anti-compacton pair.

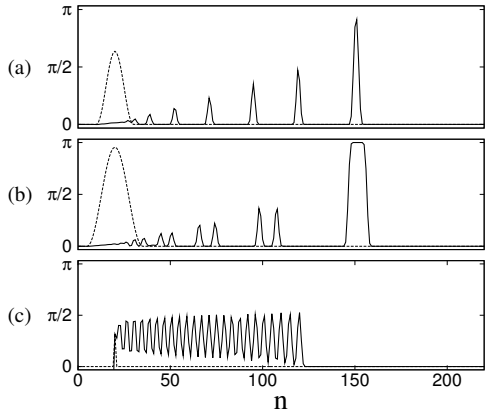

Figure 2.7: Evolution of different initial pulses for the coupling $q(v) = \cos v$ and $v^* = 0$. The initial conditions were set according to (2.38). (a) $w = 10$ and $A = 2$, (b) $w = 15$ and $A = 3$ and (c) $w = 1$ and $A = 1$. The dashed line shows the initial condition $v_n(t = 0)$ and the solid line the lattice at the time $t = 100$.

Evolution of an initial pulse

First, we consider the evolution of an initial $\cos$-pulse in the lattice (2.9) with the coupling $q(v) = \cos v$. Hence, the initial condition is

$$v_k(0) = \begin{cases} v^* + \frac{A}{2}\left[1 + \cos\left(\frac{k-k_0}{w}\pi\right)\right] & \text{for } |k - k_0| < w \\ v^* & \text{else,} \end{cases} \tag{2.38}$$

where A is the amplitude, k_0 is the center and w is the half width of the pulse.

In Fig. 2.7 we have used $v^* = 0$ and one can observe compactons and kovatons arising from the initial pulse. In Fig. 2.7(a) a wave train of compactons emerges out of the initial pulse. The speed of the compactons increases with the amplitude. In Fig. 2.7(b) we have increased the width and the amplitude of the pulse and one kovaton can be observed. In Fig. 2.7(c) a narrow initial pulse creates a wave source, emitting periodic waves. This behavior has also been observed in [30]. In [68] the authors showed that periodic waves can emerge from the above initial condition.

Transition to chaos in a finite lattice

Wave trains shown in Fig. 2.7 are obtained for an effectively infinite lattice; during the calculation times the boundaries are not reached. In a finite lattice with periodic boundaries, collisions between waves occur, and it can be observed that at large times eventually a chaotic regime appears. In Fig. 2.8 we show the evolution of an initial $\cos$-pulse with $v^* = 0.1$. The upper plot shows the initial decomposition of this pulse into

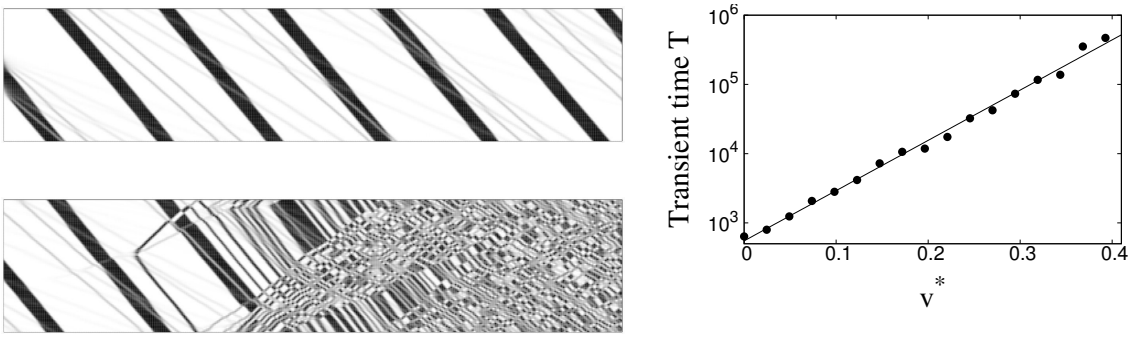

Figure 2.8: Transition to chaos. Left panel: The background is $v^* = 0.1$ and the lattice contains of $N = 100$ sites with periodic boundary conditions. The field is shown in a gray scale versus time (horizontal axis) and space (vertical axis). Upper plot: A kink and several solitons emerge out of an $\cos$-pulse. The time interval is $0 \leq t \leq 400$. Lower plot: Emergence of chaos after a collision of two solitons which creates a soliton–anti-soliton pair. The time interval is $2600 \leq t \leq 3000$. Right panel: Transient times to chaos for different backgrounds v^*. The length of the lattice is $N = 32$ and the initial $\cos$-pulse is used. In order to obtain an average of the transient times we also varied the width of the initial pulse from 5 to 15 and calculated the transient time as the average over the transient times for different initial pulses. The line is an exponential fit and the transient times scales with $T \sim \exp 16.7 v^*$.

one kink and several solitary waves. These structures appear to survive collisions quite unaffected. The lower plot shows, that after some transient time chaos emerges. The chaotic state begins to develop after a collision producing a large-amplitude soliton–anti-soliton pair. Then an avalanche of soliton–anti-soliton collisions is triggered resulting in a fast chaotization.

In Fig. 2.8 we show also a remarkable dependence of the average transient time, after which chaos establishes, on the parameter v^*. For larger values of v^* the transient time is exponentially large, which means extreme stability of the solitary waves. Qualitatively, this stability can be attributed to a smallness of effects of discreteness of the lattice for large v^*. Here, the waves are relatively wide, thus they are well approximated in the QCA, which is close to the integrable Korteweg-de Vries equation. For small v^* the waves are close to compactons that are short and for them the discreteness that causes non-elasticity of collisions is essential. Furthermore, the number of emitted waves decreases with increasing v^* and the velocity of the waves is bounded from below. These two effects reduce the possibility that two waves interact with each other, resulting in an increased transient time.

2.4 Higher-dimensional phase lattices

A generalization of the chain of coupled phase oscillators (2.9) is a two- or higher-dimensional lattice. Each phase oscillator is here coupled to its nearest neighbors in a regular higher-dimensional geometry.

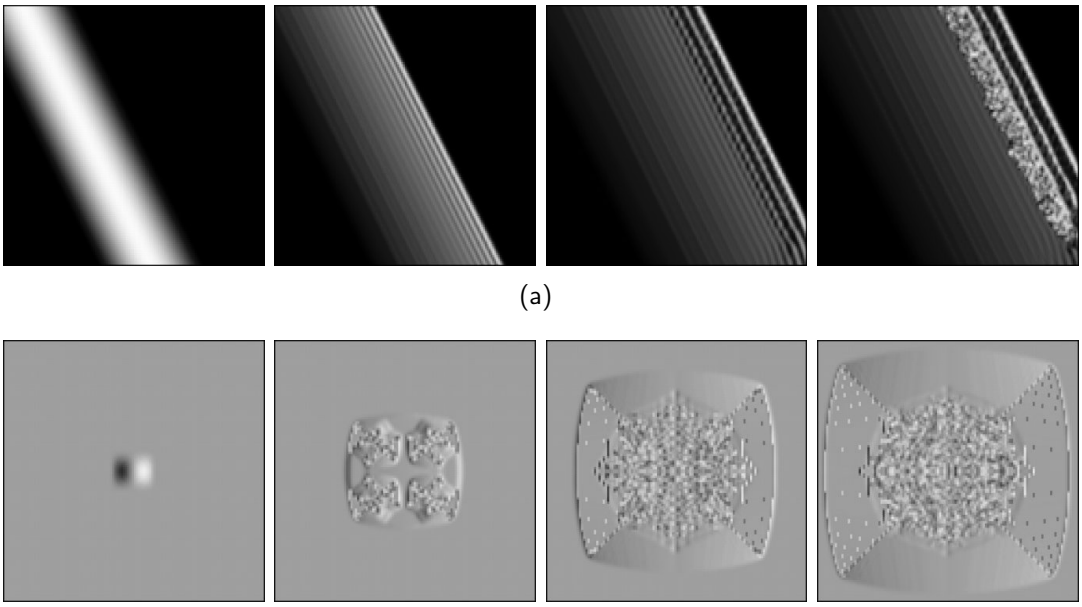

(a)

(b)

Figure 2.9: Emergence of wave fronts in a dispersively coupled van der Pol oscillator lattice (2.39) of dimension 120×120. Here, the phase difference in i-direction $v_{i,j} = \varphi_{i+1,j} - \varphi_{i,j}$ is shown for different times ($t = 0, 2000, 4000, 4000, 5000$ from left to right). The phase is defined via $\varphi_{i,j} = \arctan(\dot{x}_{i,j}/x_{i,j})$. In (a) the initial condition is a homogeneous state perturbed by a phase modulated front and in (b) a localized initial pulse. The emergence of traveling fronts is clearly visible and these fronts are compact.

First, we give an example where coupled phase oscillator lattices are of interest – a two-dimensional square lattice of dispersively coupled van der Pol oscillators:

$$\ddot{x}_{i,j} = \mu(1 - x_{i,j}^2)\dot{x}_{i,j} - x_{i,j} + \varepsilon\mu\Delta_D x_{i,j} \ . \tag{2.39}$$

$\mu = 0.2$, $\varepsilon = 0.08$ and $\Delta_D x_{i,j} = x_{i+1,j} + x_{i,j+1} + x_{i-1,j} + x_{i,j-1} - 4x_{i,j}$ is the two-dimensional discrete Laplacian. The phase of each oscillator can approximately be defined as $\varphi_{i,j} = \arctan(\dot{x}_{i,j}/x_{i,j})$. In Fig. 2.9 we show the evolution of two exemplary initial conditions. In detail, we show the evolution of the phase differences $u_{i,j} = \varphi_{i+1,j} - \varphi_{i,j}$ in i-direction. In Fig. 2.9(a) the initial condition is a homogeneous state, which is perturbed by a phase modulated front. From these initial perturbation one can clearly recognize the emergence of traveling fronts. These fronts are compact. After some transient time, some of these fronts are destroyed and a chaotic state establishes. In Fig. 2.9(b) the evolution of a localized pulse is shown. Again, the emergence of traveling compact fronts is visible. In the center of the excited region the phases are chaotic.

The generalization of the chain (2.5) for a two-dimensional square lattice reads

$$\dot{\varphi}_{i,j} = \omega_0 + q(\varphi_{i+1,j} - \varphi_{i,j}) + q(\varphi_{i-1,j} - \varphi_{i,j}) + q(\varphi_{i,j+1} - \varphi_{i,j}) + q(\varphi_{i,j-1} - \varphi_{i,j}) \ . \tag{2.40}$$

This equation can always be transformed into a rotating frame, such that ω_0 vanishes. In the following we will omit this term. Furthermore we assume a purely dispersive coupling $q(\varphi) = q(-\varphi)$. The differences in i and j direction are introduced as

$$u_{i,j} = \varphi_{i+1,j} - \varphi_{i,j} \quad \text{and} \qquad v_{i,j} = \varphi_{i,j+1} - \varphi_{i,j} \ . \tag{2.41}$$

They have to fulfill

$$u_{i,j+1} - u_{i,j} = v_{i+1,j} - v_{i,j} \ , \tag{2.42}$$

because $\varphi_{i,j} + u_{i,j} + v_{i+1,j} = \varphi_{i+1,j+1}$ and $\varphi_{i,j} + v_{i,j} + u_{i,j+1} = \varphi_{i+1,j+1}$. Eq. (2.42) can be written as $\nabla_D \times (u, v)^T = 0$, where ∇_D is the discrete nabla operator. Therefore, the differences $(u_{i,j}, v_{i,j})$ and the phases $\varphi_{i,j}$ allow the analogy to classical continuous fields: the vector field (u, v) is rotation free and φ is the according potential.

Taking now the time derivative of (2.41) and inserting the equation for the phases (2.40) yields

$$\dot{u}_{i,j} = q(u_{i+1,j}) - q(u_{i-1,j}) + q(v_{i+1,j}) + q(v_{i+1,j-1}) - q(v_{i,j}) - q(v_{i,j-1}) \tag{2.43a}$$

$$\dot{v}_{i,j} = q(v_{i,j+1}) - q(v_{i,j-1}) + q(u_{i,j+1}) + q(u_{i-1,j+1}) - q(u_{i,j}) - q(u_{i-1,j}) \ , \tag{2.43b}$$

where $q(v) = q(-v)$ has been used. This equation is the model for compact traveling wave fronts.

2.4.1 Quasi-continuous approximation

One tool to study traveling wave phenomena is the approximation of the lattice equations in terms of a continuous variable. The success of this method has been shown in the last sections, where one-dimensional phase compactons have been described by their continuous counterparts.

To derive a QCA for the two-dimensional phase lattice we will approximate the phases in (2.40), which are replaced by the continuous variable $\varphi(x, y)$ and $\varphi_{i\pm1,j}$, $\varphi_{i,j\pm1}$ are Taylor-expanded up to third order. Next, one defines $u = h\varphi_x$ and $v = h\varphi_y$ and differentiates the equation for the phases into x- and y- direction to obtain

$$\begin{aligned}\dot{u} =& 2h\partial_x\Big(q(u) + q(v)\Big) + h^3\Bigg\{\frac{1}{3}\,q'(u)u_{xxx} + \frac{5}{6}\,q''(u)u_x u_{xx} + \frac{1}{4}\,q^{(3)}(u)u_x^3 \\ &+ \frac{1}{3}\,q'(v)v_{xyy} + \frac{1}{3}\,q''(v)v_x v_{yy} + \frac{1}{2}\,q''(v)v_y v_{xy} + \frac{1}{4}\,q^{(3)}(v)v_x v_y^2\Bigg\}\end{aligned} \tag{2.44a}$$

$$\begin{aligned}\dot{v} =& 2h\partial_y\Big(q(u) + q(v)\Big) + h^3\Bigg\{\frac{1}{3}\,q'(v)v_{yyy} + \frac{5}{6}\,q''(v)v_x v_{yy} + \frac{1}{4}\,q^{(3)}(v)v_y^3 \\ &+ \frac{1}{3}\,q'(u)u_{xxy} + \frac{1}{3}\,q''(u)u_y u_{xx} + \frac{1}{2}\,q''(u)u_x u_{xy} + \frac{1}{4}\,q^{(3)}(u)u_y u_x^2\Bigg\} \ .\end{aligned} \tag{2.44b}$$

The full derivation of this equation is given in appendix A.4.

In the one-dimensional case we have shown that it is also possible to derive a QCA from the Taylor expansion of the difference variables. Of course, such an expansion can also be applied to the two-dimensional phase lattice (2.43). Here, one has to expand $u_{i\pm1,j\pm1}$ and $v_{i\pm1,j\pm1}$ in Eq. (2.43). Unfortunately, this expansion introduces terms like $[q(v)]_{xx}$ which are of dissipative nature. Hence, this expansion is not suitable for the comparison with the lattice.

Now, we look for traveling wave front solutions in the form

$$u(x,y,t) = u(t - b_1 x - b_2 y) = u(s) \ , \quad v(x,y,t) = v(t - b_1 x - b_2 y) = v(s) \ , \tag{2.45}$$

with b_1 and b_2 being the inverse velocities in x and y direction satisfying $b_1 = \cos\theta/\lambda$ and $b_2 = \sin\theta/\lambda$. λ is the front velocity and θ the propagation direction of the wave. We insert this ansatz into Eq. (2.44) and integrate every equation from 0 to t, assuming, that $u(0) = u^* = \text{const}$ and $v(0) = v^* = \text{const}$. The resulting set of ordinary differential equations for $u(s)$ and $v(s)$ fulfills $b_1(v(s) - v^*) = b_2(u(s) - u^*)$ and one finally obtains

$$\begin{aligned} u \ = \ & u^* + 2b_1\Big(q\big(u^*\big) + q\big(v^*\big) - q\big(u\big) - q\big(\tan(\theta)u\big)\Big) - \frac{b_1^3}{3}\big[q\big(u\big)\big]_{ss} \\ & - \frac{b_1 b_2^2}{3}\big[q\big(\tan(\theta)u\big)\big]_{ss} + \frac{b_1^3}{12}q''\big(u\big)u_s^2 + \frac{b_2^4}{12b_1}q''\big(\tan(\theta)u\big)u_s^2 \ . \end{aligned} \tag{2.46}$$

The term $v^* - \tan(\theta)u^*$ has been omitted for simplicity. The one-dimensional case can be recovered by setting $b_2 = 0$. For $b_1 = b_2$ both components are equal $u = v$.

Kinks between two fixed points of Eq. (2.46) might exist. One fixed point is given by the integration constants u^* and v^*. The other one has to fulfill $u(s) = \bar{u}^* = \text{const}$. and $v(s) = \bar{v}^* = \text{const}$. This yields the condition

$$\bar{u}^* - u^* = -2b_1\, G\big(u^*, v^*, \bar{u}^*, \bar{v}^*\big) \quad , \quad \bar{v}^* - v^* = -2b_2\, G\big(u^*, v^*, \bar{u}^*, \bar{v}^*\big) \ , \tag{2.47}$$

where $G\big(u^*, v^*, \bar{u}^*, \bar{v}^*\big) = q(\bar{u}^*) + q(\bar{v}^*) - q(u^*) - q(v^*)$. From this equation alone, one can not compute $\bar{u}^*$, $\bar{v}^*$ or the velocity. It only relates the three variables.

In principle one can solve the equations for the traveling waves numerically, either by transforming them to a four-dimensional ordinary differential equation or by some more advanced algebraic differential equation methods [69]. Here, we want to give an analytical solution for small amplitudes. In the surrounding of u^*, v^* the coupling function can be approximated by a Taylor series. For $q(v) = \cos v$ and $u^* = v^* = 0$ the linear term vanishes and $q(u) \approx q(0) - 1/2u^2$. Inserting this approximation into (2.46) yields

$$u = b_1(u^2 + v^2) + \frac{b_1^4 + b_2^4}{4b_1}u_s^2 + \frac{b_1^4 + b_2^4}{3b_1}uu_{ss} \ . \tag{2.48}$$

Remember, that $v(s) = b_2/b_1 u(s)$. One solution is

$$u(s) = \frac{7}{5}\lambda\cos\theta \ \cos^2\left(\sqrt{\frac{3}{7}}\frac{2\lambda}{\sqrt{3+\cos(4\theta)}}\ s\right) \ . \tag{2.49}$$

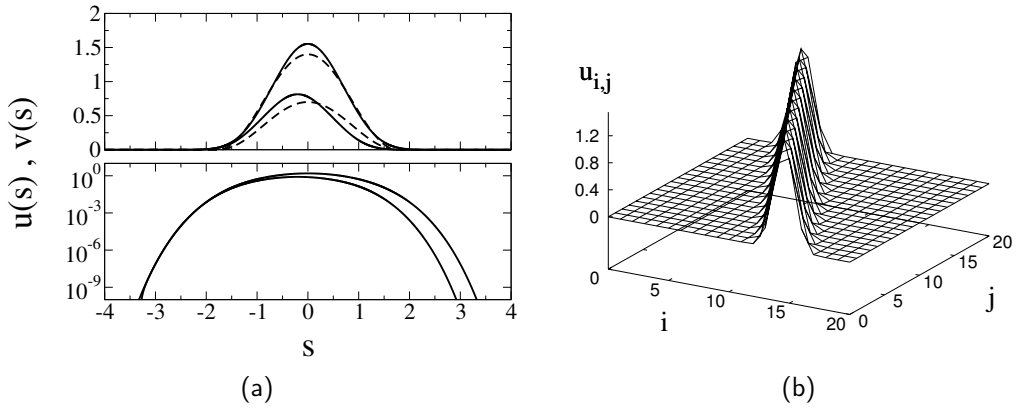

Figure 2.10: (a): Top panel: sectional view of a compact front in the two-dimensional lattice (2.43) with $\lambda = 2/\sqrt{5} \approx 0.89$ and $\theta = \arccos 2/\sqrt{5} \approx 0.46$ (corresponding to $b_1 = 0.8$ and $b_2 = 0.4$). The solid lines are the shapes of the u and the v part, where u is the larger one. Note, that u and v are not centered at the same s. The dashed line is the solution of the QCA (2.44). Bottom panel: the same plot in logarithmic scale. (b) The shape of the compact front in the lattice; only the u component is shown.

From this periodic solution one can construct a compact traveling wave front solution

$$\big(u(s), v(s)\big)^T = \begin{cases} \big(C_1 \cos^2 \omega s, C_2 \cos^2 \omega s\big)^T & \text{for } |s| \le \frac{\pi}{2\omega} \\ (0,0)^T & \text{else,} \end{cases} \tag{2.50}$$

where the parameters C_1, C_2, ω are determined by (2.49). At $s = \pi/(2\omega)$ every term in (2.44) degenerates to zero and one can glue together the trivial $(u, v)^T = (0, 0)^T$ and the periodic solution. In Fig. 2.10 we show this compact front in comparison with the front in the lattice, both solutions coincide very well. For the full coupling function $q(v)$ we assume that the front will behave like the small-amplitude front near u^*, v^* and only the shape of the hump will be affected by the full coupling.

2.4.2 Traveling compact wave fronts in the lattice

Now, we will investigate traveling waves in the lattice. Therefore, we take the plane wave ansatz

$$u_{i,j} = u(t - b_1 i - b_2 j) \quad \text{and} \quad v_{i,j} = v(t - b_1 i - b_2 j) \ , \tag{2.51}$$

where b_1 and b_2 are the inverse velocities, defined in Eq. (2.45). From $u_{i,j+1} - u_{i,j} = v_{i+1,j} - v_{i,j}$ it follows that the traveling wave fulfills

$$v(s - b_1) - v(s) = u(s - b_2) - u(s) \ , \tag{2.52}$$

such that one can compute $v(s)$ from the knowledge of $u(s)$. We insert the traveling wave ansatz into (2.43) and obtain

$$\begin{aligned} \dot{u} &= q\big(u(s-b_1)\big) - q\big(u(s+b_1)\big) + q\big(v(s-b_1)\big) + \\ &\quad q\big(v(s-b_1+b_2)\big) - q\big(v(s)\big) - q\big(v(s+b_2)\big) \qquad (2.53a) \\ \dot{v} &= q\big(v(s-b_2)\big) - q\big(v(s+b_2)\big) + q\big(u(s-b_2)\big) + \\ &\quad q\big(u(s+b_1-b_2)\big) - q\big(u(s)\big) - q\big(u(s+b_1)\big) \ , \qquad (2.53b) \end{aligned}$$

which is a set of advance-delay equations with different delays and advances. Again, the one-dimensional case (2.29) can be recovered by setting either $b_1 = 0$ or $b_2 = 0$ and $b_1 = b_2$ yields a scaled version of Eq. (2.29). Next, we integrate (2.53a) from 0 to s and assume that $u(s < b1 + b2) = u^*$ and $v(s < b1 + b2) = v^*$

$$u - u^* = 2b_1\Big(q(u^*) + q(v^*)\Big) - \int_{s-b_1}^{s+b_1} q(u)\mathrm{d}t - \int_{s-b_1}^{s} q(v)\mathrm{d}t - \int_{s-b_1+b_2}^{s+b_2} q(v)\mathrm{d}t \qquad (2.54a)$$

$$v - v^* = 2b_2\Big(q(u^*) + q(v^*)\Big) - \int_{s-b_2}^{s+b_s} q(v)\mathrm{d}t - \int_{s-b_2}^{s} q(u)\mathrm{d}t - \int_{s-b_2+b_1}^{s+b_2} q(u)\mathrm{d}t \ . \qquad (2.54b)$$

The kink condition can be derived if one assumes that a $s_1 > s_0$ exists with $u(s > s_1) = \bar{u}^* = \text{const}$ and $v(s > s_1) = \bar{v}^* = \text{const}$. This results in (2.47). Now, it is possible to construct a numerical scheme to solve Eq. (2.54). For simplicity, we restrict ourself to $q(v) = \cos v$ with $u^* = v^* = 0$. Eq. (2.54) reads then

$$u = 4b_1 - \int_{s-b_1}^{s+b_1} \cos u\mathrm{d}t - \int_{s-b_1}^{s} \Big\{ \cos v(t) + \cos v(t+b_2)\Big\}\mathrm{d}t = \mathcal{F}(u,v) \ . \qquad (2.55a)$$

Then, one chooses an initial profile u_0 and iterates

$$\begin{pmatrix} u_{k+1} \\ v_{k+1} \end{pmatrix} = \left(\frac{||(u_k, v_k)||}{||(\tilde{u}, \tilde{v})||}\right)^{3/2} \begin{pmatrix} \tilde{u} \\ \tilde{v} \end{pmatrix} \ , \qquad (2.55b)$$

where

$$\tilde{u} = \mathcal{F}(u_k, v_k) \quad \text{and} \quad \tilde{v}(s+b_1) = \tilde{v}(s) + \tilde{u}(s+b_2) - \tilde{u}(s) \ . \qquad (2.55c)$$

$||\cdot||$ denotes the L_1-norm $||(u,v)|| = \int \sqrt{u^2+v^2}\mathrm{d}s$ and the normalization ensures that the solution does not converge to the constant solution $u(s) = v(s) = 0$. The part for $v(s)$ in Eq. (2.55c) is a delay equation, which can easily be solved if $v(s < b_1 + b_2) = \text{const}$. In Fig. 2.10(a) we show the sectional shape of a two-dimensional compact front with $\lambda = 2/\sqrt{5}$ and $\theta = \arccos 2/\sqrt{5}$. Its compact properties, i.e. their super-exponential tails are clearly visible in the logarithmic scale. Note, that the components u and v have different widths and that their maxima are shifted. In Fig. 2.10(b) we show the shape of the front in the lattice.

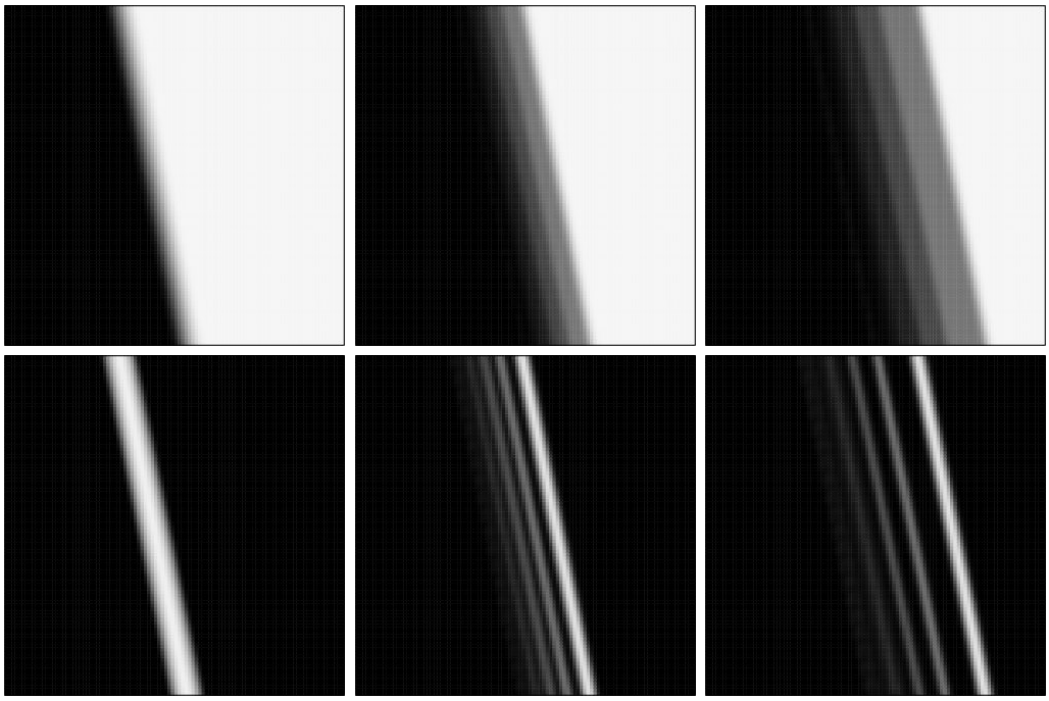

Figure 2.11: Evolution of an initial step in $\varphi_{i,j}$ or an initial pulse in $u_{i,j}$ and $v_{i,j}$. The amplitudes of the initial pulse are $u_{max} = 2.30179$, $v_{max} = 0.459599$, the width is $w = 10$ and the orientation is $\theta = \pi/16$. The upper row shows the field $\varphi_{i,j}$ at times $t = 0, 10, 20$, whereas the lower row shows the phase differences $u_{i,j}$. It is clearly visible that the initial front evolves into a train of traveling wave fronts which are the compact wave fronts.

2.4.3 Numerical studies

Evolution of an initial step

In the last section we have studied the properties of traveling wave fronts in the two-dimensional phase lattice. Here, we address the question about their appearance from physically realizable initial conditions.

We start with the most simple scenario allowing for the emergence of traveling wave fronts: an initial step in $\varphi_{i,j}$ rotated against the i-axes by an angle θ. To model the sectional step we choose a cosine where the amplitude and the width w of the step are parameters. Such a step refers to a pulse in the differences $u_{i,j}$ and $v_{i,j}$ with amplitudes u_{max} and v_{max}. In Fig. 2.11 we show the evolution of the step. The initial width of the step is $w = 10$ and the orientation is $\theta = \pi/16$; the amplitudes in the difference coordinates are $u_{max} = 2.302$ and $v_{max} = 0.456$. During the evolution, the step decomposes into a train of traveling compact steps, which can be clearly seen in Fig. 2.11. In the difference coordinates these steps are compact solitary fronts. In Fig. 2.12(a) we plot

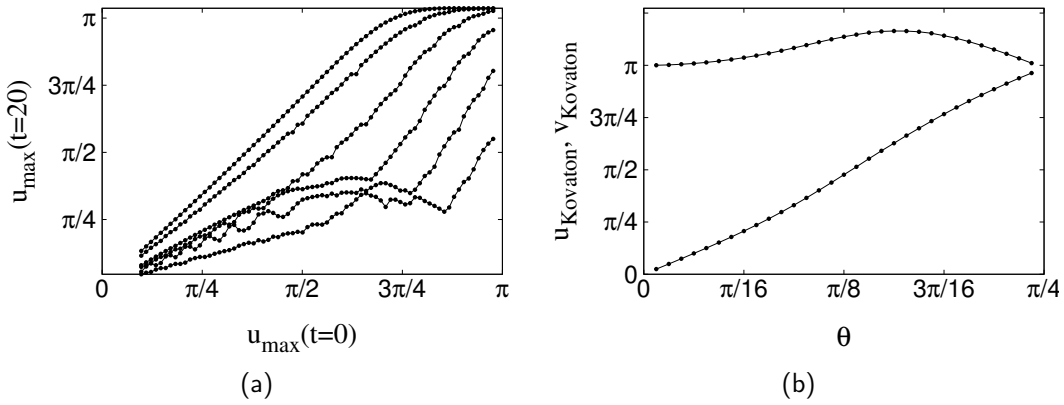

Figure 2.12: Compact traveling wave fronts are emitted from an initial pulse: (a) shows the amplitudes u_{max} of the emitted pulses in dependency on the initial amplitude. The width of the initial pulse is $w = 10$ and its orientation against the i-axis is $\theta = \pi/16$. Note, that a kovaton front appears at approximately $u_{max}(t = 0) = 3.5$. In (b) the height $u_{\mathrm{Kovaton}}, v_{\mathrm{Kovaton}}$ of the emitted kovatons are plotted in dependency on the orientation angle θ.

the amplitudes of the emitted compact fronts in dependence of the amplitude of the initial pulse. The width is fixed to $w = 10$ and the orientation to $\theta = \pi/16$.

From the study of the evolution of an initial step one can also observe another traveling wave structure – kovatons, which are traveling kink–anti-kink pairs in the difference coordinate frame. In Fig. 2.13 we show the shape of a kovaton, which emerged from an initial step. In Fig. 2.12(b) height of the kovaton fronts in dependence of the angle θ are plotted.

Evolution of localized initial data

Having studied the evolution of fronts in the phase lattice, we turn our attention to general localized initial conditions. A particular initial setup in this context is a single excited lattice site, see Fig. 2.14. In this situation two effects are observed: First, regular fronts emerge from the initial excited lattice site. The shape is not exactly circular, which is due to the direction-dependent propagation velocity. These fronts are similarity to the kovaton or kink fronts observed in the evolution of steps. They have a compact support and their height depends on the propagation direction. The second important observation is the formation of a chaotic region and a spreading of this region. The spreading is slower than the propagation of the front.

To specify the propagation of the chaotic region we use a simple variance based approach to calculate the spreading velocity of this region. Therefore, we compute the variance of $\sin(v_{i,j})$ for all i, j in a time window of length $T_{window} = 20$. In the upper left plot in Fig. 2.15 we show $\sin(v_{i,j})$ for $i = 100, j = 100$. The chaotic region approximately

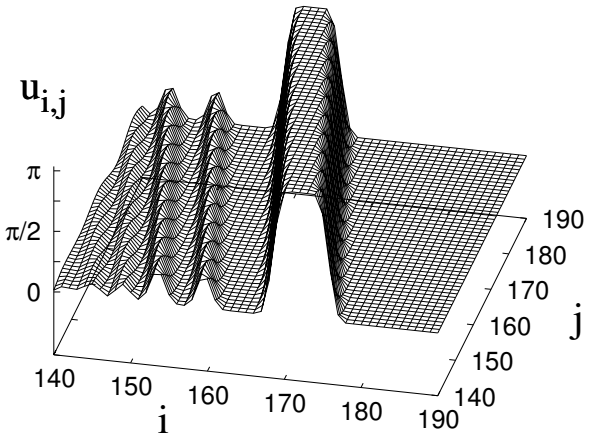

Figure 2.13: Here, a kovaton front emerging from an initial step is shown. The initial width is $w = 15$, the orientation $\theta = \pi/16$ and the initial amplitudes are $u_{max} = 3.07581$ and $v_{max} = 0.612852$.

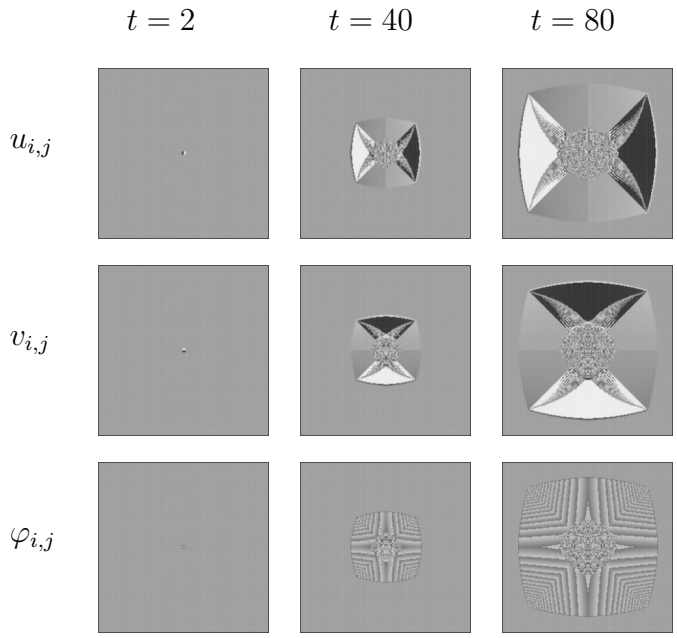

Figure 2.14: Single site initial conditions. Snapshots of the phase lattice for three different times $t = 2, 40, 80$. The dimension of the lattice is 256×256. The fronts are compact and refer to kink solutions.

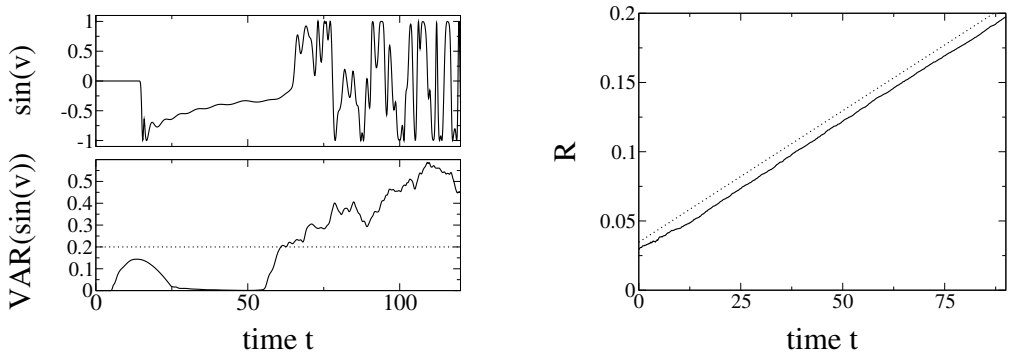

Figure 2.15: The upper left plot shows $\sin(v_{100,100})$ and the lower left plot shows the variance of $\sin(v_{100,100})$ in a time window of $T = 100$. When the chaotic front reaches this point the variance grows immediately. The dotted line is the threshold 0.2 which is used to compute N_{ch}. On the right panel the time dependence of the radius of the chaotic region $R = \sqrt{N_{ch}/\pi}$ is plotted. It follows a linear growth with $R = 0.0018991t + 0.02667$, which is a simple diffusion process.

reaches the site at $t = 60$, and then the variance immediately grows, see the lower plot on the left in Fig. 2.15. To determine now the spreading velocity we count the number of lattices sites N_{ch} with a variance larger than 0.2. Assuming that the chaotic region grows approximately circular we can define the radius $R = \sqrt{N_{ch}/\pi}$. The evolution of R is shown in the right panel of Fig. 2.15. This growth is linear and proportional to $R \sim Dt$ width the diffusion constant $D = 0.047272\sqrt{\pi}$.

2.5 Conclusion

Summarizing this chapter, we have shown that many interesting and important traveling wave phenomena can be found in dispersively coupled phase oscillator lattices. We have seen that one particular property of such lattices is the strongly nonlinear coupling function where linear terms are totally absent. This gives a link to the theory of compactons which exists in systems with nonlinear dispersion. In fact, it could be shown that the small amplitude limit of the quasi-continuous approximation of the phase lattice is exactly the $K(2, 2)$ equation, which is the classical compacton equation.

In the full lattice equations compactons also exists. Here, they are not defined on a compact support but their tails decay with a super-exponential rate. We have calculated this rate and compared the lattice compacton with their quasi-continuous counterpart. Besides compactons we could also observe a variety of other traveling wave structures, namely kinks with compact or exponential tails or classical solitary waves with exponential tails. Furthermore, a solitary wave with oscillating and exponentially decaying tails could be found.

Finally, we studied a two-dimensional phase oscillator lattice. Again, the strongly non-

linear coupling function is responsible for the emergence of compact structures. In particular, we have shown that traveling two-dimensional fronts with super-exponential tails do exist.

Chapter 3

Compactons in Hamiltonian lattices

Hamiltonian lattices arise in many fields of theoretical physics. For example, they play an important role in the understanding of the statistical properties of macroscopic systems. A first attempt into this direction was the Fermi-Pasta-Ulam experiment [31], which concentrated numerically on the thermalization properties of a lattice of coupled nonlinear oscillators. The outcome of this experiment was surprising: for some initial conditions thermalization was not observed and a recurrence phenomena established. A full understanding is still missing and subject of current research [32, 70, 71]. Furthermore, Hamiltonian lattices have been studied in connection with heat transfer and thermal conductance [33] or wave transmission [72].

Another direction of research on Hamiltonian lattices are discrete breathers [17, 18], which are genuine nonlinear excitations of the lattice. Breathers are spatially localized and time-periodic structures, where the frequency is located outside of the (linear) phonon spectrum. Discrete breathers can be found in a variety of physical setups, for example in coupled wave guide arrays [43, 44]. For more applications see the review [18] and references therein.

Anderson localization [73–75] and related topics are usually described by Hamiltonian lattices. Here, localization is induced by disorder and the localization mechanism can be thought of as an infinite series of wave scattering events on impurities, such that the wave can not leave a finite region. Recently, the interplay of disorder and nonlinearity has attracted a lot of attention in the scientific community. Here, one basic question deals with the destruction of Anderson localization by nonlinearity [34, 76, 77].

The general form of a Hamiltonian lattice of N sites is

$$H = \sum_k \frac{p_k^2}{2} + V_k(q_k) + W_k(q_1, q_2, \dots q_N) \ , \tag{3.1a}$$

where q_k and p_k are the generalized coordinates and momenta and can be vector-like. $V_k(q_k)$ is the onsite potential and $W_k(q_1,\ldots,q_N)$ is the interaction potential. In many cases, the interaction is assumed to be of nearest-neighbor type $W_k(q_1,\ldots,q_N) = W(q_{k+1},q_k)$. The equations of motions are obtained from the Hamiltonian equations

$$\ddot{q}_k = -\frac{\partial H}{\partial q_k} = -V'(q_k) - \frac{\partial W(q_{k+1},q_k)}{\partial q_k} - \frac{\partial W(q_k,q_{k-1})}{\partial q_k} \ . \tag{3.1b}$$

Some of the examples mentioned above are not described by the Hamiltonian (3.1) but fit better into the class of complex valued Hamiltonian systems related to the discrete nonlinear Schrödinger equation. Such systems are the subject of chapter 4 in the context of strongly nonlinear interaction and compact structures.

The special feature of our work are strongly nonlinear Hamiltonian systems, where linear interaction terms are totally absent. In particular, the motivating example of the granular chain in the introduction is exactly of this type. Here, the force between two granular balls follows the Hertzian law $F \sim \delta^{3/2}$, where δ is the overlap between the balls [39, 40]. Granular chains have been studied first by V. I. Nesterenko in the context of pulse propagation in mid 1980s [1, 78]. Nesterenko also coined the term "sonic vacuum" for the absence of linear waves in these systems.

3.1 The basic model

The basic model of this chapter is a Hamiltonian lattice of the type

$$H = \sum_k \frac{p_k^2}{2} + \frac{1}{n+1}|q_{k+1}-q_k|^{n+1} \ . \tag{3.2}$$

It has only one parameter – the nonlinearity index n; an onsite potential is not present. The absolute value of the differences has to be introduced to ensure that the potential possesses a minimum. The linear lattice can be reproduced by setting $n=1$. However, this case is not very interesting and we will restrict ourself to $n>1$.

In the granular chain the nonlinearity index is usually $n=3/2$ which resembles the Hertzian law and describes the repulsive force between two spheres in contact. For other contact geometries different values of n have to be used. Since the interaction is attractive if $q_{k+1}-q_k>0$, the Hamiltonian (3.2) can not describe the granular chain in all details. To account for the absence of an attracting force the coupling potential has to be modified to $\frac{1}{n+1}[q_{k+1}-q_k]_-^{n+1}$, where $[q]_-=0$ for $q>0$ and q for $q<0$.

We want to mention here, that the mass or an coupling strength does not appear in Eq. (3.2). Such constants can be removed by scaling of q and t and we set them without loss of generality to 1. Note further, that the interaction is non-smooth, despite for the values $n=1,3,5,\ldots$.

The equations of motion read

$$\ddot{q_k} = |q_{k+1} - q_k|^n \,\mathrm{sign}(q_{k+1} - q_k) - |q_k - q_{k-1}|^n \,\mathrm{sign}(q_k - q_{k-1}) \ . \tag{3.3}$$

They can be written in terms of the differences $Q_k = q_{k+1} - q_k$ between adjacent lattice sites

$$\ddot{Q}_k = |Q_{k+1}|^n \,\mathrm{sign}(Q_{k+1}) - 2\,|Q_k|^n \,\mathrm{sign}(Q_k) + |Q_{k-1}|^n \,\mathrm{sign}(Q_{k-1}) \ . \tag{3.4}$$

In the following we will omit the signum function for simplicity. The Hamiltonian (3.2) possesses two conservation laws: energy and total momentum. The first one corresponds to the time invariance of the Hamiltonian, whereas the second one is due to the invariance of arbitrary coordinate shifts $q \mapsto q + q_0$. Furthermore, the overall momentum can be trivially set to zero by transforming to a moving reference frame.

The lattice (3.2) has a remarkable scaling property

$$q = a\tilde{q}\,, \quad p = a^{\frac{n+1}{2}}\tilde{p}\,, \quad H = a^{n+1}\tilde{H}\,, \quad t = a^{\frac{1-n}{2}}\tilde{t}\ . \tag{3.5a}$$

With these relations it is always possible to scale the system such that $H = 1$. Larger energies correspond then to larger amplitudes and smaller time scales, but the spatial structure is untouched. Furthermore, a traveling wave $q_k(t) = q(k - \lambda_0 t)$ with velocity λ_0 generates a family of traveling waves with the same spatial profile but different amplitudes and velocities, being related via

$$\lambda = \lambda_0 a^{(n-1)/2} \ . \tag{3.5b}$$

In the last chapter, an approximation of the lattice in terms of a continuous variable turned out to be very successful. In particular, it could be shown that traveling waves exist in both models and that they coincide very well. To derive a quasi-continuous approximation of (3.2) two ways are possible. The first one is a *direct expansion* of the lattice variables q_k and the second one an *expansion of the differences* Q_k.

For the direct expansion of the original lattice variables one approximates $q_{k\pm1}$ in (3.3) by a Taylor series of order 4. Inserting the series and collecting all terms up to order of h^{n+3} yields

$$[q]_{tt} = h^{n+1}[q_x^n]_x + \frac{h^{n+3}}{12}\left([q_x^n]_{xxx} - \frac{n(n-1)}{2}[q_x^{n-2}q_{xx}^2]_x\right) \ , \tag{3.6}$$

where h is the lattice spacing. This equation is the long wave approximation of Nesterenko [39, 78]. To simplify and to compare it with the QCA for differences we differentiate (3.6) with respect to x, define $\tilde{Q} = hq_x$ and set $h = 1$:

$$[\tilde{Q}]_{tt} = [\tilde{Q}^n]_{xx} + \frac{1}{12}\Big([\tilde{Q}^n]_{xxxx} - \frac{n(n-1)}{2}[\tilde{Q}^{n-2}\tilde{Q}_x^2]_{xx}\Big) \ . \tag{3.7}$$

Note, that the lattice spacing h is not a small parameter and the cutoff at order 4 is more or less arbitrary. To justify the QCA one has to compare its solutions with those of the full lattice problem.

The expansion of the difference coordinates is very similar. One approximates $Q_{k\pm1}$ by a Taylor expansion of fourth order and inserts this approximation into (3.4)

$$[Q(x,t)]_{tt} = [Q^n(x,t)]_{xx} + \frac{1}{12}\,[Q^n(x,t)]_{xxxx} \quad . \tag{3.8}$$

This equation differs by a coefficient $[Q^{n-2}Q_x^2]_{xx}$ from Eq. (3.7). In [9] both approximations have been compared from a general point of view.

Equations (3.7) and (3.8) belong to a class of strongly nonlinear PDEs, because the dispersion term with the fourth derivative is nonlinear. The equations do not possess linear wave solutions (this situation has been called "sonic vacuum" by V. Nesterenko), but it has nontrivial nonlinear ones. In this way it is very similar to a family of strongly nonlinear generalizations of the Korteweg-de Vries equation, studied in [6], and can be considered as a strongly nonlinear version of the Boussinesq equation [7].

3.2 Traveling solitary waves

The topic of this section are localized traveling waves in the lattice equations (3.2) and their quasi-continuous approximations (3.7) and (3.8). We will start our considerations with the QCA where we can find analytical traveling wave solutions. In the lattice, we tackle the problem numerically. The results of both models are compared with each other. Contrary to the previous chapter, we do not analyze the problem in all details. We are only interested in compacton solutions which can only exist around $Q = 0$. Different backgrounds $Q \neq 0$ are not considered here.

3.2.1 Quasi-continuous approximation

The models (3.7) and (3.8) describe the lattice as a continuous medium. We seek traveling solitary waves in the usual form $Q(x,t) = Q(x-\lambda t) = Q(s)$ where λ is the velocity. Inserting this ansatz into Eqs. (3.7) and (3.8) and integrating twice yields

$$\lambda^2 Q = Q^n + \frac{1}{12}[Q^n]_{ss} - \frac{n(n-1)}{24}Q^{n-2}Q_s^2 \qquad \text{direct} \tag{3.9a}$$

$$\lambda^2 Q = Q^n + \frac{1}{12}\,[Q^n]_{ss} \qquad \text{differences .} \tag{3.9b}$$

Note, that we have assumed that the solution tends to zero as $s \to \pm\infty$. The second equation also appears in the traveling wave ansatz for the $K(n,n)$-equation in [6]. Both

equations can be solved [79, 80] for an arbitrary power n by

$$Q(s) = |\lambda|^m A_1 \cos^m(B_1 s) \qquad \text{with} \qquad m = \frac{2}{n-1} \tag{3.10a}$$

where the coefficients A and B differ for both approximations

$$A_1 = \left(\frac{2}{1+n}\right)^{\frac{1}{1-n}}, \qquad B_2 = \sqrt{6\frac{(n-1)^2}{n(n+1)}} \qquad \text{direct} \tag{3.10b}$$

$$A_2 = \left(\frac{n+1}{2n}\right)^{\frac{1}{1-n}}, \qquad B_2 = \sqrt{3}\,\frac{n-1}{n} \qquad \text{differences.} \tag{3.10c}$$

The solutions (3.10) do not satisfy boundary conditions, moreover, they intersect with another, trivial solution $Q = 0$. Remarkably, because of the degeneracy of Eqs. (3.9a) and (3.9b) at zero, one can merge periodic solutions (3.10) with the trivial solution $Q = 0$ (see a detailed discussion in [6, 7]):

$$Q(s) = \begin{cases} |\lambda|^m A_i \cos^m(B_i s) & |s| < \frac{\pi}{2B_i} \\ 0 & \text{else,} \end{cases} \tag{3.11}$$

with $i = 1, 2$. This gives a compacton – a solitary wave with compact support – according to the definition in [6, 7]. For other, non-solitary solutions of (3.7) see e.g. [39, 80]. Note that due to the symmetries $x \to -x$, $Q \to -Q$, solitary waves with both signs of velocity λ and of amplitude A are the solutions.

It is important to check the validity of solution (3.11) by substituting it back to (3.7) or (3.8). Then no terms are singular for the case $m > 2$ only, i.e. for $n < 2$. Thus, the constructed compacton solution (3.11) is, strictly speaking, not valid for strong nonlinearities $n \geq 2$. This conclusion is, however, only of small relevance for the original lattice problem. Indeed, the PDE (3.7) or (3.8) is only an approximation of the lattice problem: because the spatial extent of solution (3.11) is finite, there is no small parameter allowing us to break Taylor-expansion somewhere. Just breaking it after the fourth derivative is arbitrary and can be justified only by the fact that in this approximation one finds reasonable solutions at least for some values of n. A real justification can come only from a comparison with the solutions of the lattice equations, to be discussed in the next subsection. And there we will see that the solution can be found for nonlinearities with $n > 2$.

3.2.2 Traveling waves in the lattice

In the lattice we use the same traveling wave ansatz as for the phase lattice $Q_k(t) = Q(k - \lambda t) = Q(s)$ with the wave velocity λ. Mathematically, the existence of traveling

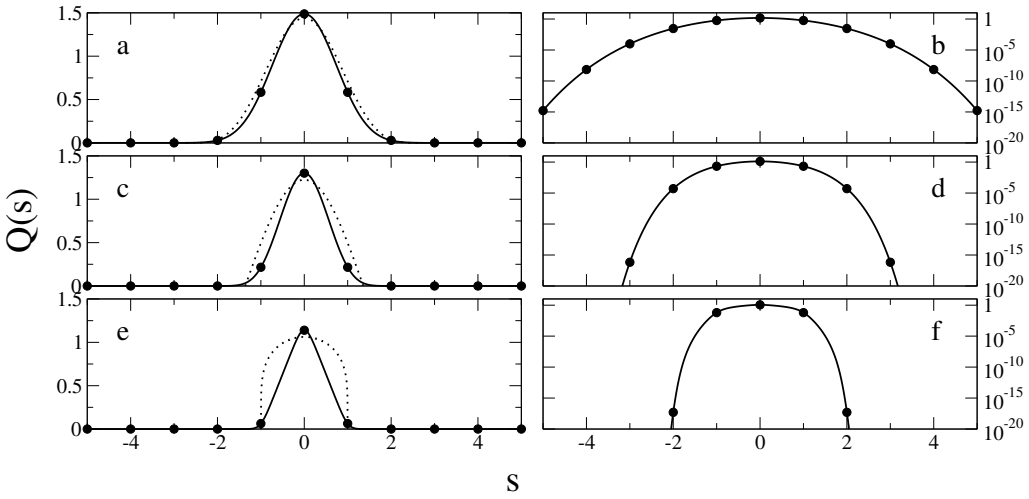

Figure 3.1: The traveling waves obtained from (3.14) for various powers n. Markers show the wave on the lattice, dotted lines show the corresponding solutions of the quasi-continuous approximation (3.8). Left column: normal scale, right column: logarithmic scale. (a,b) $n = 3/2$; (c,d) $n = 3$, (e,f) $n = 11$.

waves in (3.3) has been shown in [61, 81]. Inserting the ansatz into the equations of motion (3.4) yields

$$\lambda^2 Q''(s) = Q^n(s-1) - 2Q^n(s) + Q^n(s+1) \ . \tag{3.12}$$

We use the scaling relation (3.5) to set $\lambda = 1$. As shown in [82] the advance-delay differential equation can be written in integral form

$$Q(s) = \int_{s-1}^{s+1} (1 - |s - \xi|) Q^n(\xi) \mathrm{d}\xi \ , \tag{3.13}$$

with a triangular kernel. Now, following the approach of V. Petviashvili [65, 66], we are able to construct a numerical scheme to solve the integral equation (3.13), which is quite similar to that one for the phase compactons (2.34). Starting with some initial guess Q_0, one iterates

$$Q_{i+1} = \left(\frac{||Q_i||}{||Q_*||} \right)^{\alpha} Q_* \quad \text{and} \qquad Q_* = \int_{s-1}^{s+1} (1 - |s - \xi|) Q_i^n(\xi) \mathrm{d}\xi \ . \tag{3.14}$$

To compute the norm we have used the L_1 norm, but any other norm can be used too. The normalization with $\alpha = \frac{n}{n-1}$ ensures that the scheme converges to the desired solution. The integral has been computed numerically by a 4th-order Lagrangian integration scheme [67]. In Fig. 3.1 the traveling waves solution for various nonlinearities n are shown. Using the logarithmic scale one clearly recognizes the compact nature of the waves. Interestingly, the numerical scheme can be applied even to huge nonlinearities $n > 20$.

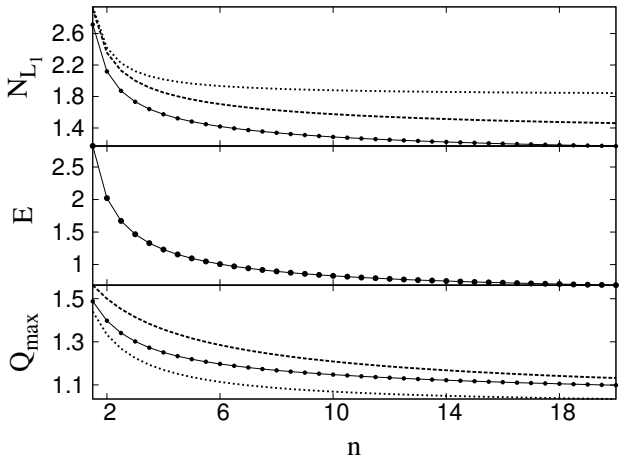

Figure 3.2: The dependency of the amplitude Q_{max}, the energy E and the L_1-norm N_{L_1} of a compacton on the nonlinearity index n. In this plots $\lambda = 1$. For comparison, the curves from the quasi-continuous approximation are shown with dashed lines for the Eq. (3.7) and with dotted lines for Eq. (3.8).

In Fig. 3.2 we show some properties of the found waves in dependence of the nonlinearity index n. In detail, we show the total energy E, the L_1-norm N_{L_1} and the amplitude $Q_{\max}$. Remarkably, the effective width N_{L_1}/Q_{max} decreases with increasing nonlinearity index and it seems that the profile of the compacton converges to a triangular shape as $n \to \infty$.

The stability of the compactons has been shown by direct numerical simulation, see Figs. 3.5, 3.6 and 3.7. They travel through the lattice without distortion, even if the initial state is perturbed. A general theory for the stability of traveling waves in Hamiltonian lattices like Eq. (3.2) has been developed in a series of papers by Gero Friesecke and Robert Pego [83–86] based on rigorous perturbation arguments. The stability of solitary waves in dissipative lattices has been studied in [87].

Estimation of the tails

It has been shown in the previous section that the solitary waves in the QCA possess a compact support. In the lattice, this is surely not the case. The integral equation (3.13), which has to be fulfilled for solitary waves, is nonlocal and therefore a truly compact wave is not possible. But one can estimate the decay of the tails. Therefore, we start with Eq.(3.13) and use the ansatz $Q(s) = e^{-f(s)}$:

$$Q(s) = \int_{s-1}^{s+1} (1 - |s - \xi|) e^{-nf(\xi)} \mathrm{d}\xi \ . \tag{3.15}$$

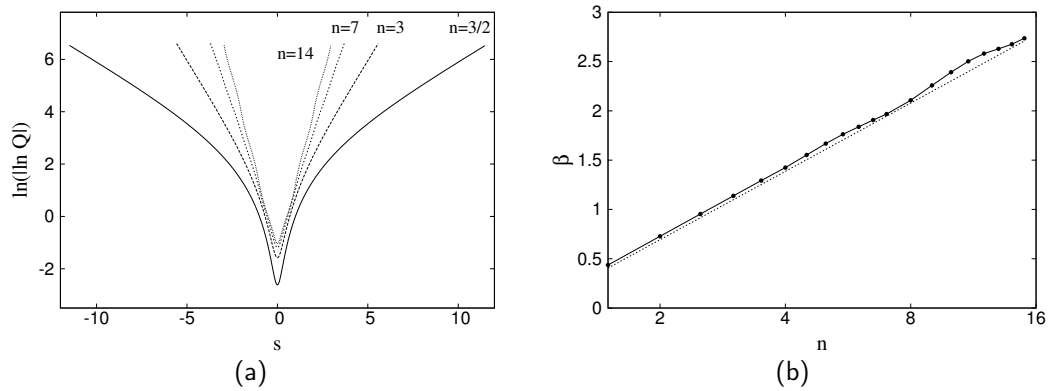

Figure 3.3: (a) The tails of the compactons in double logarithmic scale. (b) Comparison of the estimate (3.19) with the compactons obtained from (3.14).

Now, we assume that the tails of $Q(s)$ decay very fast or equivalently that $f(x)$ is a monotonically increasing function. Then, the integrand in (3.15) has a maximum close to $s-1$ and one can expand $f(\xi)$ into a Taylor series around $s-1$, keeping only the first-order term:

$$Q(s) \approx \int_{s-1}^{s+1} (1-|s-\xi|) \exp\big\{ -nf(s-1) - nf'(s-1)(\xi-(s-1))\big\} \mathrm{d}\xi \ . \tag{3.16}$$

This approximation is also know as Laplace method. Now, we shift the integration range

$$Q(s) \approx e^{-nf(s-1)} \int_{0}^{2} \xi e^{-nf'(s-1)\xi} \mathrm{d}\xi \tag{3.17}$$

where we also replace the decreasing part of the kernel with ξ. Since this integrand decreases very fast, we can set the upper bound of the integration to infinity and we obtain by partial integration

$$Q(s) = e^{-f(s)} \approx \frac{e^{-nf(s-1)}}{\big[nf'(s-1)\big]^2} \ . \tag{3.18}$$

Taking the logarithm yields $-f(s) = -nf(s-1) - 2\log[nf'(s-1)]$. Since we expect that $f(s)$ is rapidly growing we can neglect the logarithmic term $f(s) = nf(s-1)$. This equation is solved by $f(s) = Cn^s = Ce^{\log(n)s}$ where C is an arbitrary constant. Finally, we obtain the super-exponential decay:

$$Q(s) = e^{-f(s)} \approx e \exp\Big[-C \exp\big(\log(n)s\big)\Big] \ . \tag{3.19}$$

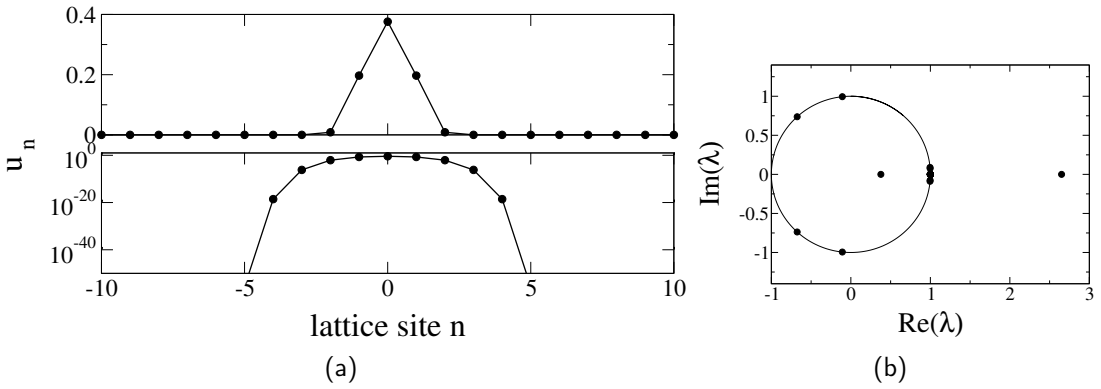

Figure 3.4: (a) Spatial profile u_k of the compact breather solution $q_k(t) = (-1)^k f(t) u_k$ in (3.3). (b) The eigenvalues of the according monodromy matrix. One eigenvalue has an absolute value larger than one, such that the compact breather is unstable.

This expression was first obtained by Chatterjee [88] using a direct expansion of the advance-delayed equation (3.12). Note, that the velocity λ enter this equation via the scaling of $Q(s)$.

In Fig. 3.3(a) we show the tails of the compactons for various values of n and in Fig. 3.3(b) we compare the estimated decay rate (3.19) with compactons obtained numerically from the traveling wave scheme (3.14). To obtain the double logarithmic decay rate $\beta = d\log(|\log(Q(s))|)/ds$, we first compute $\log(|\log(Q(s))|)$ and then the derivative is calculated using a spline smoothing scheme [89]. The numerical value of β is shown in Fig. 3.3(b). Both coincide very well.

Discrete compact breathers

For $n = 3$ Eq. (3.2) has also been studied in the context of discrete breathers [90, 91]. It could be shown that a discrete breather can be obtained by the separation ansatz $q_k(t) = (-1)^k f(t) u_k$ which results in $f''(t) = C f(t)^3$ and $C u_k = (u_{k+1} + u_k)^3 + (u_k + u_{k-1})^3$, where C is a constant. The temporal component can be solved by $f(t) = A\mathrm{cn}(A\sqrt{C}t, 1/\sqrt{2})$. $\mathrm{cn}(x, n)$ is the Jacobi elliptic function with modulus n. The spatial part can be solved by an iterative Petviashvili scheme, see appendix B.1. For $C = 1$ the spatial profile is shown in Fig. 3.4. The tails of the breather decay with a super-exponential rate, hence this breather is compact. The stability of the compact breather can be studied using Floquet theory. In Fig. 3.4 the eigenvalues of the monodromy matrix are shown. One eigenvalues has an absolute value larger than one, hence, the breather is unstable.

3.3 Numerical experiments of the 1D chain

3.3.1 Appearance of compactons from initial conditions

The compact solitary waves constructed in the previous section are of relevance only if they evolve from rather general, physically realizable initial conditions. For an experimental significance (see [1, 92] for experiments with Hertz beads) it is furthermore important, that the emerging compact waves establish on relatively short distances, otherwise dissipation (which has not been considered here) will suppress their formation. We illustrate this process in Fig. 3.5. There, we show a numerical simulation of (3.3) on a finite lattice of length $N = 128$ with open boundaries $\ddot{q}_1 = |q_2 - q_1|^n \mathrm{sign}(q_2 - q_1)$ and $\ddot{q_N} = -|q_N - q_{N-1}|^n \mathrm{sign}(q_N - q_{N-1})$. One of the quantities we report is the local energy

$$\mathcal{E}_k = \frac{p_k^2}{2} + \frac{1}{2(n+1)} \left(|q_{k+1} - q_k|^{n+1} + |q_k - q_{k-1}|^{n+1} \right) \ . \tag{3.20}$$

As initial condition we have chosen a kink in the variables q_k: $q_k = (n+1)^{1/(n+1)}$ for $k > 64$ and $q_k = 0$ elsewhere. This profile has unit energy and it corresponds to localized initial condition for the differences $Q_k = \delta_{k,64} \cdot (n+1)^{1/(n+1)}$. The evolution is shown in Fig. 3.5. From the initial pulse of Q, a series of compactons with alternating signs is emitted in both directions. Of course, compactons with large amplitude are faster which is nicely illustrated in the plot. We expect that at large times, compactons with small amplitudes will continue to detach. For other nonlinearities n the plots look very similar and compactons are emitted in every case, see also [93].

In the next numerical experiment we studied the emergence of compactons not from a sharp step in the coordinates q_k, but from localized random initial conditions. In Fig. 3.6(a) we show a typical evolution in a lattice of length $N = 512$ (with nonlinearity index $n = 3$) resulting from random initial conditions q_k in the small region $N/2 - 5 \leq k < N/2 + 5$ around the center of the lattice. In this region the coordinates q_k have been chosen as independent random numbers, identically and symmetrically uniformly distributed around zero, while $p_k(0) = 0$. Furthermore, the energy of the lattice was set to $E = 1$ by rescaling. In the particular realization of Fig. 3.6(a) two compactons emerge to the right and four compactons to the left. In the center of the lattice a chaotic region establishes and slowly spreads over the lattice, possibly emitting more compactons on a longer time scales. In Fig. 3.6(b) we perform a statistical analysis of this setup by showing the energy distribution of compactons emitted from localized random initial conditions as described above. This distribution was obtained from 60000 simulations, in each simulation the energy of the emitted compactons have been determined and counted. The functional form of the distribution obeys in very good approximation $P(E) \sim E^{-a \log(E) - b}$, with $a = 0.57$ and $b = 5.47$.

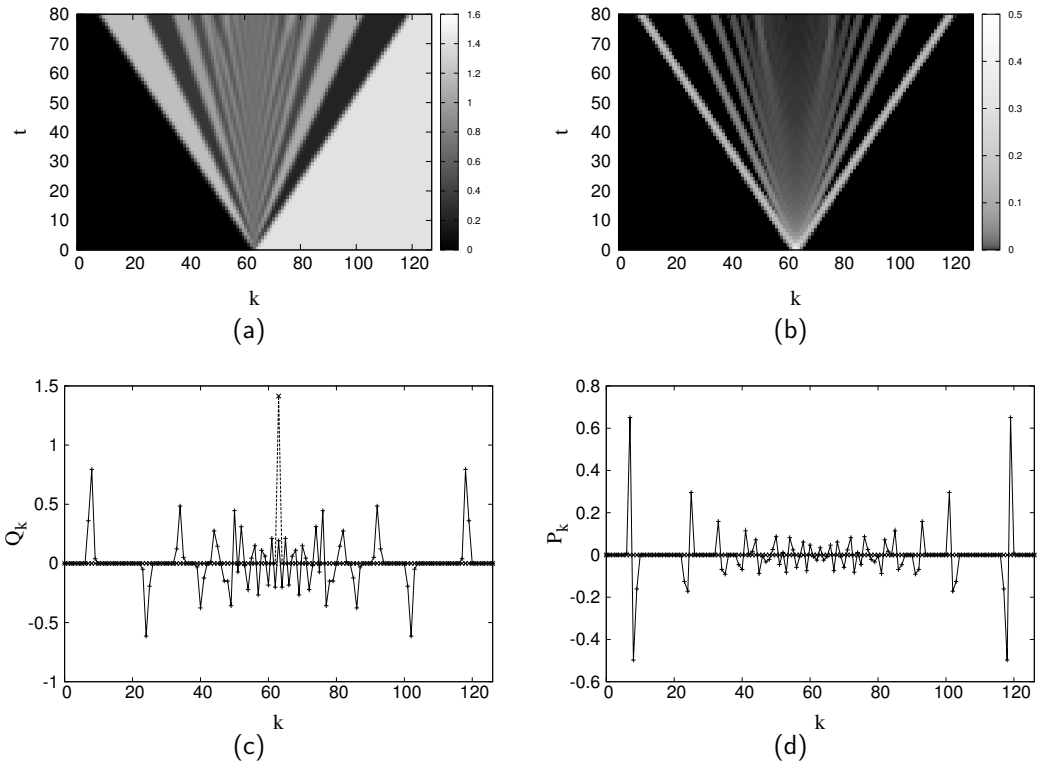

Figure 3.5: Evolution of compactons from an initial kink and for the nonlinearity index $n = 3$; the lattice length is $N = 128$ and open boundary conditions are used. Different plots show different quantities of the lattice: (a) the coordinates q_k; (b) the energy $\mathcal{E}_k$ defined in (3.20); (c) the difference coordinates $Q_k = q_{k+1} - q_k$ at time $t = 80$, the initial state at $t = 0$ is shown here as the dashed line and (d) the difference momenta $P_k = p_{k+1} - p_k$ at $t = 80$. The compactons originating from this initial state are clearly separated near the borders of the chain, those in the middle part are still overlapping.

3.3.2 Collisions of compactons

As we have demonstrated above, compactons naturally appear from initial conditions. Their stability during the evolution can be characterized by studying their stability due to collisions. In Fig. 3.7 we exemplarily show the collision of two compactons heading towards each other. They survive the collision but this process is not completely elastic, some small perturbations (that presumably on a very long time scale may evolve into small-amplitude compactons) appear. In [94] a method to systematically study the collision of solitary waves in lattices was introduced. This method can be applied to Eq. (3.2) and a similar study of collision of discrete compactons in DNLS-type lattices has been performed in section 4.3.

Because of the non-elasticity of the collisions, the initial compactons get destroyed on a

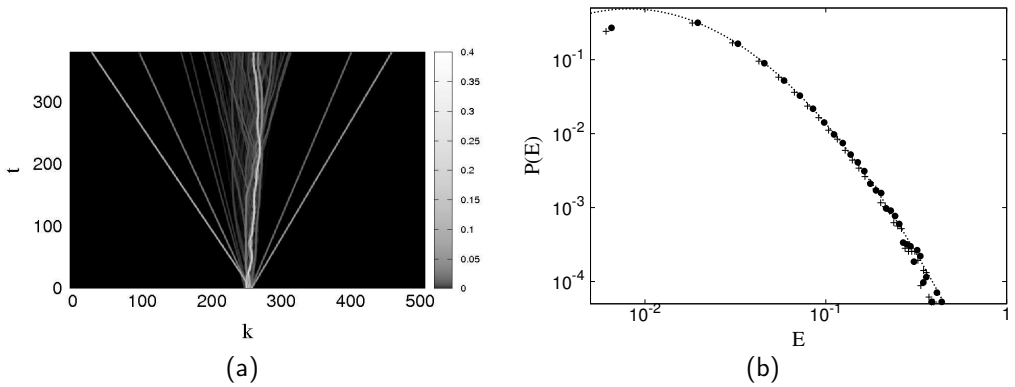

Figure 3.6: (a) Compactons emerging from localized random initial conditions. The nonlinearity index is $n = 3$. The gray scale corresponds to the energy (3.20) of the lattice site. (b) Energy distribution of the compactons emitted from localized random initial conditions. The statistics was obtained from 60000 simulations; in each simulation the lattice was integrated to the time $T = 1000$ and the energy distribution of the compactons emerged to the right (black circles) and to the left (crosses) have been determined. The distributions obeys in very good approximation $P(E) \sim E^{-a \log(E)-b}$, with $a = 0.57$ and $b = 5.47$.

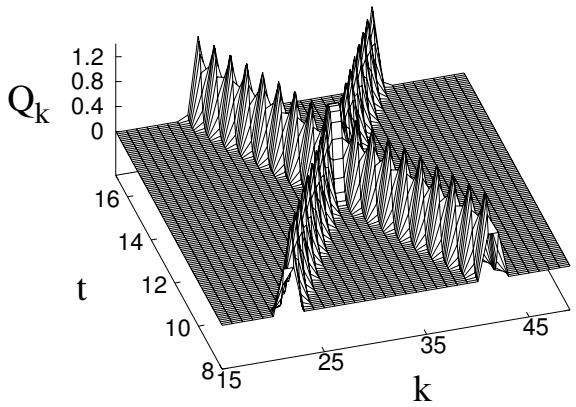

Figure 3.7: Collisions of compactons in the Hamiltonian lattice with $n = 3$, shown are the difference coordinates Q_k.

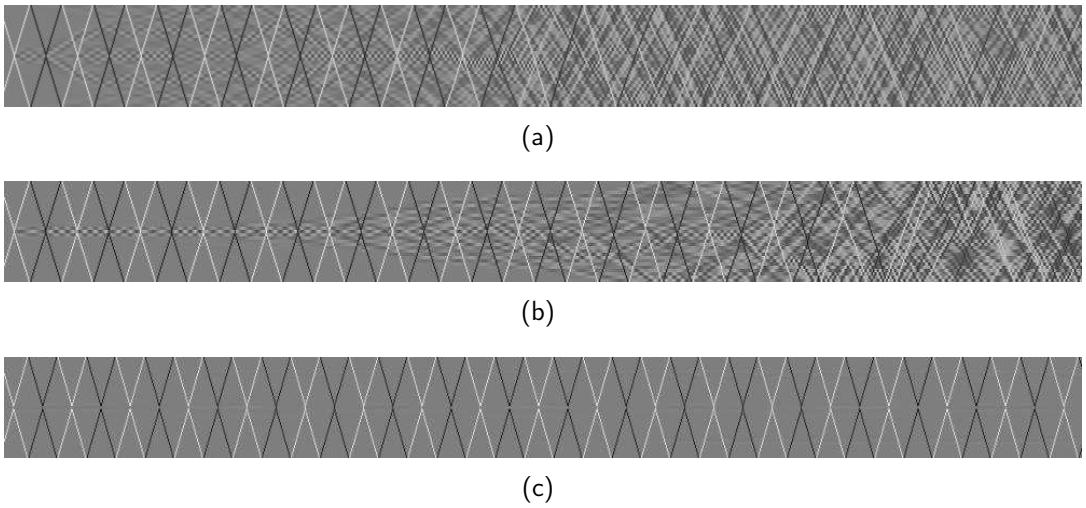

Figure 3.8: Collisions of compactons and emergence of chaos after multiple collisions. Different plots show different nonlinearity indices (a) $n = 3$, (b) $n = 9/2$ and (c) $n = 11$. Time increases from left to right and the difference coordinates Q_k are shown in gray scale. Remarkably, the elasticity of the collision increases with increasing nonlinearity index n, so that practically no irregularity appears at $n > 10$.

finite lattice and a chaotic state appears, as illustrated in Fig. 3.8. There, we show the evolution of two compactons with the same amplitude for three different nonlinearities: $n = 3, 9/2, 11$. In the first two cases the chaotic state establishes relatively fast. In the third simulation with $n = 11$ the situation is different. Here, the chaotic state does not appear even on a very long time scale. We run the simulation for times up to $T = 2 \cdot 10^5$, but could not observe the development of a chaotic state. We have checked this phenomenon also for higher values of n with the same result. Presumably, these initial conditions lie on a stable quasi-periodic orbit or are extremely close to one.

3.3.3 Chaos in a finite lattice

As demonstrated above, in a finite lattice general initial conditions evolve into a chaotic state. For characterization of chaos we use Lyapunov exponents. The chaotic state of the lattice has also been characterized in [40, 95] by the means of the velocity distribution of the lattice sites. It has been found that the lattice possesses a quasi-non-equilibrium phase, characterized by a Boltzmann-like velocity distribution but without energy equipartition.

First, we check that chaos in the lattice is extensive, i.e. the Lyapunov exponents form a spectrum when the system size becomes large and the energy density H/N remains constant (Fig. 3.9(a)). This property allows us to extend the calculations of finite

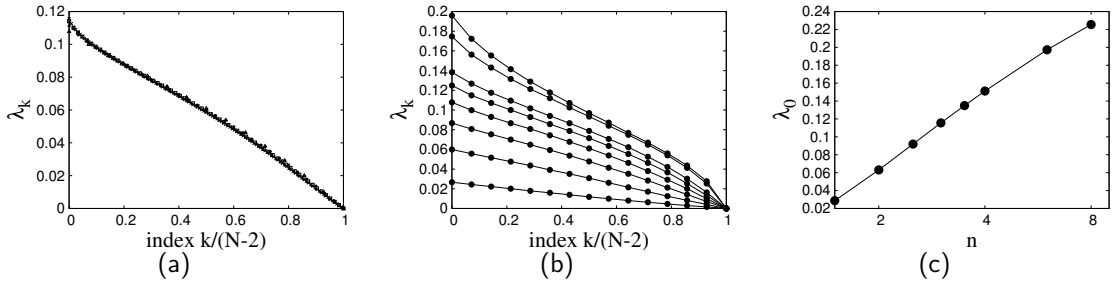

Figure 3.9: Lyapunov exponents of the Hamiltonian (3.2). (a) The Lyapunov spectra for one fixed nonlinearity index $n = 3$ and different values of lattice length $N = 16, 32, 64, 128$. The index axis is normalized to 1. (b) The Lyapunov spectra λ_j for various values of the nonlinearity index n (from bottom to top: $n = 3/2, 2, 5/2, 3, 7/2, 4, 6, 8$) and fixed lattice length $N = 16$. Larger values of n produce stronger chaos that smaller ones. (c) The largest Lyapunov exponent λ_1 for different values of n. The horizontal axis is logarithmic, thus one can see that roughly $\lambda_0 \sim \text{const} \cdot \log(n)$.

lattices to the thermodynamic limit. Note, that due to the two conservation laws, four Lyapunov exponents vanish; we have not found any more vanishing exponents, indicating the absence of further hidden conserved quantities.

For a lattice of length $N = 16$ the dependence of the Lyapunov exponents on the nonlinearity is shown in Fig. 3.9(b). For a fixed total energy (we have set $H = N = 16$ in these calculations) the Lyapunov exponents grow with the nonlinearity index. The plot presented in Fig. 3.9(c) indicates that $\lambda_{max} \propto \log n$, although we did not consider very high nonlinearity indices to make a definite conclusion on the asymptotics for large n.

We stress here that because of the scaling of the strongly nonlinear lattices under consideration, chaos is observed for arbitrary small energies – only the Lyapunov exponents decrease accordingly.

3.4 Higher-dimensional lattices

The Hamiltonian (3.2) can be generalized easily onto two- or higher-dimensional lattices. Similar systems have been widely studied in different contexts and setups. For example, traveling fronts have been investigated in [96–103] or discrete two-dimensional breathers in [104]. Other studies concentrated on two-dimensional discrete solitons [105] and discrete vortices [106]. In the context of compact structures two-and higher-dimensional compactons have been found in generalizations of the $K(m, n)$ equation [107] and their discrete counterparts [108].

The Hamiltonian for the two-dimensional square lattice reads

$$H = \sum_{i,j} \frac{p_{i,j}}{2} + \frac{1}{n+1}\left|q_{i+1,j} - q_{i,j}\right|^{n+1} + \frac{1}{n+1}\left|q_{i,j+1} - q_{i,j}\right|^{n+1} , \tag{3.21}$$

where (i,j) are the lattice indices. Other geometries like hexagonal or honeycomb lattices are also possible but will not be considered here. The equations of motion read

$$\ddot{q}_{i,j} = \left(q_{i+1,j} - q_{i,j}\right)^n - \left(q_{i,j} - q_{i-1,j}\right)^n + \left(q_{i,j+1} - q_{i,j}\right)^n - \left(q_{i,j} - q_{i,j-1}\right)^n . \quad (3.22)$$

For simplicity, we have omitted the signum function here. The system has two conservation laws – energy and total momentum. Furthermore, the scaling (3.5) is valid here. Eq. (3.22) can also be written in terms of the difference variables $U_{i,j} = q_{i+1,j} - q_{i,j}$ and $V_{i,j} = q_{i,j+1} - q_{i,j}$

$$\ddot{U}_{i,j} = U^n_{i+1,j} - 2U^n_{i,j} + U^n_{i-1,j} + V^n_{i+1,j} - V^n_{i,j} - V^n_{i+1,j-1} + V^n_{i,j-1} \quad (3.23a)$$

$$\ddot{V}_{i,j} = V^n_{i,j+1} - 2V^n_{i,j} + V^n_{i,j-1} + U^n_{i,j+1} - U^n_{i,j} - U^n_{i-1,j+1} + U^n_{i-1,j} . \quad (3.23b)$$

The differences are rotation free $\nabla_D \times (U,V)^T = U_{i,j+1} - U_{i,j} - (V_{i+1,j} - V_{i,j}) = 0$.

3.4.1 Quasi-continuous approximation

Here, we study the lattice (3.22) by means of the QCA. Therefore, the lattice variables are described by a continuous variable $q_{i,j} \approx q(x,y)$ and neighboring sites are Taylor expanded to fourth order. The calculations are rather lengthy, such that we restrict ourself to the special case $n = 2$ and set the lattice spacing $h = 1$. Then, the quasi-continuous analogon of (3.22) reads

$$\ddot{q} = \Big[(q_x)^2\Big]_x + \Big[(q_y)^2\Big]_y + \frac{1}{6}\Big(\big[(q_{xx})^2\big]_x + \big[(q_{yy})^2\big]_x + q_x q_{xxxx} + q_y q_{yyyy}\Big) . \quad (3.24)$$

For the general case with arbitrary n and h the equation is given in Appendix B.2. In principle one could also derive a quasi-continuum of the difference equations (3.23), but in this case terms proportional to h^3 arise, breaking the symmetry of the original problem.

A continuous analogon for differences variables can be obtained by introducing the variables $q_x = U/h$ and $q_y = V/h$ and differentiation of (3.24) with respect to x and y:

$$\ddot{U} = \Big[U^2\Big]_{xx} + \Big[V^2\Big]_{xy} + \frac{1}{6}\Big\{UU_{xxxx} + 3U_xU_{xxx} + 2(U_{xx})^2 \\ VV_{xyyy} + V_xV_{yyy} + 2V_{xy}V_{yy} + 2V_{xyy}V_y\Big\} \quad (3.25a)$$

$$\ddot{V} = \Big[U^2\Big]_{xy} + \Big[V^2\Big]_{yy} + \frac{1}{6}\Big\{VV_{yyyy} + 3V_yV_{yyy} + 2(V_{yy})^2 \\ UU_{xxxy} + U_xU_{xxy} + 2U_{xx}U_{xy} + U_{xxx}U_y\Big\} . \quad (3.25b)$$

The full formula for arbitrary exponents n is also given in appendix B.2.

Next, we seek traveling wave solutions of this partial differential equation. Especially, we look for plane traveling fronts in the form

$$U(x,y,t) = U(t - b_1 x - b_2 y) = U(s) \tag{3.26a}$$
$$V(x,y,t) = V(t - b_1 x - b_2 y) = V(s)\ , \tag{3.26b}$$

where b_1 and b_2 are the inverse velocities into x and y-direction: $b_1 = \cos\theta/\lambda$, $b_2 = \sin\theta$. λ is the absolute value of the velocity and θ is the propagation direction of the wave. Inserting this ansatz into the equations (3.25) and integrating twice over s yields

$$U = b_1^2 U^2 + b_1 b_2 V^2 + \frac{b_1^4}{12}\Big((U_s)^2 + 2UU_{ss}\Big) + \frac{b_1 b_2^3}{12}\Big((V_s)^2 + 2VV_{ss}\Big) \tag{3.27}$$
$$V = b_2^2 V^2 + b_1 b_2 U^2 + \frac{b_2^4}{12}\Big((V_s)^2 + 2VV_{ss}\Big) + \frac{b_1^3 b_2}{12}\Big((U_s)^2 + 2UU_{ss}\Big)\ . \tag{3.28}$$

Multiplying the first of these equations by b_2 and the second by b_1 and subtracting both equations results in $b_2 U = b_1 V$, such that V can be expressed in terms of U. The resulting equation reads then

$$U = \frac{b_1^3 + b_2^3}{b_1} U^2 + \frac{b_1^5 + b_2^5}{4b_1}\Big((U_s)^2 + 2UU_{ss}\Big)\ , \tag{3.29}$$

and has a periodic solution

$$U(s) = A\cos^2\omega s \quad \text{with} \qquad A = \frac{3}{2}\frac{b_1}{b_1^3 + b_2^3}\ ,\ \ \omega = \sqrt{\frac{b_1^3 + b_2^3}{b_1^5 + b_2^5}}\ . \tag{3.30}$$

As in the one-dimensional case this solution touches the trivial solution $U = 0$. Due to the strong degeneracy of (3.25) both solutions can be combined and form the compact front solution

$$\Big(U(s), V(s)\Big)^T = \begin{cases} (A\cos^2\omega s, b_2 b_1^{-1} A\cos^2\omega s)^T & \text{for } s \le \frac{\pi}{2\omega} \\ (0,0)^T & \text{else.} \end{cases} \tag{3.31}$$

In the previous section, we have seen that the one-dimensional compacton solution is not a strong solution of the underlying partial differential equation, since not every term is singular. In this sense, the two-dimensional front is also not a strong solution of (3.25). But as we will see in Fig. 3.10(b) below it describes the compact front in the lattice quite well.

3.4.2 Traveling waves in the lattice

Now, we search for traveling front solution of the lattice (3.23) fulfilling

$$U_{i,j}(t) = U(t - b_1 i - b_2 j) = U(s) \tag{3.32a}$$
$$V_{i,j}(t) = V(t - b_1 i - b_2 j) = V(s)\ . \tag{3.32b}$$

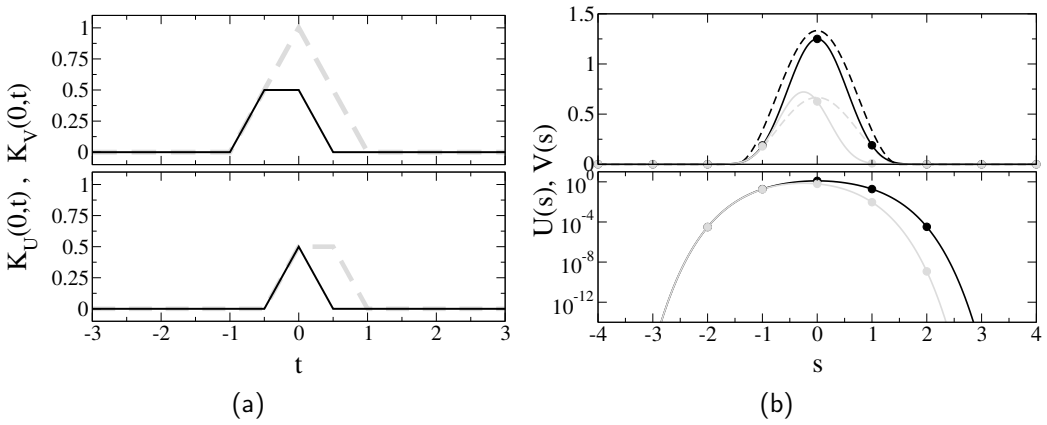

Figure 3.10: (a): The kernels in (3.35) at the position $s = 0$ for $b_1 = 1$ and $b_2 = 1/2$, or equivalently $\lambda = \sqrt{5}/2$ and $\theta = \arctan 1/2$. Upper panel: dashed line shows the kernel $K_{U1}(s,t)$ for $s = 0$ and the bold line $K_{V1}(s,t)$. Lower panel: dashed line shows $K_{U2}(s,t)$ and the bold line $K_{V2}(s,t)$. (b) The shape of the traveling wave solution obtained by the numerical scheme (3.36). The velocities are again $b_1 = 1$ and $b_2 = 1/2$. The black (grey) line is the traveling front solution $U(s)$ ($V(s)$), whereas the black (grey) dots symbolize the wave on the lattice. The dashed lines show the solution of the QCA.

This ansatz implies, that the traveling wave has to obey

$$U(s - b_2) - U(s) = V(s - b_1) - V(s) \ , \tag{3.33}$$

which follows directly from the definitions of the difference coordinates. Inserting (3.32) into (3.23) yields an advance-delay equation

$$\begin{aligned} U_{ss}(s) &= U(s + b_1)^n - 2U(s)^n + U(s - b_1)^n + \\ &\quad V(s - b_1)^n - V(s)^n + V(s + b_2)^n - V(s - b_1 + b_2)^n \qquad (3.34a) \\ V_{ss}(s) &= V(s + b_2)^n - 2V(s)^n + V(s - b_2)^n + \\ &\quad U(s - b_2)^n - U(s)^n + U(s + b_1)^n - U(s - b_2 + b_1)^n \ . \qquad (3.34b) \end{aligned}$$

As already noticed above, these equations are difficult solve and analyze, even numerically. Nevertheless, we can integrate them twice and obtain

$$U(s) = \int_{s-b_1}^{s+b_1} K_{U1}(s,t)U(t)^n \mathrm{d}t + \int_{s-b_1}^{s+b_2} K_{V1}(s,t)V(t)^n \mathrm{d}t \tag{3.35a}$$

$$V(s) = \int_{s-b_2}^{s+b_2} K_{V2}(s,t)V(t)^n \mathrm{d}t + \int_{s-b_2}^{s+b_1} K_{U2}(s,t)U(t)^n \mathrm{d}t \ . \tag{3.35b}$$

For $b_1 = 1$ and $b_2 = 1/2$ the kernels are shown in Fig. 3.10(a) and the definition is given in (B.4) and (B.5). The full derivation of Eqs. (3.35) is shown in appendix B.3. Now,

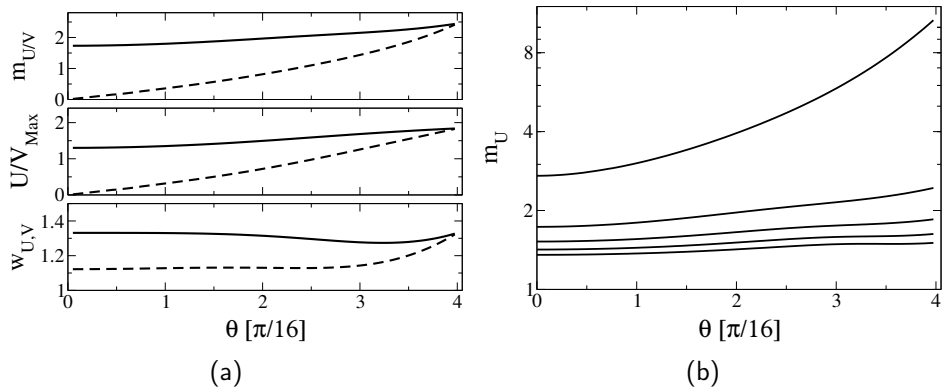

Figure 3.11: Quantitative characterization of the traveling wave fronts in the lattice. Panel (a) shows the mass (m_U, m_V), the maximas ($U_{\max}$, $V_{\max}$) and the width ($w_U = m_U/U_{\max}$, $w_V = m_V/V_{\max}$) in dependence of the propagation direction θ and for fixed nonlinearity $n = 3$ and velocity $\lambda = 1$. The solid lines are the values for U, whereas the dashed lines the values for V. In panel (b) the dependence of the mass m_U on the propagation direction θ for various values of the nonlinearity index n is plotted. The mass scale is logarithmic and the lines refer to $n = 3/2, 3, 9/2, 6, 15/2$ (from top to bottom).

we contruct a numerical method based on Eqs. (2.34) and (3.14) to solve the integral equation. Therefore, we start from an initial wave profile $U_0(s)$, $V_0(s)$ and iteratively apply

$$U^\star(s) = \int_{s-b_1}^{s+b_1} K_{U1}(s,t)U_i(t)^n \mathrm{d}t + \int_{s-b_1}^{s+b_2} K_{V1}(s,t)V_i(t)^n \mathrm{d}t \tag{3.36a}$$

$$V^\star(s) = V^\star(s-b_1) + U^\star(s-b_2) + U^\star(s) \tag{3.36b}$$

$$\begin{pmatrix} U_{i+1} \\ V_{i+1} \end{pmatrix} = \left(\frac{||(U_i, V_i)||}{||(U^\star, V^\star)||} \right)^\alpha \begin{pmatrix} U^\star \\ V^\star \end{pmatrix} , \tag{3.36c}$$

with $\alpha = n/(n-1)$. As norm, we have used the L_2-norm:

$$||(U,V)|| = \left\{ \int \Big(U^2(\tau) + V^2(\tau) \Big) \mathrm{d}\tau \right\}^{1/2} .$$

The normalization is necessary to avoid convergence to the constant solution $U = V = 0$.

In Fig. 3.10(b) we show the shape of the solitary wave for the nonlinearity $n = 3$ and $b_1 = 1$ and $b_2 = 1/2$. First, one notices that the profiles are not centered at the same positions. This is due to the fact, that the U and V component of the wave are mapped on the same range s although the wave is more narrow in in V-component. Secondly, one observes again the super-exponential decaying tails, which results from the nonlinear coupling.

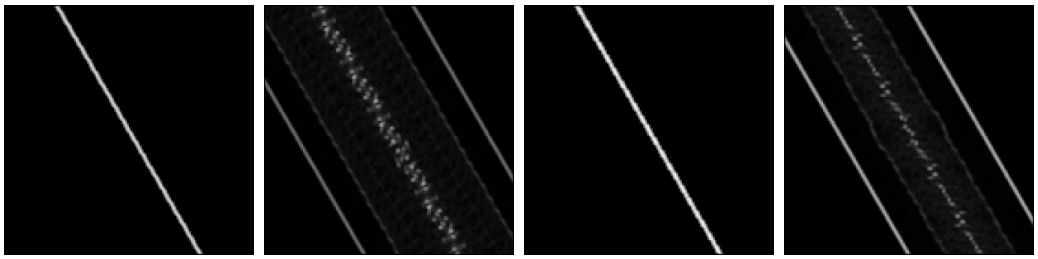

(a) (b) (c) (d)

Figure 3.12: Evolution of compact traveling wave fronts from plane initial conditions. The nonlinearity index is $n = 3$ and the lattice size is 136×136. (a) An initial step in the coordinate space as defined in the text. Shown is the local energy (3.37). The height of the step is 1 and its orientation against the x-axis is $\theta = \pi/6$. (b) The state of the lattice at $t = 100$. One can see, that traveling compact fronts have been emerged. (c) An initial pulse in the momentum space. The orientation of this pulse is $\theta = \pi/6$. Shown is the local energy. (d) The state of the lattice at $t = 50$. Again, one recognized the formation of a series of compact traveling fronts.

To give a quantitative characterization of the wave fronts we have calculated its mass $m_U = \int U(s)\mathrm{d}s$, $m_V = \int V(s)\mathrm{d}s$, the maximas $U_{\max}$, $V_{\max}$ and the width $w_U = m_U/U_{\max}$, $w_V = m_V/V_{\max}$. In Fig. 3.11(a) we show these quantities in dependence on the propagation direction θ and for the nonlinearity $n = 3$. The velocity of the front was fixed to $\lambda = 1$. Results for other velocities can be obtained by the scaling relation (3.5). It is clear that for $\theta = 0$ the mass and the maxima of V vanish, since this case refers to the quasi one-dimensional case where only U is present. For $\theta = \pi/4$ both components are equal and possess the same values of $m_{U/V}$ and U/V_{max}. In the parameter region $0 < \theta < \pi/4$ one observes an increase of the mass and an increase of the maxima. In Fig. 3.11(b) the mass m_U is shown in dependence on θ for various nonlinearity indices n. One can clearly see, that for increasing nonlinearity the mass decreases.

3.4.3 Numerical studies

Now, we study the lattice directly, that is we solve Eq. (3.22) numerically. The main focus is on the emergence of compact traveling wave fronts. To present the results we use the local energy defined by

$$\begin{aligned}\mathcal{E}_{i,j} &= \frac{p_{i,j}}{2} + \frac{1}{2(n+1)}\Big(|q_{i+1,j} - q_{i,j}|^{n+1} + |q_{i,j+1} - q_{i,j}|^{n+1} \\ &\quad |q_{i,j} - q_{i-1,j}|^{n+1} + |q_{i,j} - q_{i,j-1}|^{n+1}\Big)\,, \end{aligned} \tag{3.37}$$

which is the sum of the kinetic energy and the half of the interaction energy of each particle.

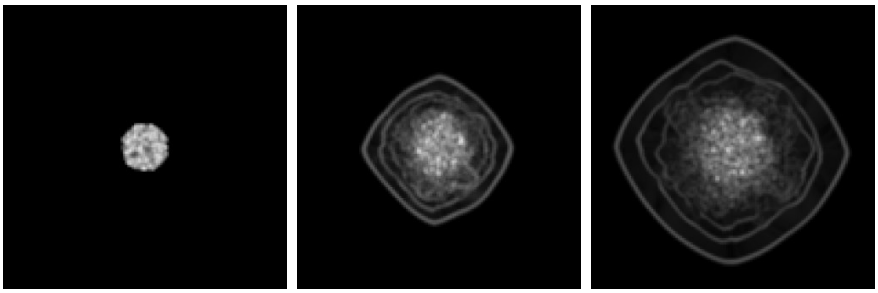

(a) (b) (c)

Figure 3.13: Evolution of random initial conditions in a circular region of the lattice. The nonlinearity is $n = 3$, the lattice dimension is 128×128. Shown is the energy defined in Eq. (3.37) for (a) $t = 0$, (b) $t = 10$ and (c) $t = 20$.

The easiest initial condition one could imagine to allow the emergence of compact traveling wave fronts is a plane step in the coordinate space q rotated by an angle θ against the x-axis. In Fig.3.12(a) we show the local energy (3.37) of such an initial condition. The height of the step is 1 and its orientation against the x-axis is $\theta = \pi/6$. The step refers in the energy representation to a plane pulse. In Fig. 3.12(b) the energy state of the lattice is shown at time $t = 100$. One can see that at least two compact traveling wave fronts have emerged and the orientation of these fronts are identical to the initial orientation of the step. Nevertheless, the initial step does not fully decompose into a series of traveling fronts. A significant part of the energy remains at the location of the initial excitation.

Similar to a step is a pulse in momentum space p. In Fig. 3.12(c) the local energy (3.37) for such a pulse is shown which is indistinguishable from the step in q. The state of the lattice at time $t = 50$ is shown in Fig. 3.12(d). Again, one recognizes a series of compact traveling fronts having the sane orientation as the initial pulse.

Other interesting phenomena related to the formation of traveling wave fronts can be observed if random localized initial conditions are investigated. In Fig. 3.13 the evolution of a random circular region in q is shown for the nonlinearity $n = 3$. The momenta are initially 0 and the radius of the circular region is $r = 10$. From this initial excitation wave fronts emerge radially and the front is compact, hence, it possesses super-exponentially-decaying tails. In Fig. 3.13 one can see at least two radial fronts. We assume, that more front have been emerged which are not visible in this plots, due to their small amplitudes and finite observation times. The fronts can be considered as deformed versions of the plane traveling compact wave fronts. During our observation they have been stable but its amplitude and radial velocity decrease during the spreading process.

3.5 Long-range interacting systems

In this section we study Hamiltonian lattices where the interaction is not limited to the nearest neighbors. An example is a chain of charged particles, where the interaction between the sites follows the long-range Coloumb law. Another examples is a chain of electric or magnetic dipoles. Lattices with long-range interaction have been widely studied in physical, biological and mathematical sciences [109–111]. In the context of traveling waves it could be shown that long-range interaction may result in solitary waves with algebraic tails in contrast to the usual exponential decay [112].

The motivation of this section is the question, if long-range interaction will destroy the super-exponential decay of the solitary waves. Therefore, we study a one-dimensional Hamiltonian lattice similar to Eq. (3.2) but with additional coupling terms

$$H = \sum_k \left\{ \frac{p_k^2}{2} + \frac{1}{n+1} \sum_{j=1}^{m} \alpha_j |q_{k+j} - q_k|^{n+1} \right\} . \tag{3.38}$$

The coefficients α_j denote the strength of the interaction and m is the interaction range. We want to stress here, that the motivation to study Eq. (3.38) is purely mathematical. A realistic physical model with long-range interaction will typically include linear terms, which can not result in compact tails.

The energy of the Hamiltonian (3.38) can be scaled to $H = 1$ by the scaling relation (3.5) and the equations of motion are

$$\ddot{q}_k = \sum_{j=1}^{m} \alpha_j \Big((q_{k+j} - q_k)^n - (q_k - q_{k-j})^n \Big) . \tag{3.39}$$

For the sake of simplicity we restrict ourself to odd n. Otherwise we have to introduce the sign function in the equations of motion. But the results presented here are valid for general nonlinearities. If one introduces the difference coordinates $Q_k = q_{k+1} - q_k$ the equations of motions are transformed to

$$\ddot{Q}_k = \sum_{j=1}^{m} \alpha_j \Big\{ (w_{k+1}^{(j)})^n - (w_{k-j+1}^{(j)})^n - (w_k^{(j)})^n + (w_{k-j}^{(j)})^n \Big\} , \tag{3.40a}$$

where

$$w_k^{(j)} = \sum_{i=0}^{i<j} Q_{k+i} \tag{3.40b}$$

are the sums of the differences.

Now, we look for traveling waves in the form $Q_k(t) = Q(s) = Q(k - \lambda t)$ with the wave velocity λ. Inserting this ansatz into (3.40) yields

$$Q_{ss} = \sum_{j=1}^{m} \alpha_j \Big\{ \big(w^{(j)}(s+1)\big)^n - \big(w^{(j)}(s-j+1)\big)^n - \big(w^{(j)}(s)\big)^n + \big(w^{(j)}(s-j)\big)^n \Big\} . \tag{3.41}$$

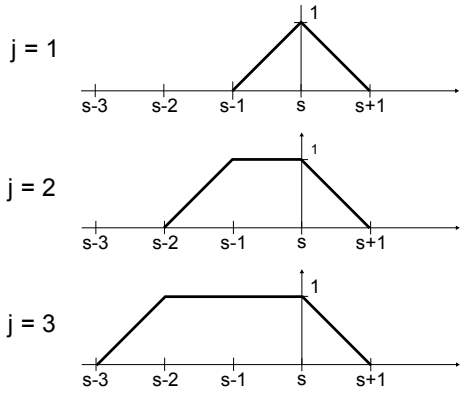

Figure 3.14: The Kernel K_j defined in (3.42b) for $j = 1, 2, 3$.

Note, that we have already set the wave velocity to $\lambda = 1$. Next, we integrate (3.41) twice and obtain

$$Q(s) = \sum_{j=1}^{m} \alpha_j \int_{s-j}^{s+1} K_j(\tau, s) \left(w^{(j)}(\tau)\right)^n \mathrm{d}\tau \ . \tag{3.42a}$$

To derive this equation we have used $Q(-j < s < m) = 0$. The kernel $K_j(\tau, s)$ is defined via

$$K_j(\tau, s) = \begin{cases} j - (s - \tau) & \text{for } s - j \leq \tau \leq s - j + 1 \\ 1 & \text{for } s - j + 1 \leq \tau \leq s \\ 1 - (\tau - s) & \text{for } s \leq \tau \leq s + 1 \ . \end{cases} \tag{3.42b}$$

In Fig. 3.14 we show $K_j(\tau, s)$ for various values of j. The complete derivation of (3.42) is shown in appendix B.4.

Now, we use a modification of the Petviashvili's scheme (3.14) to compute the traveling solutions. Therefore, one defines a starting pulse $Q_0(s)$ and then iterates

$$Q_\star = \sum_{j=1}^{m} \alpha_j \int_{s-j}^{s+1} K_j(\tau, s) \big(w_i^{(j)}(\tau)\big)^n \mathrm{d}\tau \quad \text{and} \quad Q_{i+1} = \left(\frac{||Q_i||}{||Q_\star||}\right)^\alpha Q_\star \ , \tag{3.43}$$

where $\alpha = (n + 1)/n$ ensures convergence of the algorithm. In the following we will present results for two specific interactions: constant and exponential interaction.

Constant coupling

In Fig. 3.15(a) we show the shape of the traveling wave solution obtained from the numerical scheme (3.43) for a uniform coupling $\alpha_j = \text{const.} = 1$. The nonlinearity index

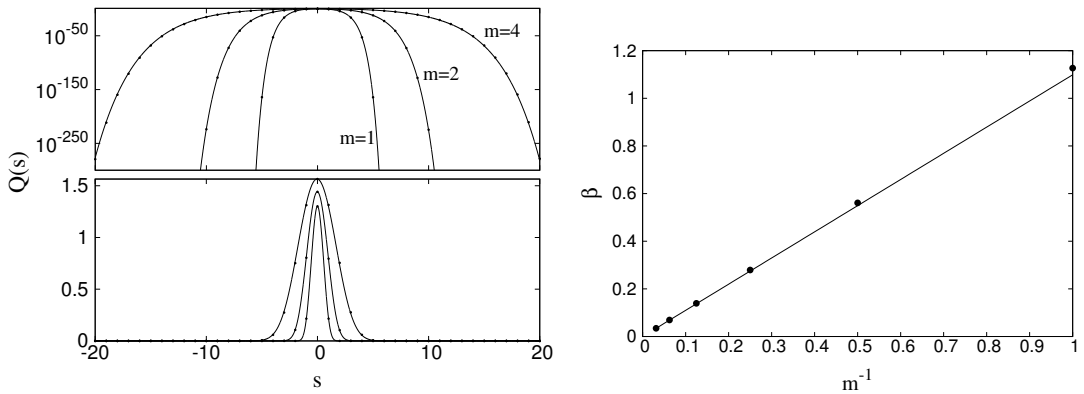

Figure 3.15: (a) Traveling waves in the Hamiltonian lattice (3.38) with constant coupling coefficient $\alpha_j = \text{const.}$, the power of the nonlinearity is $n = 3$. (b) Numerical findings and analytical estimation of the double logarithmic decay rate β of the tails of the compacton.

is $n = 3$ and the interaction length varies $m = 1, 2, 4$. For all interaction ranges m the according solitary wave possesses super-exponential decaying tails. Furhtermore, one observes that the width of the wave becomes larger with increasing m.

For the constant coupling $\alpha_j = 1$ we can estimate the decay of the tails. Therefore, the ansatz $Q(s) \sim \mathrm{e}^{-f(s)}$ is used, where the function $f(s)$ has to be determined. Since the tails of the wave are considered one can impose monotony on $f(s)$. Inserting the ansatz into Eq. (3.42a) yields

$$\mathrm{e}^{-f(s)} \sim \sum_{j=1}^{m} \int_{s-j}^{s+1} K_j(\tau, s) \left(\mathrm{e}^{-f(\tau)} + \mathrm{e}^{-f(\tau+1)} + \cdots + \mathrm{e}^{-f(\tau+(j-1))} \right)^n \mathrm{d}\tau \ . \tag{3.44}$$

Using the Laplace method we can approximate this integral and obtain

$$\mathrm{e}^{-f(s)} = \frac{\mathrm{e}^{-nf(s-m)}}{\left[nf'(s-m)\right]^2} \ . \tag{3.45}$$

Taking the logarithm of this equation and neglecting the term with $\log(nf'(s-m))$ yields the function $f(x) = \exp(\log n/ms)$ and finally for $Q(s)$

$$Q(s) \sim \exp(-\exp(\frac{\log n}{m}s)) = \exp(-\exp(\beta s)) \ . \tag{3.46}$$

The full derivation of (3.46) is given in appendix B.5. In Fig. 3.15(b) we show the coefficient β obtained from the traveling waves generated with (3.43) and compare it with the theoretical values (3.46). Numerical findings and our analytical estimation of β agree very well.

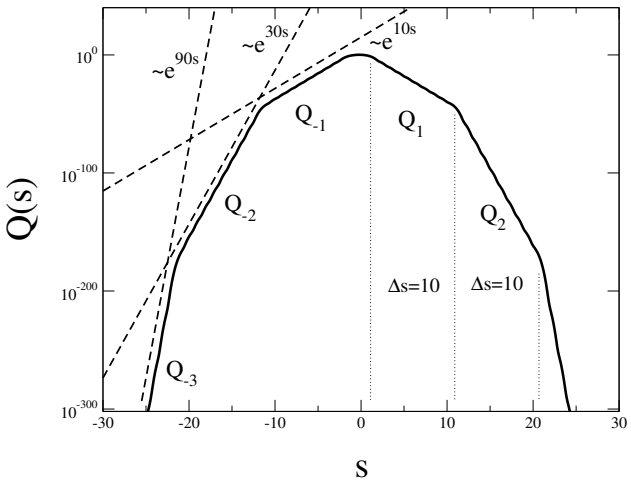

Figure 3.16: The shape of a compacton in (3.38) with an exponential decaying interaction strength (3.47) with $\kappa = 10$ and $m = 10$. This solitary wave solution consists of exponential tails of length $m = 10$ and the first three segments follow $Q(s) \sim \exp(-10s)$, $Q(s) \sim \exp(-30s)$ and $Q(s) \sim \exp(-90s)$.

Exponential coupling

Next, we present results for an exponential decaying interaction, also known as Kac-Baker interaction [113, 114]

$$\alpha_j \sim \mathrm{e}^{-\kappa j} \ , \tag{3.47}$$

with κ being the inverse penetration depth. In Fig. 3.16 we show the shape of a compact traveling solitary wave for $m = 10$ and $\kappa = 10$. This wave consists of a series of exponentially decaying segments $\ldots$, $Q_{-2}(s)$, $Q_{-1}(s)$, $Q_1(s)$, $Q_2(s)$, $\ldots$, where the peak is located between Q_{-1} and Q_1. Each segment has approximately the length m and it decays with

$$Q_k(s) \sim \exp\Big(- \mathrm{sign}(k)\kappa n^{|k-1|} s \Big) \ . \tag{3.48}$$

In Fig. 3.16 the first three segments decay with $\exp(-10s)$, $\exp(-30s)$ and $\exp(-90s)$. Some examples for varying parameters κ and m are shown in Fig. 3.17. One clearly observes that the length of segments is m and that the penetration depth κ changes the slope of the segments according to (3.48).

Note, that for finite m the waves always possesses super-exponential decaying tails – the result of the decay for the constant interaction is an upper bound for the case of exponential interaction. For infinite m we assume that the tails follow an exponential function.

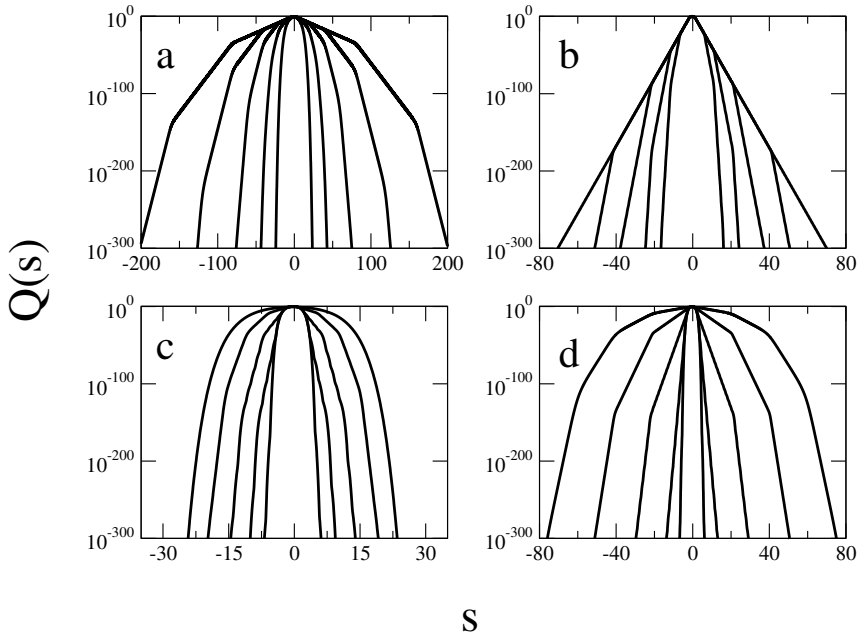

Figure 3.17: The shape of the compactons in the Hamiltonian lattice (3.38) with exponential coupling and varying interaction length m and strength κ. (a) The penetration depth is fixed to $\kappa = 1$ and m varies from 5, 10, 20, 40, 80, the according wave solutions are shown from inside to outside. (b) The same plot as in (a), but with different interaction strength $\kappa = 10$. (c) Here, the interaction length is fixed to $m = 5$ and κ varies 1, 4, 16, 64, 256. (d) The same plot as in (b), but with $m = 20$. One remarkable feature of all compacton solutions are the piecewise exponentially decaying tails, where the length of the pieces is approximately m.

3.6 Conclusion

In this chapter, we have investigated strongly nonlinear Hamiltonian lattices. Such systems play a major role in the description of compression pulses in granular chains. By means of the quasi-continuum and by an iterative Petviashvili's method we could show that compactons exists. Furthermore, we studied the lattice directly by numerical solution of the initial value problem to show how compactons emerge from initial data and how they collide. The extensive chaotic state of the strongly nonlinear Hamiltonian has been characterized by Lyapunov exponents and the Lyapunov spectrum.

Two generalizations of the one-dimensional chain have been introduced: First, a two- or higher-dimensional lattice, which is important for real-world applications especially in the context of granular and atomic systems. Again, the strongly nonlinear interaction between the particles causes super-exponential traveling waves which appear in the form of traveling fronts. Secondly, we studied a lattice with long-range interaction. Here, we have been interested in the question for the existence of the super-exponential tails. Interestingly, it could be shown that the tails remain compact if the interaction range

is finite. For an infinite range the super-exponential tails vanish, even in the case of an exponential decaying coupling.

Chapter 4

Compactons in discrete Schrödinger systems

In this section we study compactons in systems which are related to the discrete nonlinear Schrödinger Equation (DNLS)

$$\mathrm{i}\dot{\Psi}_k = \Psi_{k+1} + \Psi_{k-1} + \beta|\Psi_k|^2\Psi_k \ . \tag{4.1}$$

Here, Ψ_k is the complex field at lattice site k and β is the nonlinearity parameter. The DNLS is widely used in physical and mathematical setups, where some fields of applications have been presented in section 1.3.

4.1 The basic model

The DNLS is a Hamiltonian system and can be derived from

$$H = \sum_k \Psi_k\Psi^*_{k+1} + \Psi^*_k\Psi_{k+1} + \frac{\beta}{2}|\Psi_k|^4 \ , \tag{4.2}$$

where $(\cdot)^*$ denotes the complex conjugate. Ψ_k and Ψ^*_k are the canonical variables and the equations of motion can be obtained from $\mathrm{i}\dot{\Psi}_k = \partial H/\partial\Psi^*_k$ and $\mathrm{i}\dot{\Psi}^*_k = -\partial H/\partial\Psi_k$. See also appendix C.1 for the properties of Hamiltonian systems of type (4.1).

In the following, Hamiltonians are studied which possess a global phase invariance, meaning that $\Psi_k \mapsto \Psi_k\mathrm{e}^{\mathrm{i}\varphi}$ does not changes the Hamiltonian or the equations of motion. The Noether theorem relates this phase invariance to the norm conservation [115]

$$N = \sum_k |\Psi_k|^2 \ . \tag{4.3}$$

In this chapter, we want to study traveling waves with compact or quasi-compact support in equations related to the DNLS. In previous chapters we have seen that such structures arise if the interaction between two neighboring lattice sites is purely nonlinear. Therefore, a promising candidate to find compactons in DNLS-type models is

$$H = \sum_k \left(|\Psi_k|^2 + |\Psi_{k+1}|^2\right)\left(\Psi_k^*\Psi_{k+1} + \Psi_k\Psi_{k+1}^*\right) . \tag{4.4}$$

The terms $\Psi_k|^2|\Psi_{k+1}|^2$ and $\left(\Psi_k^2\Psi_{k+1}^{*2} + \Psi_k^{*2}\Psi_{k+1}^2\right)$ are also coupling terms of the same order, but they can not be responsible for wave propagation, which results from $\dot{\Psi}_k = 0$ for $\Psi_k = 0$, see appendix C.2. The equation of motion are given by

$$\mathrm{i}\dot{\Psi}_k = |\Psi_{k+1}|^2\Psi_{k+1} + |\Psi_{k-1}|^2\Psi_{k-1} + 2|\Psi_k|^2\left(\Psi_{k+1} + \Psi_{k-1}\right) + \Psi_k^2\left(\Psi_{k+1}^* + \Psi_{k-1}^*\right) . \tag{4.5}$$

Although Eq. (4.4) might look a bit artificial and arbitrary, a similar Hamiltonian describes a waveguide array embedded in a material with Kerr nonlinearity [116]. In this setup the coupling between two waves-guides is nonlinear. Furthermore, nonlinear interaction in the DNLS has also been studied in the context of disorder [117] and tight-binding approximation [118]. Nonlinear coupling also describes the evolution of the DNLS in terms of the linear eigenmodes [119].

In Eq. (4.4) a scaling similar to (3.5) exists

$$\Psi = a\tilde{\Psi} , \quad H = a^4\tilde{H} , \quad t = a^{-2}\tilde{t} , \quad N = \sum_k |\Psi_k|^2 = a^2\tilde{N} . \tag{4.6}$$

This is due to the fact, that each term in Eq. (4.4) is of order four. As a consequences, any traveling wave with velocity λ can be rescaled to $\lambda = 1$. An interesting case occurs, if the state $\Psi_k(t)$ can be written as $\Psi_k = u_k(t)\mathrm{e}^{\mathrm{i}\varphi}\mathrm{e}^{\mathrm{i}k\pi/2}$ with $u_k(t) \in \mathbb{R}$, $\varphi \in \mathbb{R}$. Then, the equations of motion Eqs. (4.5) reduce to

$$\dot{u}_k = u_{k+1}^3 - u_{k-1}^3 + u_k^2\left(u_{k+1} - u_{k-1}\right) , \tag{4.7}$$

which are very similar to the phase oscillator lattice (2.9). In the next section we will see that compactons exist in this reduced model.

In Chapters 2 and 3 the QCA has been used to describe the lattice and its traveling wave solutions. Of course, Eq. (4.5) can also by approximated by continuous equations. But unfortunately, we could not find any traveling wave solutions in the continuum models, such that we avoid the introduction of the QCA here.

4.2 Traveling waves

Now, we study traveling waves in the reduced equations (4.7). In the next section it is demonstrated that traveling waves also exist in the full equation (4.5), although they

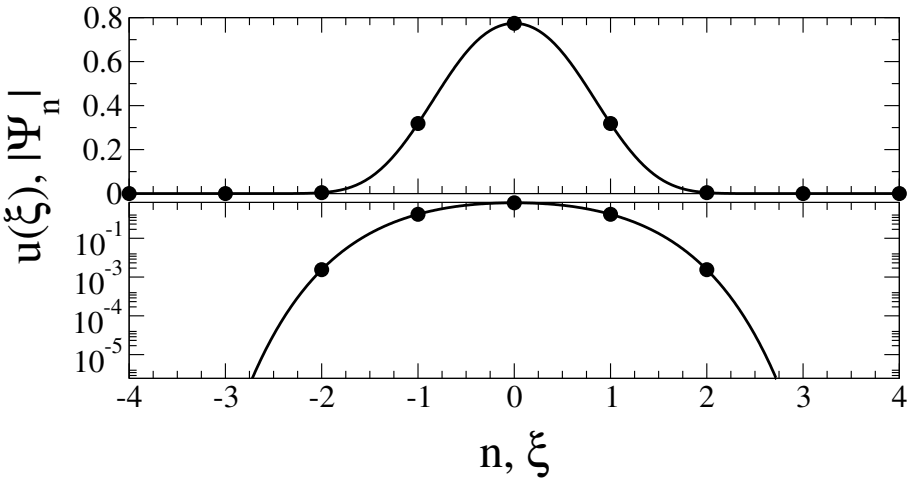

Figure 4.1: The shape of the compacton in model (4.5) for $\lambda = 1$. The straight line shows the solution $u(\xi)$ of (4.9) and the dots show the $|\Psi_k|$ on the lattice. In the logarithmic plot the super-exponential tails can be recognized.

are not stable on large time scales. We seek waves in the form

$$u_k(t) = u(k - \lambda t) \ , \tag{4.8}$$

where λ is the wave velocity. Inserting this ansatz into (4.7) yields

$$-\lambda \dot{u}(s) = u(s+1)^3 - u(s-1)^3 + u(s)^2 u(s+1) - u(s)^2 u(s-1) \ . \tag{4.9}$$

As mentioned above, the wave velocity can be scaled to $\lambda = 1$. Next, we integrate Eq.(4.9) from 0 to s. Unfortunately the integral does not become local, meaning that the part from 1 to $s-1$ does not cancels out:

$$u(s) - u(0) = -\int_0^s \Big[u(\xi+1)^3 - u(\xi-1)^3 + u(\xi)^2 u(\xi+1) - u(\xi)^2 u(\xi-1) \Big] \mathrm{d}\xi \ . \tag{4.10}$$

Nevertheless, this equation can be solved numerically by an iterative scheme, which is based on the approach of Petviashvili [65, 66] and which has been explored in the previous chapters. First, an initial pulse $u_0(s)$ is chosen. Then, the pulse is iterated via

$$u_{i+1} = \left(\frac{||u_i||}{||u_\star||} \right)^\alpha u_\star \qquad \text{with} \tag{4.11}$$

$$u_\star(s) = u_i(0) - \int_0^s \Big[u_i(\xi+1)^3 - u_i(\xi-1)^3 + u_i(\xi)^2 \Big(u_i(\xi+1) - u_i(\xi-1) \Big) \Big] \mathrm{d}\xi \ ,$$

until the scheme converges. The normalization avoids that the trivial solution $u(s) = 0$ is reached; the exponent is $\alpha = 3/2$ and the L_2-norm $||u|| = \left[\int u(s)^2 \mathrm{d}s \right]^{1/2}$ is chosen,

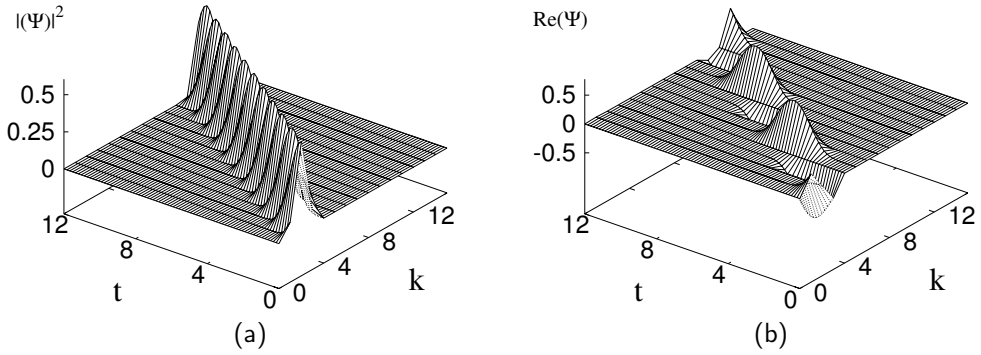

Figure 4.2: The evolution of the compacton in the lattice. Both panels show the same wave function, in (a) the norm and in (b) its real part. The phase shift between two neighboring sites is always $\pi/2$, such that the real part vanishes at every second lattice site when the compacton passes trough.

but any other norm can be used as well. In Fig. 4.1 the envelope $u(\xi)$ and the absolute value of the wave function $|\Psi_k|$ are shown. As expected, the tails converge to zero with a super-exponential rate. The evolution of an compacton in the lattice is shown in Fig. 4.2. One can see the phase shift $\pi/2$ between two neighboring sites, such that the real part of the wave function vanishes every second lattice site.

Another method for solving the traveling wave ansatz in DNLS-type equations has been proposed in [120], where the authors investigated an iterative Petviashvili's method in Fourier space. Nonetheless, they could show that a true traveling wave solution in the DNLS (4.1) can not be obtained by this method.

4.3 Numerical experiments

In this section we study the lattice equations (4.4) directly by numerical solution of the initial value problem. We will show that compactons evolve from rather general initial conditions and that they are stable under collisions.

Emergence of compactons from initial conditions

The most simple scenario is a single excited site at position k_0. Since the lattice obeys the scaling relation (4.6) and is invariant under an arbitrary phase shift one can use $\Psi_k(t=0) = \delta_{k,k_0}$ for the initial state. This kind of initial condition can be written as $\Psi_k = u_k \mathrm{e}^{\mathrm{i}\varphi} \mathrm{e}^{\mathrm{i}k\pi/2}$ for an appropriate choice of u_k. Therefore, the dynamics can be described be the reduced model (4.7) and we expect that compacts will emerge. The temporal evolution is shown in Fig. 4.3. The initial excitation triggers the emergence of

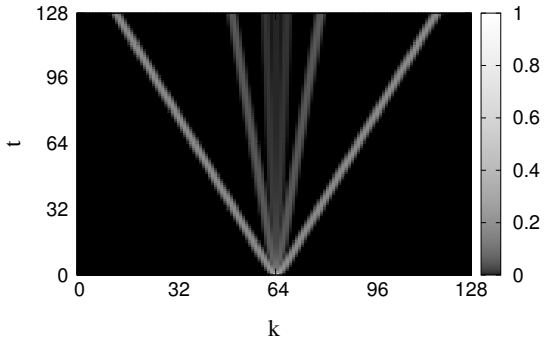

Figure 4.3: Evolution of compactons from a single excited site in (4.4). The color coding represents $|\Psi_k|^2$.

a sequence of compactons evolving to the left and right. These compactons are ordered by their amplitudes, which results from the scaling (4.6) – a large amplitude implies a large velocity.

A more complicated situation arises if two neighboring lattice sites are excited. Here, the initial conditions can be generally written as

$$\Psi_k(t=0) = \delta_{k,k_0} + r_0 \mathrm{e}^{\mathrm{i}\phi_0}\, \delta_{k,k_0+1} \ . \tag{4.12}$$

The amplitude and the phase at site k_0 are fixed, whereas at site k_0+1 the amplitude is r_0 and the phase is ϕ_0. In Fig.4.4 the evolution is shown for three exemplary parameters (r_0, ϕ_0). The left panel shows the evolution from $r_0 = 0.5, \phi_0 = \pi/2$. This initial condition matches the reduced model (4.7) and a sequence of compactons emerge to the left. In the middle panel the parameters are $r_0 = 1.0, \phi_0 = \pi/4$ which does not obey Eq. (4.7). Remarkably, a traveling solitary wave emerges, but this wave is not a true compacton. In the direction of motion it possesses a compact tail but at its back it leaves a small disturbance and looses energy. We will call this type of traveling solitary wave a quasi-compacton. Its energy loss can be also seen by the deceleration of the wave. In the right panel the parameters are $r_0 = 0.5$, $\phi_0 = \pi$ and one observes that the initial energy is localized for a finite time near the initial excitations. After a transient time this localized state spreads and possibly splits into some compactons or traveling waves.

Summarizing, three different situations have been observed: the emergence of compactons, the emergence of quasi compactons and energy localization. Here, detailed studies should be carried out. Especially, the emergence of the quasi compactons is not observed in the phase oscillator (2.9) or the Hamiltonian lattice (3.2) and seems to be a generic feature of the DNLS with nonlinear interaction. Further studies should also take more general initial conditions into account, like randomly initialized parts of the lattice.

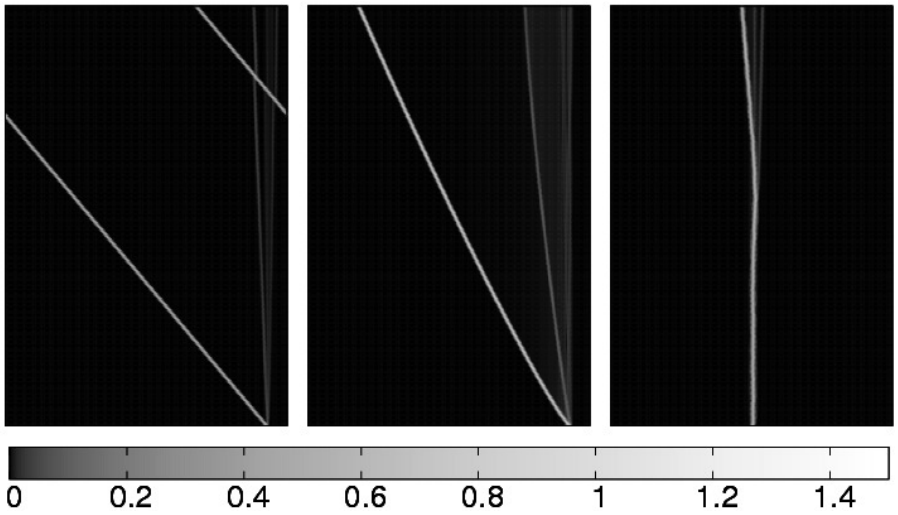

Figure 4.4: Evolution of the lattice (4.4) from two neighboring excited sites (4.12). The lattice length is $N = 256$ and the integration time $T = 256$. The x-axis is the lattice index, the y-axis is the time and the color coding represents $|\Psi_k|^2$. In the left panel $r_0 = 0.5$, $\phi_0 = \pi/2$, in the middle panel $r_0 = 1.0$, $\phi_0 = \pi/4$ and in the right panel $r_0 = 0.5$, $\phi_0 = \pi$.

Collisions of compactons

We have shown that compactons emerge from rather general initial conditions, although they might not be perfect and lose energy. Here, we study their stability due to collisions. The tails of the compactons decay very fast and the lattice can be prepared with two compactons heading towards each other and which do not interact initially. The setup is the following: First, we prepare the lattice with two compactons with different velocities and phases heading towards each other. Then, the lattice equations (4.5) are solved numerically until the collision has been finished and the resulting velocities λ_1 and λ_2 of the first and second compacton are measured. A similar study has been performed in FPU-type lattices [94].

We initialize the first compacton with the velocity $\lambda = 1$ and phase $\phi = 0$, such that its initial state can be written as $\Psi_k^{(1)}(t = 0) = u_k \mathrm{e}^{\mathrm{i}\pi k/2}\mathrm{e}^{\mathrm{i}\phi}$. u_k is calculated from (4.11) and the peak of the compacton is centered at k_1. The second compacton is created with velocity λ_0 and phase ϕ_0 but it is centered at a different lattice site k_2. Both compactons do not touch each other. Note, that the initial conditions do not reduce the equations of motion to Eq. (4.7).

In Fig. 4.5 the velocities after the collision are shown in dependence on λ_0 and ϕ_0. It is clearly visible that the collision are not always elastic. In some parameter regions the compactons gain or lose energy during the interaction. Surprisingly, one can also see that the faster compacton can gain energy.

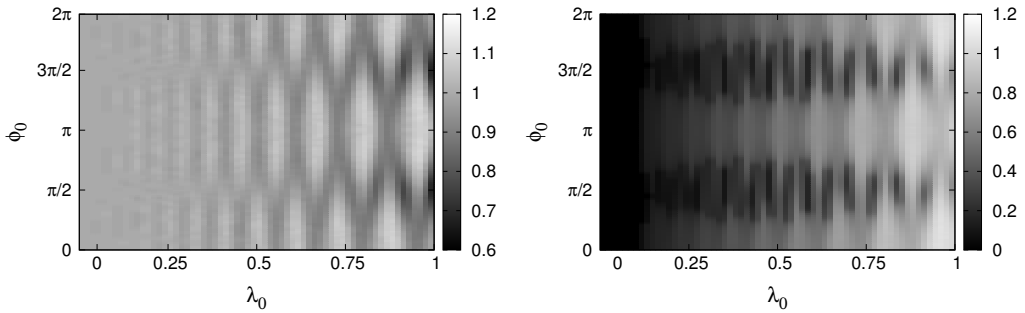

(a) λ_1 (b) λ_2

Figure 4.5: Velocities after the collision of two compactons. The initial velocity of the first compacton is $\lambda = 1$ and its phase is $\phi = 0$. See the text for a definition of the non-trivial phase. The second compacton possesses the initial velocity λ_0 and phase ϕ_0. The dependency of the velocities on these two parameters (λ_0, ϕ_0) is shown in the plots; on the left for the first compacton and on the right for the second compacton. It can be seen from this plots, that the collision are not always ideal. In some parameter regions the compactons gain or lose energy from the collision.

4.4 Conclusion

Here, a variant of the discrete nonlinear Schrödinger equation with nonlinear interaction has been introduced and studied. As we have seen in the previous chapters, nonlinear interaction may lead to compact traveling waves, which can be also observed in this model. As a particularity, the compactons in the DNLS-type lattice have a special form: the phase difference between two neighboring sites is exactly $\pi/2$. We have computed their spatial shape by means of the Petviashvili's method and we could show that this compactons emerge from specially prepared initial conditions.

For general initial conditions we have observed traveling waves which radiate energy and leave a small perturbation of the lattice. Nevertheless, in the direction of motion their tails decay super-exponentially such that we call them quasi-compactons. The exact properties of these kinds of waves have to be determined and are left as an open question.

Chapter 5

Conclusion and Outlook

Strongly nonlinear lattices play an important role in many scientific disciplines. An unusual feature of such lattices is the absence of linear terms and consequently linear waves are not present. Linearization techniques will not work and advanced analysis methods have to be introduced. In this work we have studied strongly nonlinear lattices numerically and analytically in the context of traveling waves. In particular, we have investigated compactons – traveling solitary waves with compact or quasi-compact support – in different physical setups.

5.1 Phase oscillator lattices

In this part we have studied lattices of dispersively coupled phase oscillators. Such lattices are conservative and are similar to Hamiltonian systems. Traveling waves are described by an advance-delay equation, possessing terms going forward and backward in time. In general, these equations are very difficult to solve, even numerically. But here, the advance-delay equation can be transformed into an integral equation which is solved numerically by an iterative scheme, known as Petviashvili's method. With the help of this method and by comparison with the quasi-continuous approximation it is possible to show that a large variety of traveling wave structures exist in one-dimensional chains. In particular, we have investigated solitary waves with super-exponentially decaying or quasi-compact tails – the compactons. Furthermore, solitary waves with oscillatory but exponentially decaying tails are described and a new class of kinks with one exponential and one compact tail are introduced. All wave structures are stable against collisions and emerge from physically realizable initial conditions.

We also studied a higher-dimensional lattice as a generalization of the chain of phase oscillators. There, we demonstrated that traveling solitary wave fronts with quasi-compact support exist. These waves have been successfully investigated by a generalization of the Petviashvili's method and by a two-dimensional quasi-continuum approach.

5.2 Hamiltonian lattices

In the second part of this work we have investigated a strongly nonlinear Hamiltonian lattice of FPU-type. A particular realization of such a lattice is a chain of hard spheres, where the contact force between two neighboring spheres follows the Hertzian law $F \sim \delta^{3/2}$. We could show that traveling solitary waves are basic excitations in these lattices. They emerge from physically realizable initial conditions and are stable against small perturbations and collisions. The shape of the wave could be computed numerically by an enhancement of the Petviashvili's method and analytically from the quasi-continuous approximation of the equations of motion. It turns out that the tails of the wave decay with a super-exponential rate. Hence, these waves are compactons. Furthermore, compact breathers exist in such lattices, although they are unstable.

As an important feature of nonlinear systems in general and strongly nonlinear ones in particular we have studied the chaotic state of the lattice. This state emerges from a variety of different initial conditions. One possibility is due to multiple collisions of compactons: although compactons are stable against collisions this process is not purely elastic and a small part of the compacton's energy remains at the position of the collision. This energy might trigger a multiple scattering process which results in the chaotic state. Of course, the chaotic state also appears from random initial conditions. We characterize chaos by Lyapunov-exponents and demonstrate that the thermodynamic limit is reached for small system sizes.

Two generalizations of the one-dimensional chain have been studied: A two-dimensional square lattice and a strongly nonlinear Hamiltonian with long-range interaction. In the 2D-lattice solitary traveling fronts have been found and analyzed by the help of the Petviashvili's method and the QCA. Due to the strongly nonlinear interaction these waves are quasi compact and we demonstrated how they emerge from localized initial conditions. For the long-range interacting Hamiltonian the motivation of our studies has been the question for the existence of the compact tails. It could be shown, that for finite interaction ranges the tails always remain compact. For an infinite interaction range the particular case of an exponentially decaying coupling strength has been investigated in detail. In this case the quasi-compact tails are lost and decay exponentially.

5.3 Discrete nonlinear Schrödinger lattices

In the third and last part some results concerning compactons in lattices similar to the discrete nonlinear Schrödinger equation are presented. The model we have used here is a strongly nonlinear version of the DNLS and we could show, that compactons also exist in this model. They have a specific form; the phase difference between two lattice sites is exactly $\pi/2$. We could compute the shape of the compactons with the help of

the Petviashvili's method and we have shown that these compactons emerge from initial conditions fulfilling the phase relation. For general initial conditions quasi-compactons could be observed. These objects are stable, at least during the observation time but they radiate energy and are not exact traveling wave solutions.

5.4 Open questions and outlook

Influence of dissipation: In this work, we have studied lattices which conserve energy or are at least conservative. The influence of dissipation has been totally neglected. In this context many interesting and important questions arise. The existence of traveling waves is not clear, as well as their stability and life time. Another issue concerns the super-exponential decay of the tails. It is assumed, that the tails remain compact if dissipation is also strongly nonlinear. For example, this is the case for realistic friction in granular chains [121, 122].

Stability of compactons: The stability of compactons has been studied in terms of numerical simulations and collisions between the compactons. A general theory based on perturbation arguments has not been worked out so far. This could be carried out with the help of the works from G. Friesecke and R. Pego [83–86].

Destruction of compactons due to inhomogeneities and disorder: Another major question is the behavior of compactons in the presence of local inhomogeneities and disorder. We assume that three major phenomena can be observed: absorption of energy, scattering and transmission, see Fig. 5.1 for an illustrative example of such processes in the Hamiltonian lattice (3.2). It is a major task to understand this behavior as well as characterizing them qualitatively and quantitatively and to give statistical measures like the mean-free path of compactons in a disordered medium.

Statistical properties: The statistical properties of the lattice and the traveling waves have not been studied in all details. For example, a detailed analysis of the collisions would be very interesting and would give valuable insights and hints for applications. The life-time of compactons and the creation of small-amplitude compactons from the collisions are important questions in this direction. Another direction is the question of the emergence of compactons from initial conditions which could be investigated statistically. A third topic are the thermodynamic properties of strongly nonlinear lattices, like heat transport or thermalization. The existence of a compacton or a kink gas in such lattices could also be addressed in this topic.

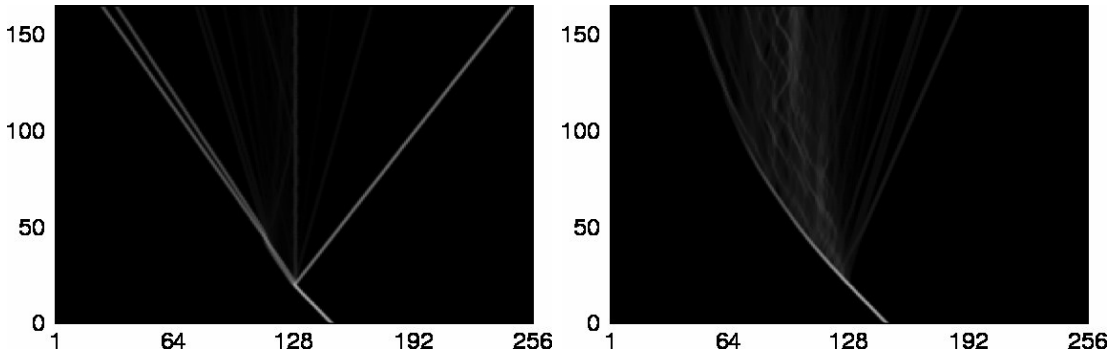

Figure 5.1: Scattering of compacton on inhomogeneities in (3.2) with nonlinearity $n = 3$. The inhomogeneities have been introduced by adding a local linear terms $\omega_k^2 q_k^2/2$. On the left plot the scattering on 10 sites with random eigenfrequencies ω_k is shown. One observes that some part of the compacton is reflected but some energy also tunnels through the inhomogeneity. On the right panel the apsorption of a compacton in a disordered region is shown. Here, all lattice sites with $k < 128$ posseses a local random potential and the compacton is slowly decelerated and absorbed.

Different topologies: In this work, only regular lattice topologies have been studied. It would be desirable to enhance the results to irregular topologies like networks or networks of regular pieces. Strongly nonlinear lattices are predestinate candidates to study such systems, since their excitations are super-exponentially localized and can be easily detected. Furthermore, the two- or three-dimensional lattices could be investigated with different topologies like hexagonal or honeycomb geometry.

Appendix A

Compactons in phase oscillator lattices

A.1 Averaging of the phase equations

The coupling function $\tilde{q}$ in (2.3) can be expressed as a Fourier series

$$\tilde{q}\left(\varphi_l, \varphi_k\right) = \sum_{i,k=-\infty}^{\infty} A_{i,j} \mathrm{e}^{\mathrm{i}(i\varphi_k + j\varphi_l)} \ . \tag{A.1}$$

Now, we write

$$\varphi_k = \omega_k t + \phi_k \ , \tag{A.2}$$

where ϕ_k is small due to the weak coupling. Then the terms with $i\omega_k + j\omega_l \approx 0$ are in resonance. Consider $\omega_k = \omega_l = \omega$. Inserting Eq. (A.2) into Eq. (A.1) and separating the resonant terms where $i = -j$ yields

$$\tilde{q}\left(\varphi_l, \varphi_k\right) = \sum_{i} A_{i,-i} \mathrm{e}^{\mathrm{i}i(\phi_l - \phi_k)} + \sum_{i,j,i\neq -j} A_{i,j} \mathrm{e}^{\mathrm{i}(i\phi_l + j\phi_k)} \mathrm{e}^{\mathrm{i}\omega t(i+j)} \ . \tag{A.3}$$

All summands in the second term of this equation oscillate fast. After averaging over one period only the resonant terms remain and we can write

$$\tilde{q}\left(\varphi_l, \varphi_k\right) \approx \sum_{i} A_{i,-i} \mathrm{e}^{\mathrm{i}i(\varphi_l - \varphi_j)} = q(\varphi_l - \varphi_k) \ . \tag{A.4}$$

If the frequencies are not equal the above equation can not be valid. But, if one assumes that ω_k is a rational multiple of ω_l ($r\omega_l = s\omega_k$ with r and s being integers without a common divisor) the resonant terms have the form

$$A_{ri,-si} \mathrm{e}^{\mathrm{i}i(r\phi_l - s\phi_k)} \ .$$

Then, the analogon of (A.4) reads

$$\tilde{q}\left(\varphi_l, \varphi_k\right) \approx \sum_i A_{ri,-si} \mathrm{e}^{\mathrm{i}i(r\varphi_l - s\varphi_k)} = q(r\varphi_l - s\varphi_k) \ . \tag{A.5}$$

A.2 Quasi continuous approximation of the phases

In this section we derive a quasi-continuous approximation of the phase variables in (2.5). That is, we Taylor expand $\varphi_{k\pm1}$ up to order 3

$$\varphi_{k\pm1} = \varphi \pm h\frac{\partial}{\partial x}\varphi + \frac{h^2}{2}\frac{\partial^2}{\partial x^2}\varphi \pm \frac{h^3}{6}\frac{\partial^3}{\partial x^3}\varphi \ , \tag{A.6}$$

where h is the lattice spacing. Inserting (A.6) into (2.5) yields

$$\dot{\varphi} = q\left(h\varphi_x + \frac{h^2}{2}\varphi_{xx} + \frac{h^3}{6}\varphi_{xxx}\right) + q\left(h\varphi_x - \frac{h^2}{2}\varphi_{xx} + \frac{h^3}{6}\varphi_{xxx}\right) \ . \tag{A.7}$$

Note, that we have used $q(v) = q(-v)$. To compare this equation with (2.14) we introduce $v = h\varphi_x$, differentiate (A.7) with respect to x, and multiply it with h. This yields

$$v_t = h\frac{\partial}{\partial x}\left\{q\left(v + \frac{h}{2}v_x + \frac{h^2}{6}v_{xx}\right) + q\left(v - \frac{h}{2}v_x + \frac{h^2}{6}v_{xx}\right)\right\} \ . \tag{A.8}$$

Now, we are nearly done and develop this equation in h:

$$\begin{aligned} v_t &= 2h\frac{\partial}{\partial x}q(v) + h^3\frac{\partial}{\partial_x}\left(\frac{1}{4}q''(v)v_x^2 + \frac{1}{3}q'(v)v_{xx}\right) \\ &= 2\left[h\frac{\partial}{\partial x} + \frac{h^3}{6}\frac{\partial^3}{\partial x^3}\right]q(v) - \frac{h^3}{12}\frac{\partial}{\partial x}\left(q''(v)v_x^2\right) \ . \end{aligned} \tag{A.9}$$

A.3 Transition from solitary to periodic waves in the QCA

To investigate the behavior of (2.18) in the vicinity of the critical wave velocity $\lambda_C = -2q'(v^*)$ we develop Eq. (2.17) up to second order in u and v around the fixed point 0, v^*:

$$\dot{v} = u \quad , \qquad \dot{u} = -\frac{3}{a}(\lambda + 2a)v + \frac{3b}{a^2}(\lambda + a)v^2 - \frac{b}{a}u^2 \ , \tag{A.10}$$

with $a = q'(v^*)$ and $b = q''(v^*)$. Introducing the control parameter $\mu = \lambda + 2a$ and using the scaling $v \mapsto b^{-1}v$ and $t \mapsto \sqrt{a/3}t$ yields

$$\ddot{v} = -\mu v + \frac{1}{a}(\mu - a)v^2 - \frac{1}{a}u^2 \ . \tag{A.11}$$

We are interested in the behavior of this equation in the vicinity of the critical velocity $\lambda_C = -2a$ or equivalently $\mu_C = 0$, such that $\mu - a \approx -a$. This yields the final equation

$$\ddot{v} = -\mu v - v^2 - \frac{1}{a}u^2 \ . \tag{A.12}$$

A.4 QCA of the two-dimensional phase lattice

Here, we derive the QCA of Eq. (2.40). Therefore, the phases $\varphi_{i,j}$ are replaced by a continuous variable $\varphi(x, y)$ and the phase variables $\varphi_{i\pm1,j}$, $\varphi_{i,j\pm1}$ are Taylor expanded up to third order expanded by $\varphi_{i\pm1,j} = \varphi \pm h\varphi_x + h^2/2\varphi_{xx} \pm h^3/6\varphi_{xxx}$ and $\varphi_{i,j\pm1} = \varphi \pm h\varphi_y + h^2/2\varphi_{yy} \pm h^3/6\varphi_{yyy}$. h denotes the lattice spacing and the subscripts are the partial derivatives into the x and y direction. Inserting the expansion into (2.40) and using the symmetry relation $q(v) = q(-v)$ yields

$$\begin{aligned}\dot{\varphi} \ = \ & q\left(h\varphi_x + \frac{h^2}{2}\varphi_{xx} + \frac{h^3}{6}\varphi_{xxx}\right) + q\left(h\varphi_x - \frac{h^2}{2}\varphi_{xx} + \frac{h^3}{6}\varphi_{xxx}\right) + \\ & q\left(h\varphi_y + \frac{h^2}{2}\varphi_{yy} + \frac{h^3}{6}\varphi_{yyy}\right) + q\left(h\varphi_y - \frac{h^2}{2}\varphi_{yy} + \frac{h^3}{6}\varphi_{yyy}\right) \ .\end{aligned} \tag{A.13}$$

Without the explicit knowledge of the coupling function, this equation can not be simplified further. But one can define $u = h\varphi_x$ and $v = h\varphi_y$ and differentiate (A.13) into x- and y- direction to obtain

$$\begin{aligned}\dot{u} =& 2h\partial_x\Big(q(u) + q(v)\Big) + h^3\Big\{\frac{1}{3}\,q'(u)u_{xxx} + \frac{5}{6}\,q''(u)u_x u_{xx} + \frac{1}{4}\,q^{(3)}(u)u_x^3 \\ & + \frac{1}{3}\,q'(v)v_{xyy} + \frac{1}{3}\,q''(v)v_x v_{yy} + \frac{1}{2}\,q''(v)v_y v_{xy} + \frac{1}{4}\,q^{(3)}(v)v_x v_y^2\Big\}\end{aligned} \tag{A.14a}$$

$$\begin{aligned}\dot{v} =& 2h\partial_y\Big(q(u) + q(v)\Big) + h^3\Big\{\frac{1}{3}\,q'(v)v_{yyy} + \frac{5}{6}\,q''(v)v_x v_{yy} + \frac{1}{4}\,q^{(3)}(v)v_y^3 \\ & + \frac{1}{3}\,q'(u)u_{xxy} + \frac{1}{3}\,q''(u)u_y u_{xx} + \frac{1}{2}\,q''(u)u_x u_{xy} + \frac{1}{4}\,q^{(3)}(u)u_y u_x^2\Big\} \ .\end{aligned} \tag{A.14b}$$

Appendix B

Compactons in Hamiltonian lattices

B.1 Compact breathers

We study compact breathers in the the Hamiltonian (3.2) with $n = 3$. We look for breathers in the form of $q_k(t) = (-1)^k u_k f(t)$. Inserting this ansatz into (3.3) and separating the time and the space dependence yields

$$\begin{aligned} \ddot{f} + Cf^3 &= 0 \\ (u_{k+1} + u_k)^3 + (u_k + u_{k-1})^3 &= Cu_k \ , \end{aligned}$$

where C is a constant. The first equation can be solved by $f(t) = A\mathrm{cn}(\omega t, \frac{1}{\sqrt{2}})$, where $\omega = A\sqrt{C}$. The solution for the lattice part can be obtained iteratively. First one defines an initial state u_k^0 and then iterates

$$\begin{aligned} u_k^\star &= \frac{1}{C}\left((u_{k+1}^i + u_k^i)^3 + (u_k^i + u_{k-1}^i)^3\right) \\ u_k^{i+1} &= u_k^\star \left(\frac{||u^i||}{||u^\star||}\right)^{3/2} \ , \end{aligned}$$

where i is the iteration index.

B.2 QCA for the two-dimensional lattice

The equations of motion for the lattice are given by (3.22). The quasi-continuous approximation is derived by introducing $q_{i,j} \approx q(x, y)$ and neighboring sites are expanded

by a Taylor series of order 4, for example $q_{i+1,j} \approx q + hq_x + h^2/2q_{xx} + h^3/6q_{xxx} + h^4/24q_{xxxx}$, where h is the spatial difference. This yields

$$\begin{aligned}\ddot{q} &= nh^{n+1}\Big([q_x]^{n-1}q_{xx} + [q_y]^{n-1}q_{yy}\Big) + h^{n+3}\Bigg\{\frac{n}{12}\Big([q_x]^{n-1}q_{xxxx} + [q_y]^{n-1}q_{yyyy}\Big) \\ &+ \frac{n(n-1)}{6}\Big([q_x]^{n-2}q_{xx}q_{xxx} + [q_y]^{n-2}q_{yy}q_{yyy}\Big) \\ &+ \frac{n(n^2-3n+2)}{24}\Big([q_x]^{n-3}[q_{xx}]^3 + [q_y]^{n-3}[q_{yy}]^3\Big)\Bigg\}\,. \end{aligned} \tag{B.1}$$

A continuous analogon for differences of the lattice variables can be obtained by introducing the variables $q_x = U/h$ and $q_y = V/h$ and differentiation of (B.1) with respect to x and y:

$$\begin{aligned}\ddot{U} &= h^2\Big([U^n]_{xx} + [V^n]_{xy}\Big) + h^4\Bigg\{A_1\Big(U^{n-1}U_{xxxx} + V^{n-1}V_{xyyy}\Big) \\ &\quad B_1\Big(U^{n-2}(3U_xU_{xxx} + 2U_{xx}^2) + V^{n-2}(V_xV_{yyy} + 2V_{xy}V_{yy} + 2V_{xyy}V_y)\Big) \\ &\quad +C_1U^{n-3}[U_x]^2U_{xx} + V^{n-3}\Big(C_2V_xV_yV_{yy} + C_3V_{xy}[V_y]^2\Big) \\ &\quad +D_1\Big(U^{n-4}[U_x]^4 + V^{n-4}V_x[V_y]^3\Big)\Bigg\}\end{aligned} \tag{B.2a}$$

$$\begin{aligned}\ddot{V} &= h^2\Big([U^n]_{xy} + [V^n]_{yy}\Big) + h^4\Bigg\{A_1\Big(V^{n-1}V_{yyyy} + U^{n-1}U_{xxxy}\Big) \\ &\quad B_1\Big(V^{n-2}(3V_yV_{yyy} + 2[V_{yy}]^2) + U^{n-2}(2U_xU_{xxy} + 2U_{xx}U_{xy} + U_{xxx}U_y)\Big) \\ &\quad +C_1V^{n-3}[V_y]^2V_{yy} + U^{n-3}\Big(C_2U_xU_{xx}U_y + C_3U_{xy}[U_x]^2\Big) \\ &\quad +D_1\Big(V^{n-4}[V_y]^4 + U^{n-4}[U_x]^3U_y\Big)\Bigg\}\,.\end{aligned} \tag{B.2b}$$

The constants are given by

$$A_1 = \frac{n}{12}\,,\quad B_1 = \frac{n(n-1)}{12}\,,\quad C_1 = \frac{7n(n^2-3n+2)}{24}\,,\quad C_2 = \frac{n(n^2-3n+2)}{6}$$

$$C_3 = \frac{n(n^2-3n+2)}{8} \quad \text{and} \quad D_1 = \frac{n(n^3-6n^2+11n-6)}{24}\,.$$

B.3 Integral equation for traveling fronts in the 2D lattice

The equations to solve are given in Eq. (3.34). For simplicity we define

$$U(s)^n = u(s)\ , \quad V(s)^n = v(s)\ , \quad F(s) = \int_{s_0}^{s} u(t)\mathrm{d}t\ , \quad G(s) = \int_{s_0}^{s} v(t)\mathrm{d}t\ . \tag{B.3}$$

Furthermore, it is assumed that a s_0 exist with $U(s < s_0+b_1+b_2) = V(s < s_0+b_1+b_2) = 0$. We start from (3.34a). Integration from s_0 to s yields

$$\begin{aligned} U_s &= F(s+b_1) - F(s) - \Big(F(s) - F(s-b_1)\Big) \\ &\quad + G(s+b_2) - G(s) - \Big(G(s-b_1+b_2) - G(s-b_1)\Big)\ . \end{aligned}$$

Integrating once more results in

$$U(s) = \int_{s}^{s+b_1} F(t)\mathrm{d}t - \int_{s-b_1}^{s} F(t)\mathrm{d}t + \int_{s}^{s+b_2} G(t)\mathrm{d}t - \int_{s-b_1}^{s-b_1+b_2} G(t)\mathrm{d}t\ .$$

Every term is now integrated partially and one obtains

$$\begin{aligned} U(s) &= tF(t)\Big|_{s}^{s+b_1} - tF(t)\Big|_{s-b_1}^{s} + tG(t)\Big|_{s}^{s+b_2} - tG(t)\Big|_{s-b_1}^{s-b_1+b_2} \\ &\quad - \int_{s}^{s+b_1} tF'(t)\mathrm{d}t + \int_{s-b_1}^{s} tF'(t)\mathrm{d}t - \int_{s}^{s+b_2} tG'(t)\mathrm{d}t + \int_{s-b_1}^{s-b_1+b_2} tG'(t)\mathrm{d}t\ . \end{aligned}$$

This equation can be simplified to

$$U(s) = \int_{s-b_1}^{s+b_1} K_{U1}(s,t)u(t)\mathrm{d}t + \int_{s-b_1}^{s+b_2} K_{V1}(s,t)v(t)\mathrm{d}t\ , \tag{B.4a}$$

with the kernels

$$K_{U1}(s,t) = b_1 - |s-t| \tag{B.4b}$$

$$K_{V1}(s,t) = \begin{cases} b_1 - (s-t) & \text{for } s-b_1 \le t \le s-b1+b_2 \\ b_2 & \text{for } s-b_1+b_2 \le t \le s \\ b_2 - (t-s) & \text{for } s \le t \le s+b_2\ . \end{cases} \tag{B.4c}$$

For the equation for $V(s)$ one obtains a similar result

$$V(s) = \int_{s-b_2}^{s+b_2} K_{V2}(s,t)v(t)\mathrm{d}t + \int_{s-b_2}^{s+b_1} K_{U2}(s,t)u(t)\mathrm{d}t \tag{B.5a}$$

with the kernels

$$K_{V2}(s,t) = b_2 - |s-t| \tag{B.5b}$$

$$K_{U2}(s,t) = \begin{cases} b_2 - (s-t) & \text{for } s-b_2 \le t \le s \\ b_2 & \text{for } s \le t \le s+b_1-b_2 \\ b_1 - (t-s) & \text{for } s+b_1-b_2 \le t \le s+b_1 \ . \end{cases} \tag{B.5c}$$

B.4 Long-range interaction: Integral equation for traveling waves

We try to find an integral equation for (3.41). Therefore, we integrate Eq. (3.41) twice and write each summand as $Q(s) = \sum \alpha_j Q_j(s)$

$$\begin{aligned} Q_j &= \int_0^s \mathrm{d}\xi \int_0^\xi \Big\{ W(\tau+1) - W(\tau-j+1) - W(\tau) + W(\tau-j) \Big\} \mathrm{d}\tau \\ &= \int_s^{s+1} F(\xi)\mathrm{d}\xi \ - \int_{s-j}^{s-j+1} F(\xi)\mathrm{d}\xi \ , \end{aligned} \tag{B.6}$$

where $F(\xi) = \int_0^\xi W(\tau)\mathrm{d}\tau$ and $W(t) = \left(w^{(j)}(t)\right)^n$. Next, we integrate this equation partially and arrive at

$$\begin{aligned} Q_j &= \xi F(\xi)\Big|_s^{s+1} - \xi F(\xi)\Big|_{s-j}^{s-j+1} - \int_s^{s+1} \xi F'(\xi)\mathrm{d}\xi + \int_{s-j}^{s-j+1} \xi F'(\xi)\mathrm{d}\xi \\ &= (s+1)F(s+1) - sF(s) - (s-j+1)F(s-j+1) + (s-j)F(s-j) \\ &\quad - \int_s^{s+1} \xi F'(\xi)\mathrm{d}\xi + \int_{s-j}^{s-j+1} \xi F'(\xi)\mathrm{d}\xi \\ &= \int_{s-j}^{s+1} K_j(\tau,s) W(\tau)\mathrm{d}\tau \ , \end{aligned} \tag{B.7}$$

where the kernel $K_j(\tau, s)$ is defined as

$$K_j(\tau,s) = \begin{cases} j-(s-\tau) & \text{for } s-j \le \tau \le s-j+1 \\ 1 & \text{for } s-j+1 \le \tau \le s \\ 1-(\tau-s) & \text{for } s \le \tau \le s+1 \ . \end{cases} \tag{B.8}$$

B.5 Long-range interaction: Estimation of the tails

To estimate the tails we start with

$$Q(s) = \sum_{j=1}^{m} \int_{s-j}^{s+1} K_j(\tau) \Big(Q(\tau) + Q(\tau+1) + \ldots Q(\tau+(j-1)) \Big)^n \mathrm{d}\tau \ . \tag{B.9}$$

Inserting the ansatz $Q(s) \sim \mathrm{e}^{-f(s)}$ yields

$$\mathrm{e}^{-f(s)} \sim \sum_{j=1}^{m} \int_{s-j}^{s+1} K_j(\tau) \Big(\mathrm{e}^{-f(\tau)} + \mathrm{e}^{-f(\tau+1)} + \ldots \mathrm{e}^{-f(\tau+(j-1))} \Big)^n \mathrm{d}\tau \ . \tag{B.10}$$

In the sum inside the integral only the first summand contributes significantly to the integral – the other terms can be neglected:

$$\mathrm{e}^{-f(s)} \sim \sum_{j=1}^{m} \int_{s-j}^{s+1} K_j(\tau) \mathrm{e}^{-nf(\tau)} \mathrm{d}\tau \ . \tag{B.11}$$

Now, we use the same argument to neglect all other terms with $j \neq m$ and obtain

$$\mathrm{e}^{-f(s)} \sim \int_{s-m}^{s+1} K_m(\tau) \mathrm{e}^{-nf(\tau)} \mathrm{d}\tau \ . \tag{B.12}$$

We approximate this integral by

$$\begin{aligned} \mathrm{e}^{-f(s)} &\sim \mathrm{e}^{-nf(s-m)} \int_{s-m}^{s+1} (\tau-(s-m)) \mathrm{e}^{-nf'(s-m)(\tau-(s-m))} \mathrm{d}\tau \\ &\sim \mathrm{e}^{-nf(s-m)} \int_{0}^{\infty} \tau \mathrm{e}^{-nf'(s-m)\tau} \mathrm{d}\tau \ = \ \frac{\mathrm{e}^{-nf(s-m)}}{\big[nf'(s-m)\big]^2} \ . \end{aligned}$$

Taking logarithm of this equation yields $f(s) = nf(s-m) + 2\log(nf'(s-m))$. Since we assume, that $f(s)$ is a rapidly decreasing function, we can neglect the last term and obtain $f(s) = nf(s-m)$ which can be solved by

$$f(s) = \mathrm{e}^{\frac{\log n}{m}s} \ . \tag{B.13}$$

Appendix C

Discrete Schrödinger systems

C.1 Properties of DNLS-type equations

For DNLS-type Hamiltonians like (4.2) the equations of motion can be obtained from $\mathrm{i}\dot{\Psi}_k = \partial H/\partial \Psi_k^*$ and $\mathrm{i}\dot{\Psi}_k^* = -\partial H/\partial \Psi_k$. The Poisson brackets are defined via

$$\big[f, g\big] = \sum_k \left(\frac{\partial f}{\partial \Psi_k} \frac{\partial g}{\partial \Psi_k^*} - \frac{\partial f}{\partial \Psi_k^*} \frac{\partial g}{\partial \Psi_k} \right) \ , \tag{C.1a}$$

and they obey the fundamental relation

$$\big[\Psi_k, \Psi_l^*\big] = \delta_{k,l} \quad , \quad \big[\Psi_k, \Psi_l\big] = 0 \quad \text{and} \quad \big[\Psi_k^*, \Psi_l^*\big] = 0 \ . \tag{C.1b}$$

The time dependency of some function $F(\Psi_k, \Psi_k^*, t)$ can then be obtained from

$$\dot{F} = -\mathrm{i}\big[F, H\big] + \frac{\partial F}{\partial t} \ , \tag{C.1c}$$

for example

$$\dot{\Psi}_k = -\mathrm{i}\big[\Psi_k, H\big] \quad \text{or} \quad \dot{\Psi}_k^* = -\mathrm{i}\big[\Psi_k^*, H\big] \ . \tag{C.1d}$$

We study Hamiltonians which can be written in the form

$$H = \sum_k \mathcal{H}_k^{(1)}(\Psi_k, \Psi_k^*) + \mathcal{H}_k^{(2)}(\Psi_k, \Psi_k^*, \Psi_{k+1}, \Psi_{k+1}^*) \ , \tag{C.2}$$

where $\mathcal{H}_k^{(1)}$ is the local one particle – or onsite – Hamiltonian and $\mathcal{H}_k^{(2)}$ is the local two particle – or interaction – Hamiltonian. Note, that both Hamiltonian may generally depend on the index k.

For systems with a global phase invariance the norm Eq. (4.3) is conserved and the according continuity equation is

$$\frac{\mathrm{d}}{\mathrm{d}t}|\Psi_k|^2 = \dot{\Psi}_k\Psi_k^* + \Psi_k\dot{\Psi}_k^* = \rho_{k,k+1} - \rho_{k-1,k} \ . \tag{C.3}$$

The quantity $\rho_{k,k+1}$ is called the probability flux from site k to site $k+1$ and its functional form has to be determined from the interaction Hamiltonian $\mathcal{H}_k^{(2)}$

$$\rho_{k,k+1} = \mathrm{i}\left(\Psi_k\frac{\partial H_k^{(2)}(\Psi_k,\Psi_k^*,\Psi_{k+1},\Psi_{k+1}^*)}{\partial\Psi_k} - \Psi_k^*\frac{\partial H_k^{(2)}(\Psi_k,\Psi_k^*,\Psi_{k+1},\Psi_{k+1}^*)}{\partial\Psi_k^*}\right) \ . \tag{C.4}$$

One can easily show that the onsite Hamiltonian $\mathcal{H}_k^{(1)}$ will not contribute to the probability flux.

With the condition of phase invariance the onsite Hamiltonian $\mathcal{H}_k^{(1)}$ can be written in the form $\mathcal{H}_k^{(1)}(\Psi_k,\Psi_k^*) = \mathcal{H}_k^{(1)}(|\Psi_k|^2)$ and this term contributes to the equations of motion in the form $\mathrm{i}\dot{\Psi}_k = \mathcal{H}_k^{(1)\prime}(|\Psi_k|^2)\Psi_k + \dots$ for example $\mathcal{H}_k^{(1)}(|\Psi_k|^2) = \beta/2|\Psi_k|^4$ yields the nonlinear onsite term in the standard DNLS (4.1).

For the interaction Hamiltonian $\mathcal{H}_k^{(2)}$ the situation is more complicated. Here, we consider interaction potentials consisting of polynomials. The order of the polynomials has to be even and each term must consist of the same number of conjugated and non-conjugated coordinates, otherwise the phase invariance of the Hamiltonian is not guaranteed. The most simple interaction Hamiltonian consist of polynomials of order two

$$\mathcal{H}_k^{(2)} = \alpha_k\left(\Psi_k\Psi_{k+1}^* + \Psi_k^*\Psi_{k+1}\right) \ , \tag{C.5a}$$

which contributes to the equations of motion by $\mathrm{i}\dot{\Psi}_k = \dots + \alpha_k\Psi_{k+1} + \alpha_{k-1}\Psi_{k-1}\dots$ and to the flux by

$$\rho_{k,k+1}^L = \mathrm{i}\,\alpha_k\left(\Psi_k\Psi_{k+1}^* - \Psi_k^*\Psi_{k+1}\right) \ . \tag{C.5b}$$

This Hamiltonian is responsible for linear interaction. The α_k's are real constants, which only depend on k.

Polynomials of order four in the interaction Hamiltonian lead to nonlinear coupling between the nodes. Four combinations of Ψ_k, Ψ_{k+1}, Ψ_k^*, Ψ_{k+1}^* exist. The according equations are shown in Appendix C.2.

Nonlinear coupling arises if the normal-or eigenmodes of the original DNLS (with a possible random onsite potential) are studied. The onsite potential can be introduced on the RHS of Eq. (4.1)

$$\mathrm{i}\dot{\Psi}_k = \Psi_{k+1} + \Psi_{k-1} + V_k\Psi_k + \beta|\Psi_k|^2\Psi_k \ , \tag{C.6}$$

where V_k is the local (and possible random) potential. The wave function can then be expressed in terms of the eigenmodes $\psi_k^{(l)}$ of the linear problem

$$\Psi_k = \sum_l C_l \psi_k^{(l)} \ , \tag{C.7}$$

which obey the equation

$$\varepsilon_l \psi_k^{(l)} = \psi_{k+1}^{(l)} + \psi_{k-1}^{(l)} + V_k \psi_k^{(l)} \ . \tag{C.8}$$

The ε_l's are the eigenvalues of the linear problem. In the linear problem each mode rotates with its frequency $-\varepsilon_l$. Using the eigenmode representation of the wave function the DNLS (C.6) transforms to

$$\mathrm{i}\dot{C}_l = \varepsilon_l C_l + \beta \sum_{l_1,l_2,l_3} V_{l,l_1,l_2,l_3} C_{l_1} C_{l_2}^* C_{l_3} \tag{C.9a}$$

$$H = \sum_l \varepsilon_l |C_l|^2 + \sum_{l,l_1,l_2,l_3} V_{l,l_1,l_2,l_3} C_{l_1} C_{l_2}^* C_{l_3} C_l^* \ , \tag{C.9b}$$

where the coefficients V_{l,l_1,l_2,l_3} are the overlaps between the eigenmodes

$$V_{l,l_1,l_2,l_3} = \sum_k \psi_k^{(l)*} \psi_k^{(l_1)} \psi_k^{(l_2)*} \psi_k^{(l_3)} \ . \tag{C.9c}$$

The coupling of the eigenmodes in (C.9) is purely nonlinear, but an infinite number of coupling terms exists. For systems with disorder the coupling strength between two neighboring modes decreases very fast, since each mode is exponentially localized. For details on disorder in DNLS-type systems, see [119] and references therein.

C.2 Interaction polynomials of order four

In this section polynomials of order four in the interaction Hamiltonian are considered. Four combinations exist:

$$\begin{aligned} \mathcal{H}_k^{(2)} &= \alpha_k \big(\Psi_k^2 {\Psi_{k+1}^*}^2 + {\Psi_k^*}^2 \Psi_{k+1}^2 \big) \quad , \\ \mathrm{i}\Psi_k &= \ldots + 2\,\Psi_k^* \big(\alpha_k \Psi_{k+1}^2 + \alpha_{k-1} \Psi_{k-1}^2 \big) + \ldots \quad , \\ \rho_{k,k+1} &= \ldots + 2 \big(\Psi_k \Psi_{k+1}^* + \Psi_k^* \Psi_{k+1} \big) \rho_{k,k+1}^L + \ldots \end{aligned} \tag{C.10}$$

$$\begin{aligned} \mathcal{H}_k^{(2)} &= \alpha_k |\Psi_k|^2 |\Psi_{k+1}|^2 \quad , \\ \mathrm{i}\Psi_k &= \ldots + \Psi_k (\alpha_k |\Psi_{k+1}|^2 + \alpha_{k-1} |\Psi_{k-1}|^2) + \ldots \quad , \\ \rho_{k,k+1} &= \ldots + 0 + \ldots \end{aligned} \tag{C.11}$$

$$\begin{aligned} \mathcal{H}_k^{(2)} &= \alpha_k|\Psi_{k+1}|^2\,(\Psi_k\Psi_{k+1}^* + \Psi_k^*\Psi_{k+1}) \quad , \\ \mathrm{i}\Psi_k &= \ldots + \alpha_k|\Psi_{k+1}|^2\Psi_{k+1} + \alpha_{k-1}\big(2|\Psi_k|^2\Psi_{k-1} + \Psi_k^2\Psi_{k-1}^*\big) + \ldots \quad , \\ \rho_{k,k+1} &= \ldots + |\Psi_{k+1}|^2\rho_{k,k+1}^L + \ldots \end{aligned} \tag{C.12}$$

$$\begin{aligned} \mathcal{H}_k^{(2)} &= \alpha_k|\Psi_k|^2\,(\Psi_k^*\Psi_{k+1} + \Psi_k\Psi_{k+1}^*) \quad , \\ \mathrm{i}\dot{\Psi}_k &= \ldots + \alpha_k\Psi_k^2\Psi_{k+1}^* + \alpha_{k-1}\big(2|\Psi_k|^2\Psi_{k+1} + |\Psi_{k-1}|^2\Psi_{k-1}\big) + \ldots \quad , \\ \rho_{k,k+1} &= \ldots + |\Psi_k|^2\rho_{k,k+1}^L + \ldots \end{aligned} \tag{C.13}$$

Remarkably, the first two combinations can not be responsible for the spreading alone. A lattice site k_0 with $\Psi_{k_0} = 0$ acts as a barrier which can not be crossed, since in this case (C.10) and (C.11) yield $\dot{\Psi}_{k_0} = 0$. Note further, that (C.12) and (C.13) are not symmetric in the lattice index k, meaning that in the Hamiltonian k and $k+1$ can not be exchanged. One can combine these two terms to obtain

$$\begin{aligned} \mathcal{H}_k^{(2)} &= \alpha_k(|\Psi_k|^2 + |\Psi_{k+1}|^2)\,(\Psi_k^*\Psi_{k+1} + \Psi_k\Psi_{k+1}^*) \quad , \\ \mathrm{i}\dot{\Psi}_k &= \ldots + \Psi_k^2(\alpha_k\Psi_{k+1}^* + \alpha_{k-1}\Psi_{k-1}^*) + 2|\Psi_k|^2(\alpha_k\Psi_{k+1} + \alpha_{k-1}\Psi_{k-1}) + \\ &\quad \alpha_k|\Psi_{k+1}|^2\Psi_{k+1} + \alpha_{k-1}|\Psi_{k-1}|^2\Psi_{k-1} + \ldots \quad , \\ \rho_{k,k+1} &= \ldots + (|\Psi_k|^2 + |\Psi_{k+1}|^2)\rho_{k,k+1}^L + \ldots \end{aligned} \tag{C.14}$$

Bibliography

[1] A. N. Lazaridi and V. F. Nesterenko, J. Appl. Mech. Tech. Phys. **26**, 405 (1985).

[2] A. Scott, *Nonlinear science: emergence and dynamics of coherent structures*, Oxford UP, Oxford, 1999.

[3] M. J. Ablowitz and P. Clarkson, *Solitons, Nonlinear Evolution Equations and Inverse Scattering*, Cambridge University Press, 1991.

[4] Y. S. Kivshar and B. A. Malomed, Rev. Mod. Phys. **61**, 763 (1989).

[5] A focus issue on "Solitons in nonintegrable systems" (ed. by Roger H. J. et al.), CHAOS **15** (2005).

[6] P. Rosenau and J. M. Hyman, Phys. Rev. Lett. **70**, 564 (1993).

[7] P. Rosenau, Phys. Rev. Lett. **73**, 1737 (1994).

[8] N. J. Zabusky and M. D. Kruskal, Phys. Rev. Lett. **15**, 240 (1965).

[9] P. Rosenau, Phys. Lett. A **311**, 39 (2003).

[10] P. Rosenau, Phys. Lett. A **118**, 222 (1986).

[11] P. Rosenau, Phys. Rev. B **36**, 5868 (1987).

[12] M. Toda, Prog. Theor. Phys. Suppl. **45**, 174 (1970).

[13] M. Toda, J. Phys. Soc. Jpn. **23**, 501 (1967).

[14] M. Toda, J. Phys. Soc. Jpn. **22**, 431 (1967).

[15] M. J. Ablowitz et al., Phys. Rev. Lett. **30**, 1262 (1973).

[16] N. N. Akhmediev, V. M. Eleonskii, and N. E. Kulagin, Theor. Math. Phys. **72**, 809 (1987).

[17] S. Flach and C. R. Willis, Phys. Rep. **295**, 181 (1998).

[18] S. Flach and A. V. Gorbach, Phys. Rep. **467**, 1 (2008).

[19] J. C. Eilbeck and M. Johansson, nlin/0211049 (2002).

[20] A. H. Nayfeh and D. T. Mook, *Nonlinear Oscillations*, Wiley, New York, 1979.

[21] S. H. Strogatz et al., Nature **438**, 43 (2005).

[22] M. Abel, S. Bergweiler, and R. Gerhard-Multhaupt, J. Acoust. Soc. Am. **119**, 2467 (2006).

[23] K. K. Likharev, *Dynamics of Josephson Junctions and Circuits*, Gordon and Breach, Philadelphia, 1991.

[24] I. Kiss, Y. Zhai, and J. Hudson, Phys. Rev. Lett. **88**, 238301 (2002).

[25] R. Kapral and K. Showalter, editors, *Chemical Waves and Patterns*, Kluwer, Dodrecht, 1995.

[26] Y. Kuramoto, *Chemical Oscillations, Waves and Turbulence*, Springer, Berlin, 1984.

[27] A. Pikovsky, M. Rosenblum, and J. Kurths, *Synchronization. A Universal Concept in Nonlinear Sciences.*, Cambridge University Press, Cambridge, 2001.

[28] A. S. Kovalev, Low Temp. Phys. **25**, 184 (1999).

[29] J. E. Prilepsky et al., Phys. Rev. B **74**, 132404 (2006).

[30] A. Pikovsky and P. Rosenau, Physica D **218**, 56 (2006).

[31] J. R. Pasta, S. M. Ulam, and E. Fermi, Studies on nonlinear problems, in *Collected works of Enrico Fermi*, volume 2, page 978, Univ. of Chicago Press, Chicago, 1965.

[32] A focus issue on "The "Fermi-Pasta-Ulam" problem – the first 50 years" (ed. by D. K. Campbell, P. Rosenau and G. Zaslavsky), CHAOS **15** (2005).

[33] S. Lepri, R. Livi, and A. Politi, Phys. Rep. **377**, 1 (2003).

[34] S. Flach, D. O. Krimer, and C. Skokos, Phys. Rev. Lett. **102**, 024101 (2009).

[35] C. Skokos et al., Phys. Rev. E **79**, 056211 (2009).

[36] O. M. Braun and Y. S. Kivshar, Phys. Rep. **306**, 1 (1998).

[37] H. M. Jaeger, S. R. Nagel, and R. P. Behringer, Rev. Mod. Phys. **68**, 1259 (1996).

[38] I. S. Aranson and L. S. Tsimring, Rev. Mod. Phys. **78**, 641 (2006).

[39] V. Nesterenko, *Dynamics of Heterogeneous Materials*, Springer, New York, 2001.

[40] S. Sen et al., Phys. Rep. **462**, 21 (2008).

[41] A. S. Davydov, J. Theor. Biol. **38**, 559 (1973).

[42] P. G. Kevrekidis, *The Discrete Nonlinear Schrödinger Equation*, Springer, Berlin, 2009.

[43] H. S. Eisenberg et al., Phys. Rev. Lett. **81**, 3383 (1998).

[44] F. Lederer et al., Phys. Rep. **463**, 1 (2008).

[45] D. N. Christodoulides and R. I. Joseph, Opt. Lett. **13**, 794 (1988).

[46] C. J. Pethick and H. Smith, *Bose-Einstein Condensation in Dilute Gases*, Cambridge University Press, Cambridge, UK, 2002.

[47] K. B. Davis et al., Phys. Rev. Lett. **75**, 3969 (1995).

[48] J. R. Ensher et al., Phys. Rev. Lett. **77**, 4984 (1996).

[49] A. J. Leggett, Rev. Mod. Phys. **73**, 307 (2001).

[50] B. P. Anderson and M. A. Kasevich, Science **282**, 1686 (1998).

[51] O. Morsch and M. Oberthaler, Rev. Mod. Phys. **78**, 179 (2006).

[52] J. Billy et al., Nature **453**, 891 (2008).

[53] G. Roati et al., Nature **453**, 895 (2008).

[54] S. Boccaletti et al., Phys. Rep. **366**, 1 (2002).

[55] J. A. Acebron et al., Rev. Mod. Phys. **77**, 137 (2005).

[56] A. Arenas et al., Phys. Rep. **469**, 93 (2008).

[57] A. Balanov et al., *Synchronization: From Simple to Complex*, Springer, 2008.

[58] S. N. Dorogovtsev, A. V. Goltsev, and J. F. F. Mendes, Rev. Mod. Phys. **80**, 1275 (2008).

[59] G. V. Osipov, *Synchronization in Oscillatory Networks*, Springer, Berlin Heidelberg, 2009.

[60] P. Rosenau and A. Pikovsky, Phys. Rev. Lett. **94**, 174102 (2005).

[61] G. Friesecke and J. Wattis, Commun. Math. Phys. **161**, 391 (1994).

[62] G. Iooss, Nonlinearity **13**, 849 (2000).

[63] G. Iooss and K. Kirchgässner, Commun. Math. Phys. **211**, 439 (2000).

[64] A. Rustichini, J. Dyn. Diff. Eq. **1**, 121 (1989).

[65] V. I. Petviashvili, Sov. J. Plasma Phys. **2**, 257 (1976).

[66] V. I. Petviashvili, Physica D **3**, 329 (1981).

[67] M. Abramowitz and I. A. Stegun, *Handbook of Mathematical Functions*, Washington, D.C., 1964.

[68] K. Ahnert and A. Pikovsky, CHAOS **18**, 037118 (2008).

[69] E. Hairer, C. Lubich, and M. Roche, *The Numerical Solution of Differential-Algebraic Systems by Runge-Kutta Methods*, Sprinter, Berlin, 1989.

[70] D. Bambusi and A. Ponno, Commun. Math. Phys. **264**, 539 (2006).

[71] G. Benettin, R. Livi, and A. Ponno, J. Stat. Phys. **135**, 873 (2009).

[72] D. Hennig and G. P. Tsironis, Phys. Rep. **307**, 333 (1999).

[73] P. W. Anderson, Phys. Rev. **109**, 1492 (1958).

[74] B. Kramer and A. MacKinnon, Rep. Prog. Phys. **56**, 1469 (1993).

[75] P. Sheng, *Introduction to Wave Scattering, Localization and Mesoscopic Phenomena*, Springer, Berlin, 2006.

[76] G. Kopidakis et al., Phys. Rev. Lett. **100**, 084103 (2008).

[77] A. S. Pikovsky and D. L. Shepelyansky, Phys. Rev. Lett. **100**, 094101 (2008).

[78] V. F. Nesterenko, J. Appl. Mech. Tech. Phys. **24**, 733 (1983).

[79] A. Rosas and K. Lindenberg, Phys. Rev. E **68**, 041304 (2003).

[80] Nesterenko, V. F., Le Journal de Physique IV **04**, C8 (1994).

[81] R. S. MacKay, Phys. Lett. A **251**, 191 (1999).

[82] D. Treschev, Disc. Cont. Dyn. Sys. **11**, 867 (2004).

[83] G. Friesecke and R. L. Pego, Nonlinearity **12**, 1601 (1999).

[84] G. Friesecke and R. L. Pego, Nonlinearity **15**, 1343 (2002).

[85] G. Friesecke and R. L. Pego, Nonlinearity **17**, 207 (2004).

[86] G. Friesecke and R. L. Pego, Nonlinearity **17**, 229 (2004).

[87] S. Chow, J. Mallet-Paret, and W. Shen, J. Diff. Eq. **149**, 248 (1998).

[88] A. Chatterjee, Phys. Rev. E **59**, 5912 (1999).

[89] K. Ahnert and M. Abel, Comput. Phys. Commun. **177**, 764 (2007).

[90] Y. S. Kivshar, Phys. Rev. E **48**, R43 (1993).

[91] B. Dey et al., Phys. Rev. E **65**, 017601 (2001).

[92] C. Coste, E. Falcon, and S. Fauve, Phys. Rev. E **56**, 6104 (1997).

[93] K. Ahnert and A. Pikovsky, Phys. Rev. E **79**, 026209 (2009).

[94] T. Jin, H. Zhao, and B. Hu, Phys. Rev. E **81**, 037601 (2010).

[95] S. Sen, K. Mohan, and J. Pfannes, Physica A **342**, 336 (2004).

[96] Y. Zolotaryuk, A. V. Savin, and P. L. Christiansen, Phys. Rev. B **57**, 14213 (1998).

[97] D. B. Duncan et al., Phys. Lett. A **158**, 107 (1991).

[98] J. Pouget, Phys. Rev. B **43**, 3582 (1991).

[99] J. Pouget, Phys. Rev. B **43**, 3575 (1991).

[100] J. Pouget, Phys. Rev. B **46**, 10554 (1992).

[101] O. A. Druzhinin and L. A. Ostrovskii, Phys. Lett. A **160**, 357 (1991).

[102] T. Y. Astakhova and G. A. Vinogradov, J. Phys. A: Math. Gen. **39**, 3593 (2006).

[103] M. Feckan and V. M. Rothos, Nonlinearity **20**, 319 (2007).

[104] J. W. Fleischer et al, Nature **422**, 147 (2003).

[105] E. Arevalo, Phys. Rev. Lett. **102**, 224102 (2009).

[106] B. A. Malomed and P. G. Kevrekidis, Phys. Rev. E **64**, 026601 (2001).

[107] P. Rosenau, J. M. Hyman, and M. Staley, Phys. Rev. Lett. **98** (2007).

[108] N. Z. Klinghoffer and P. S. Rosenau, Phys. Lett. A **374**, 252 (2009).

[109] J. F. R. Archilla, P. L. Christiansen, and Y. B. Gaididei, Phys. Rev. E **65**, 016609 (2001).

[110] A. Comech, J. Cuevas, and P. Kevrekidis, Physica D **207**, 137 (2005).

[111] M. Feckan and V. M. Rothos, Appl. Anal. Int. Jour. (2009).

[112] S. F. Mingaleev, Y. B. Gaididei, and F. G. Mertens, Phys. Rev. E **58**, 3833 (1998).

[113] G. A. Baker, Phys. Rev. **122**, 1477 (1961).

[114] M. Kac and E. Helfand, J. Math. Phys. **4**, 1078 (1963).

[115] C. Sulem and P. Sulem, *The Nonlinear Schrödinger Equation*, Springer, 1999.

[116] M. Öster, M. Johansson, and A. Eriksson, Phys. Rev. E **67**, 056606 (2003).

[117] J. Fröhlich, T. Spencer, and C. E. Wayne, J. Stat. Phys. **42**, 247 (1986).

[118] F. K. Abdullaev et al., Phys. Rev. E **77**, 016604 (2008).

[119] M. Mulansky et al., Phys. Rev. E **80**, 056212 (2009).

[120] M. J. Ablowitz, Z. H. Musslimani, and G. Biondini, Phys. Rev. E **65**, 026602 (2002).

[121] N. V. Brilliantov et al., Phys. Rev. E **53**, 5382 (1996).

[122] L. Vergara, Phys. Rev. Lett. **104**, 118001 (2010).